

Low Earth Orbit Spacecraft Slotting: Towards an Implementable Proposal

by

Miles Lifson

S.M. Aeronautics & Astronautics, MIT, 2020

S.M. Technology & Policy, MIT, 2020

B.A. Physics, Claremont McKenna College, 2013

B.A. Government, Claremont McKenna College, 2013

Submitted to the Department of Aeronautics & Astronautics
in partial fulfillment of the requirements for the degree of

DOCTOR OF PHILOSOPHY IN AERONAUTICS & ASTRONAUTICS

at the

MASSACHUSETTS INSTITUTE OF TECHNOLOGY

June 2024

© 2024 Miles Lifson. This work is licensed under a [CC BY-NC-ND 4.0](#) license.

The author hereby grants to MIT a nonexclusive, worldwide, irrevocable, royalty-free license to exercise any and all rights under copyright, including to reproduce, preserve, distribute and publicly display copies of the thesis, or release the thesis under an open-access license.

Authored by: Miles Lifson
Department of Aeronautics & Astronautics
April 1, 2024

Certified by: Richard Linares
Associate Professor of Aeronautics & Astronautics, Thesis Supervisor

Certified by: Daniel E. Hastings
Professor of Aeronautics & Astronautics

Certified by: Moriba K. Jah
Associate Professor of Aerospace Engineering and Engineering Mechanics

Certified by: Mark A. Skinner
Senior Project Leader for Space Traffic Management

Accepted by: Jonathan P. How
Professor of Aeronautics & Astronautics
Chair, Graduate Committee, Department of Aeronautics & Astronautics

Low Earth Orbit Spacecraft Slotting: Towards an Implementable Proposal

by

Miles Lifson

Submitted to the Department of Aeronautics & Astronautics
on April 1, 2024 in partial fulfillment of the requirements for the degree of

DOCTOR OF PHILOSOPHY IN AERONAUTICS & ASTRONAUTICS

ABSTRACT

The growth in the number of proposed low Earth orbit (LEO) satellites is driven primarily by large commercial communications constellations. The launch of even half of the proposed satellites would result in an order-of-magnitude increase in active spacecraft traffic, with significant implications for LEO operations. This thesis provides a framework for understanding LEO orbital use. Intelligently organizing large constellations to efficiently make use of LEO and avoid hazardous conjunctions between on-station satellites can significantly reduce risk while imposing only a minimal burden on satellite operators. This research demonstrates the design of efficient, mutually compatible orbits and shells, describes analytical tools to assess their benefits, explores trade-offs in policy implementation pathways, and estimates reductions to the collision avoidance burden for operators from the use of cross-operator compatible orbits. The proposed framework supports quantification of the efficiency of orbital shell allocations, the opportunity cost of alternatives, and the amount of remaining uncommitted volume.

Thesis supervisor: Richard Linares

Title: Associate Professor of Aeronautics & Astronautics

Dedication

*To Carolyn Berger-Ott, who taught me to love the stars
(and that the math wasn't THAT bad)*

Acknowledgments

Professor David Arnas, thank you for considerable guidance and mentorship over the last several years. I appreciate your mathematical creativity, eye for detail, and perennial willingness to help. You were always happy to read paper drafts, offer your honest feedback, and catch the small details that everyone else overlooked. You have helped shape the intellectual direction of this work and my future career plans. I deeply appreciate all of your support and advice.

Professor Richard Linares, thank you for giving me the flexibility to pursue this research. The field of space sustainability and space traffic coordination and management is the subject of significant and increasing interest but is still not the easiest topic to fund. That is especially true for work that cuts across both the policy and technical portions of the problem. You have magnificently navigated sponsors and grants to give me the opportunity to pursue my work on these topics, share our results at a variety of conferences and other venues, and engage with stakeholders. Thank you for making my work possible.

To the members of my thesis committee, I also extend my appreciation: Professor Linares, Professor Daniel Hastings, Dr. Mark Skinner, Professor Moriba Jah, and Professor Danielle Wood (who temporarily served as my committee chair in Richard's stead). Thank you for suggestions, thoughtful questions, and advice. They have enriched this thesis. Mark, I still remember you telling me at my first committee meeting that you were highly skeptical about the feasibility of orbit coordination and that it did not seem like a particularly important problem. I hope I have managed to convince you otherwise in the time since!

To my thesis readers, Professor Kerri Cahoy and Zach Folcik, thank you for taking the time to read this thesis, participate in my defense, and offer your feedback.

Professor Martín Avendaño, thank you for collaborating with me, Richard, and David on this work.

Thank you to my fellow students and researchers in the Astrodynamics, Space Robotics, and Controls Laboratory. Dan Jang, thank you for your assistance running MOCAT-MC, for presenting work on my behalf at multiple conferences when I was unable to travel, and for being a generally fantastic person who is always willing to help. Thomas Roberts, thank you for your professional advice, graphic design expertise, and your sense of perspective as we navigated the PhD process. Dr. Axel Garcia, thank you for collaborating with me on some really interesting projects, and most importantly for reminding me that the best thesis is a finished thesis. Dr. Andrea D'Ambrosio, you were a great collaborator on MOCAT modeling, and I'm so glad that you are enjoying your new position at University of Arizona. Dr. Giovanni Lavezzi, thank you for your willingness to get involved with MOCAT-SSEM and extend our intrinsic capacity work. I am glad to know that as I wrap up my time in

ARCLab, the projects will continue in good hands.

To the experts who were willing to be interviewed or talk to me informally for this project, thank you for lending your insight, practical experience, and candid feedback. With any translational project, it is critical to ensure fit between the problem and proposed solution. Your advice has been tremendously helpful to steer the direction of this work.

Thank you to Greg Henning, Deanna Mains, Marlon Sorge, and the full ADEPT team at Aerospace Corporation for answering endless questions about the model and its assumptions and providing me access to modeling data used to help verify MOCAT-MC and MOCAT-SSEM. Patrick Bauer and Dr. Mark Skinner, thank you for bringing me onto your team at Aerospace, helping me connect with the right people in the company to support my work for this thesis, and accommodating my constantly fluctuating schedule as I finished this degree.

The Orekit space dynamics library was used to perform propagation, coordinate transforms, and other functions for this work.

I gratefully acknowledge the MIT SuperCloud and Lincoln Laboratory Supercomputing Center for providing high-performance computing resources and consultation that have contributed to the research results reported within this thesis.

I wish to provide the following chapter-specific acknowledgments:

- **Chapter 3:** I thank Shiva Iyer and Apoorva Karra for their considerable assistance with using the UT Austin caspy library. I was partially supported by the MathWorks Fellowship and the MIT Portugal Partnership 2030. This work is sponsored in part by the Defense Advanced Research Projects Agency (Grant N66001-20-1-4028). The content does not necessarily reflect the position or the policy of the U.S. government. No official endorsement should be inferred. Distribution statement A: Approved for public release; distribution is unlimited. I acknowledge the support of this work by the U.S. Air Force's Office of Scientific Research under Contract Number FA9550-18-1-0115.
- **Chapter 4:** I was partially supported by the MathWorks Fellowship and the MIT Portugal Partnership 2030. This work is sponsored by the Defense Advanced Research Projects Agency (Grant N66001-20-1-4028). The content does not necessarily reflect the position or the policy of the U.S. government. No official endorsement should be inferred. Distribution statement A: Approved for public release; distribution is unlimited. I acknowledge the support of this work by the U.S. Air Force's Office of Scientific Research under Contract Number FA9550-18-1-0115.
- **Chapter 5 and 6:** This work was funded by the NASA Office of Technology, Policy, and Strategy under Grant Number NNH22ZDA001N-ESPOD.

To my parents, Jeff Lifson and Aloha Keylor, thank you for your unconditional love and support. When I started down this path, I was not sure that space policy was a thing, much less a viable career path. Your encouragement helped keep me going, even when the path was far from clear.

Thank you to Chatt Lifson Routh, my bloodhound-mix rescue, for being a (mostly) patient good boy. I cannot count the hours and Zoom calls you have spent curled up behind

me as I wrote this thesis. It would not have been the same without you. I promise there will be many more walks after my defense.

And lastly, to my wife, Carol Ann Routh, thank you for your endless patience and support as one master's degree became two, and two became a PhD. In a marriage, any academic degree, and especially a PhD, is a joint commitment. Thank you for your understanding through all the deadlines, long hours, and travel.

Contents

Title page	1
Abstract	3
Dedication	5
Acknowledgments	6
List of Figures	13
List of Tables	15
Nomenclature	18
1 Introduction	21
1.1 Research Problem	23
1.1.1 Limitations	24
1.2 Contributions	24
1.3 Organization	24
2 Literature Review	26
2.1 Risk-Based Capacity Quantification	26
2.2 Flower Constellation Theory	28
2.3 Orbital Slotting	31
2.4 Literature Review Summary	31
3 A Method for Generating Closely Packed Orbital Shells and Implications for Orbital Capacity	34
3.1 Introduction	34
3.2 Preliminaries	38
3.2.1 2D-LFCs	39
3.2.2 Non-Spherical Earth Effects	39
3.2.3 Classical Orbit Freezing	40
3.2.4 Equinoctial Elements	40
3.2.5 Other Perturbations	40
3.2.6 Other Modeling Assumptions	41

3.2.7	Overview of the Proposed Techniques and Their Potential Use	42
3.3	Definition of Osculating 2D-LFCs	43
3.3.1	Definition of Osculating 2D-LFCs under a Zonal Geopotential	43
3.3.2	Definition of Osculating 2D-LFCs under a Zonal, Sectoral, and Tesseral Geopotential	48
3.4	Simplified Shell Model	52
3.4.1	Simplified Shell Model Method	52
3.4.2	Simplified Shell Model Results	53
3.5	Shell Width Estimation	58
3.5.1	Shell Width Estimation Method	58
3.5.2	Shell Width Estimation Results	59
3.6	Shell Coordination, Number of Admissible Shells and Slots, and the Effect of Inclination Sequencing	60
3.6.1	Demonstration 1: J_2 - J_3 Shells Are Not Stable over Practical Time Periods	60
3.6.2	Demonstration 2: Coordinated Orbits Allow More Shells than Minimum-Maximum Altitude Separation, But Inclination Sequencing Matters	61
3.6.3	Experiment 1: Impact of Shell Coordination and Inclination Ordering on Number of Shells and Satellites	63
3.6.4	Experiment 2: Impact of Shell Separation Distance on Number of Admissible Shells	65
3.7	Summary	66
4	The LEO Packing Problem: Implications for Orbit Design and Policy	68
4.1	Introduction	68
4.2	The Orbit Packing Problem	69
4.2.1	Preliminaries	70
4.2.2	Capacity per Shell	72
4.2.3	Number of Shells in LEO	83
4.3	Pathways to Implementation for Orbit Coordination	85
4.3.1	Verification of Slotting Implementation Pathways with Operators	89
4.4	Recommendations	91
4.5	Summary	94
5	Space Environmental Governance and Decision Support Using Source-Sink Evolutionary Environmental Models	95
5.1	Introduction	95
5.1.1	SSEMs	96
5.1.2	Adaptive Management and Adaptive Governance	99
5.1.3	Traditional Ecological Knowledge	103
5.2	Methodology	104
5.2.1	A Sketch of an Adaptive Space Environment Management Regime	104
5.2.2	Model Specifications	108
5.2.3	Indicator Variables	110
5.2.4	Non-Zero Altitude Disposal Orbits	116

5.3	Results	117
5.3.1	Adaptive Authorization Pathway	117
5.3.2	Adaptation to Changes to Environmental Conditions	122
5.3.3	Decision Support to Changes to Behavior	122
5.4	Summary and Future Work for Chapter 5	123
6	Quantifying the Benefit of Orbit Coordination between LLCs	126
6.1	Relevant Prior Analyses	127
6.2	MOCAT-MC	127
6.2.1	Collision Modeling	127
6.2.2	Baseline Traffic Model	128
6.2.3	Method	128
6.2.4	Results	129
6.3	Conclusion	132
7	Summary and Future Work	133
7.1	Summary	133
7.2	Contributions	133
7.3	Future Work	134
7.4	Final Remarks	134
	Appendices	136
A	Initial Equinoctial Elements for Constellation Seed Orbits	137
B	Radial Distance Derivatives	138
C	LEO Operator Interview Questions	140
D	LEO Operator Interviewees	145
E	Chapter 6 Supplementary Tables	146
	References	149

List of Figures

2.1	2D-LFC with $N_o = 5, N_{so} = 7, N_c = 1$, and $a = 7000$ km, $i = 70^\circ$.	30
2.2	Sun-Synchronous Satellite Orbit Crossing at the North Pole.	32
3.1	Selected Proposed Large Constellations [475–750 km].	35
3.2	Selected Proposed Large Constellations [1000–1225 km].	35
3.3	Flowchart for Applicability of the Introduced Techniques.	42
3.4	Comparison of Sequential Constellation Shell Spacing Strategies.	43
3.5	SpaceX and Amazon Shells, Unaligned.	46
3.6	SpaceX and Amazon Shells, Aligned.	47
3.7	J_2 -Adjusted Approximate Admissible Mean Altitudes ($i = 45^\circ$).	49
3.8	Median Distance Between RGTs.	49
3.9	Hughes and China SatNet Shells.	51
3.10	Mean to Osculating Shell Geometry Comparison Example 1 ($i = 40^\circ$).	54
3.11	Mean to Osculating Shell Geometry Comparison Example 2 ($i = 87^\circ$).	55
3.12	GA Geometry Comparison Example 1 ($i = 40^\circ$).	56
3.13	GA Geometry Comparison Example 2 ($i = 87^\circ$).	56
3.14	Classical versus Numerical Orbit Freezing Geometry Comparison for Example 1.	57
3.15	Classical versus Numerical Orbit Freezing Geometry Comparison for Example 2.	58
3.16	Estimated versus Actual Shell Widths for Sample Satellites.	60
3.17	J_2 - J_3 Frozen Shells Propagated under a J_3 Model for 30 Days.	61
3.18	J_2 - J_3 Frozen Shells Propagated under a 21 by 21 Gravity Model.	61
3.19	Compatible Geopotential-Aware Shell Placement within Keplerian Separation Distance.	62
3.20	Shells Nesting Compared between Disparate and Similar Inclinations.	63
3.21	A Comparison of Random and Sequential Inclination Shell Layering Approaches.	64
3.22	Admissible Satellite Locations for Various In-Shell Separation Distances.	65
3.23	Admissible Shells for Various Shell Separation Distances.	66
4.1	Self-Safe Shells Can Be Sequentially Nested.	70
4.2	Nested Quasi-Periodic 2D-LFC Shells.	72
4.3	Distribution of a 2D-LFC ($i = 60^\circ, N_o = 246, N_{so} = 7, N_c = 224$).	75
4.4	Direct Database Capacity Results ($i = 60^\circ$).	75
4.5	Direct Database Capacity Results (any Inclination).	76

4.6	Power Law Fit ($c = 429.811$, $b = -0.8305$, $R^2 = 0.97661$).	77
4.7	Angular Distance to N_{sat} Relationship for $i = 60^\circ$.	78
4.8	Power Law Angular Distance Predictions and Actual Values for $N_{sat} = 1722$.	78
4.9	An Example of an NSI Trajectory ($N_d = 2$, $N_p = 3$).	79
4.10	NSI Capacity Curve ($i = 60^\circ$).	79
4.11	Local NSI Capacity Curve ($i = 60^\circ$).	80
4.12	NSI Prediction Error vs. Best 2D-LFCs ($i = 60^\circ$).	80
4.13	Original and Reconfigured Shells (Partial View).	82
4.14	Histogram of Slot Center Adjustments from Expansion.	83
4.15	Metrics for Shell-Stacking Efficiency.	85
4.16	Shell Tessellation for Sequence and Non-Sequential Inclinations.	86
4.17	Implementation Pathways	87
4.18	Selected Proposed LLCs.	92
5.1	A Potential Adaptive Management Cycle.	100
5.2	Adaptive Governance Overview.	102
5.3	Area vs. Mass Analysis for Station-keeping Satellites.	112
5.4	Baseline Modeling Process Diagram.	118
5.5	Baseline Constraint Satisfaction.	119
5.6	Additional Aggregate Collisions from the New Constellation (C) and Constellation Derelicts (D).	120
5.7	Additional Induced Maneuvers from the New Constellation (C) and Constellation Derelicts (D).	122
5.8	Long-term Sustainability Constraint, Evaluated with and without ASAT Test.	123
5.9	Derelict Population Increases from Five-Year Rule versus Instantaneous Disposal.	124
5.10	Derelict Population Burden from Five-Year Rule versus Instantaneous Disposal.	124
6.1	Scenario 1: Object Type Pairs for Conjunctions.	130
6.2	Scenario 1: Object Type Pairs for Conjunctions (Percentage).	130
6.3	Scenario 1: Object Type Pairs for Conjunctions, Pairs involving Constellations Only (Percentage).	131
6.4	Scenario 1: Constellation-on-Constellation Conjunctions by Constellation.	131

List of Tables

3.1	Zonal Example: Selected SpaceX and Amazon Shells.	46
3.2	RGT Example: China SatNet and Hughes Shells.	51
4.1	Best Fit Power Laws	77
5.1	Reference Scenario Properties for Adaptive Demonstrations.	109
5.2	Reference Species and Properties for Adaptive Demonstrations.	110
5.3	LLCs Included in Future Launch Model.	111
5.4	Objects in Initial Population and Future Launch Model	111
5.5	Species and Properties for Additional Species Added for Demonstration Case	121
5.6	Fragment Counts for the Simulated ASAT Missile Test	122
6.1	Collision Avoidance Failure Rate	129
1	Seed Trajectories for Constellations	137
2	LEO Operator Interviewees	145
3	Future Constellation Launch Model	146
4	Operator vs. Operator Conjunctions	147
5	Object Type vs. Object Type Conjunctions	148

Nomenclature

2D-LFC	two-dimensional lattice flower constellations
3D-LFC	three-dimensional lattice flower constellations
4D-LFC	four-dimensional lattice flower constellations
A_{\odot}	sun-exposed area of the spacecraft
ARCLab	Astrodynamics, Space Robotics, and Controls Laboratory
ASAT	anti-satellite
ASO	anthropogenic space objects
a	semi-major axis
\bar{a} ,	mean semi-major axis
B	ballistic coefficient
\dot{C}	collision rate
$C_{l,m}$	empirical constants provided by the chosen gravity field model
\dot{C}_{PMD}	post-mission disposal rate
c_D	coefficient of drag
c_R	coefficient of reflectivity
\vec{D}	drag coefficient vector
DSST	Draper Semi-Analytical Satellite Theory
DTM2000	a semi-empirical atmospheric model
d	thickness of an altitude bin
ECEF	Earth-centered Earth-fixed
ESA	European Space Agency
e	eccentricity
\bar{e}	mean eccentricity
e_x	equinoctial element e_x
e_y	equinoctial element e_y
FC	flower constellation
FCC	U.S. Federal Communications Commission
GA	genetic algorithm
GEO	geosynchronous Earth orbit
h_x	equinoctial element h_x
h_y	equinoctial element h_y
ITU	International Telecommunication Union
i	inclination
\bar{i}	mean inclination
i_1	inclination of satellite 1

i_2	inclination of satellite 2
J_l	J_l refers to either a specific zonal harmonic constants, $J_l = -C_{l,0}$, or a zonal-only model including all zonal terms up to degree l , depending on context.
JB2008	Jacchia-Bowman 2008 Empirical Thermospheric Density Model
k_1	optimization constant
k_2	optimization constant
LEO	low Earth orbit
LLC	large LEO constellation
LNT	lethal non-trackable
l_θ	true longitude
lb_e	lower bound on eccentricity during optimization
M_{ij}	mean anomaly (of the i -th satellite in the j -th plane)
MIT	Massachusetts Institute of Technology
MOCAT	MIT Orbital Capacity Assessment Tool
MOCAT-SSEM	MIT Orbital Capacity Assessment Tool Source Sink Evolutionary Model
MC	Monte-Carlo
m	mass
N	debris species
N_c	configuration number
N_d	number of days
NEAT	number of Encounters Assessment Tool
N_o	number of orbital planes
N_p	number of orbital periods
N_{sat}	number of satellites per orbit
NSI	non-self-intersecting
N_{so}	number of satellites per orbit
ODE	ordinary differential equations
\mathbf{P}	population of each species
$P_{l,m}$	Legendre polynomial of degree l and order m
p_{srp}	force of solar pressure per unit area
Q	arbitrary species in an SSEM
RAAN	right ascension of the ascending node
RGT	repeating ground-track
SBM	Standard Break-Up Model
$S_i(t)$	population of species S_i at time t
$S_{l,m}$	empirical constants provided by the chosen gravity field model
STCM	space traffic coordination and management
SSEM	source-sink evolutionary model
T_c	cycle time
T_Ω	nodal period of the orbit
$T_{\Omega G}$	nodal period of Greenwich
TEK	traditional ecological knowledge
$t_{i,j}$	propagation time for the j -th satellite in the i -th orbital plane from

	the starting epoch of $X_{0,0}$
V	volume (of the altitude bin or cube)
v	rate of change of the semi-major axis
\bar{n}	mean mean motion
$\vec{r}_{\oplus 3}$	vector from the Earth to the 3rd body
$\vec{r}_{\oplus sat}$	vector from the Earth to the satellite
$\vec{r}_{sat\odot}$	vector from the satellite to the sun
\vec{r}_{sat3}	vector from the satellite to the third body
ub_e	upper bound on eccentricity during optimization
$v_r(h)$	relative velocity (either w.r.t. atmosphere or two colliding objects)
$X_{0,0}$	seed trajectory
α_{active_i}	collision avoidance term for an active maneuverable object
$\alpha_{c_{intra}}$	fraction of collision avoidance failure for conjunctions within a particular constellation
$\alpha_{c_{inter}}$	fraction of collision avoidance failure between constellation spacecraft from different constellations
α_i	collision avoidance term
$\Gamma_{i,j}$	ground-track offset angles (Ch. 3)
Γ_{ij}	collision modifier (Ch. 5)
$\Delta t_{i,j}$	propagation times
ζ	slotting effectiveness factor
θ	true anomaly
Λ	launch rate
λ_{sat}	geocentric longitude
μ_{\oplus}	Earth's gravitational constant
μ_3	gravitational constant of a third body
ρ	atmospheric density
σ_{ij}	impact parameter for species i and j
ϕ	geocentric latitude angle
$\phi_{gc_{sat}}$	geocentric latitude
ϕ_{ij}	intrinsic collision frequency between species i and j
Ω_{ij}	right ascension of the ascending node (of the i -th satellite in the j -th plane)
$\bar{\omega}$	mean argument of perigee
ω	argument of perigee
ω_{\oplus}	Earth's angular velocity
ℓ_2	2-norm
+	quantities related to the bin immediately above the current one

Chapter 1

Introduction

Since about 2015, the number of proposed low Earth orbit (LEO) satellites and constellations has skyrocketed. This increase has been fueled by trends in technological miniaturization, more affordable launch costs, and increasing availability of the capital necessary to develop and operate large constellations. While interest is currently being driven by commercial constellations, primarily for communications applications, large constellation architectures are also of interest to nation states for the resiliency and capacity they bring to supporting various national security space missions.

Large constellations totaling more than 100,000 satellites have been proposed for LEO. For example, while technically dubious, the company E-Space has proposed constellations of more than 300,000 satellites¹. Not all of these constellations will make it to orbit, and fewer still will be completed. Nevertheless, increasing the active satellite population by more than an order of magnitude will necessitate numerous technical, operational, and policy changes to ensure the long-term sustainability of the space environment in the face of denser operations.

Large constellations with overlapping orbital altitudes have the potential to increase orbital conjunction risk as well as the operational burden associated with planning and coordinating collision avoidance maneuvers for active spacecraft controlled by different operators. For this reason, representatives of multiple operators have argued that large constellations should not overlap in orbital altitude [1], [2]. At the same time, others have raised concerns that such a practice essentially amounts to legitimizing a land grab by early entrants to the detriment of later operators.²

Orbital physical interference issues have also played out in discussions before the U.S. Federal Communications Commission (FCC). In 2020, Amazon submitted a petition for reconsideration of an FCC orbital debris rulemaking action, arguing that the FCC should adopt a 1 km separation requirement between constellations of at least 300 satellites [3]. The move drew support from some operators concerned about orbital risk from overlapping large constellations [4], and opposition from others arguing that the proposal would create a first-come, first-served priority system in LEO that would incentivize overly large orbital tolerances [5], [6]. A small constellation operator also expressed concern about how smaller

¹See <https://www.spaceintelreport.com/e-space-registers-116640-satellite-c-band-network-with-itu-through-france-300000-satellite-rwanda-network-is-no-more>, accessed 16 December 2023.

²See, for instance <https://www.theverge.com/2021/1/27/22251127/elon-musk-bezos-amazon-billionaire-s-satellites-space>, accessed 16 December 2023.

operators would interact with large constellations subject to separation requirements [7].

Issues relating to orbital tolerances have repeatedly been raised, with operators requesting large operational tolerances that exceed the as-flown range of their constellations to preserve orbital flexibility [8]–[10]. In SpaceX’s most recent license modification, the FCC side-stepped these orbital separation issues and chose to impose a requirement that SpaceX not exceed 580 km in altitude to avoid hazardous overlap with Amazon [11, p. 43]. Across this regulatory discourse, it is clear that discussion remains relatively elementary, with limited thought about orbital coordination mechanisms. Such discussion, to the extent it occurs, remains rooted in implicit first-come, first-served mechanisms or nebulous coordination requirements. There is scant justification for claimed expansive and inefficient orbital tolerances, which appear more driven by a desire for regulatory flexibility than engineering. There is also a lack of technical specificity on ways to design and operate dense compatible orbits, or even what information sharing would be required to facilitate a coordination regime.

Concerns about access to orbital volume are also present in international and geostrategic discussions. In a subsequently removed article from early 2023³, researchers at an institution affiliated with the Chinese People’s Liberation Army expressed concern about Starlink’s access to orbital volume as a competitive and strategic threat. Translated from the original Chinese, the article argues: “First, before Starlink finishes deployment, we must quickly deploy satellites on orbital tracks, protecting our influence on these orbital tracks and preventing the excessive use of these tracks by Starlink.” Further, the paper argues that, “Second, we can deploy our country’s own massive satellite constellation in orbital tracks (orbits) where Starlink is not yet deployed, gaining superiority and advantage at other altitudes, so much so that we may suppress the formation of Starlink.” There are also calls from emerging space nations that fear that established space nations will disproportionately occupy the “beachfront” orbital volume in LEO to the detriment of other nations’ ability to access and make use of LEO. For instance, this concern was raised by a representative of the Group of 77 at the 2023 meeting of the Scientific and Technical Subcommittee of the United Nations Committee on the Peaceful Use of Outer Space, where the speaker noted:

The [Group of 77] underscores that the deployment of megaconstellations, if not carried out sustainably and equitably, may pose the risk of congestion of Low Earth Orbit, which will be [a] significant disadvantage in the use and exploration of space by developing countries. Therefore, the principle of equitable access to outer space, and in particular in the LEO, needs to be observed more than ever.⁴

Concerns about orbital access in LEO are informed by previous disputes regarding geosynchronous Earth orbit (GEO). In GEO, demand for orbital access (and for associated spectrum access) has long exceeded capacity, causing particular frustration for nations with emerging space programs [13]–[15]. In LEO, large constellations will occupy significant orbital real

³The article was originally posted at <https://www.zhkzyfz.cn/CN/10.3969/j.issn.1673-3819.2023.01.022> and first reported by the *South China Morning Post* (<https://www.scmp.com/news/china/article/3211438/china-aims-launch-nearly-13000-satellites-suppress-elon-musks-starlink-researchers-say>). Both websites were accessed 24 February 2023.

⁴See <https://media.un.org/en/asset/k11/k11gbjlxh9>, accessed 16 December 2023, from approximately 52:50-53:20 and [12, p. 7]

estate, limiting both placement options for new entrants and consuming a significant portion of the allowable aggregate orbital risk budget. Orbital access can be thought of as a common-pool resource, but LEO demand is now sufficient to make the rivalrous aspect of orbital use particularly salient.

Discussions are also occurring through the International Telecommunications Union Radiocommunication Sector (ITU-R) Working Party 4A (WP4A) in the lead-up to the World Radio Conference 2023 in late November and early December 2023, where an agenda item addressed tolerances for orbital characteristics of non-geostationary satellite orbit (NGSO) space stations. Multiple suggestions have been proposed based on technical approaches, including spreading loss at zenith (i.e., linking altitude tolerances to changes in satellite signal strength due to distance), orbital period-based tolerances, and percentage-based tolerances with consideration for circular and non-circular NGSO satellites. As of July 2023, Annex 8 of the draft Annex 20 to the WP4A Chairman’s Report briefly describes potential coordination based on separation in altitude as a function of geocentric latitude [16]. While the draft acknowledges the possibility of sharing based on compatible frozen orbits, it currently reaches a conclusion that separation of 70 km in orbital altitude is necessary based on osculating altitude ranges associated with the eccentricities of various small satellites flying in non-frozen orbits. This dubious analysis is currently subject to non-consensus within the committee. At the 2023 Radiocommunication Assembly, China proposed a new question on orbit and spectrum capacity for NGSO systems for study through the ITU-R [17]. Accompanying the draft question, China provided a highly oversimplified estimate of the number of satellites that could physically coexist in LEO based on stacking 50° inclination circular Walker constellations with an intra-shell minimum separation distance of 50 km and inter-shell spacing of 20, 50, 70 or 100 km. It then compared this number against ITU coordination requests and Part II-S filings to conclude that LEO capacity is heavily oversubscribed in the 300–700 and 700–1500 km ranges.

1.1 Research Problem

Against this backdrop, it is clear that there is a need to understand congestion of physical orbital volume in LEO and that the problem is coupled with, but not the same as, broader discussions about space sustainability. It is equally clear that productive discussion on these issues requires casting them in terms of a level of technical specificity that facilitates bridging discussion at the operational and policy levels.

The goal of this thesis is to present a pragmatic framework to understand issues of orbital volume use and admissible satellite locations—also known as slots—in LEO, using a framework of intrinsic capacity arising from an imperative for physical non-conjunction between coordinated orbits for active constellation spacecraft. This framework is then applied to demonstrate potential technical solutions to challenges associated with orbital congestion in LEO and initial policy analyses on potential broad pathways toward implementation. The potential benefits associated with coordinating large constellation orbits are estimated.

1.1.1 Limitations

This work adopts several limitations to scope for a variety of reasons. First, because the overwhelming majority of planned constellation traffic for the next few decades is likely to be placed in LEO due to engineering and economic reasons, this work focuses on LEO, neglecting the regime-specific factors that would apply to an orbit coordination scheme for medium Earth orbit or the existing coordination structures for GEO. It also ignores architectures dependent on highly elliptical orbits and spacecraft without propulsion. The proposed orbit coordination measures avoid a significant source of otherwise avoidable orbital risk but do not address these types of orbits at the design stage. We assume operational collision avoidance mechanisms will be necessary for such coordination. Likewise, the work in this thesis focuses primarily on orbit coordination and orbital slots rather than questions of risk-based capacity. Risk-based capacity, which also incorporates consideration of debris, is very important but is already an ongoing topic of research and focus by an existing and much broader community [18]–[20].

1.2 Contributions

The contributions in this dissertation are:

1. Development and demonstration of slotting methods to generate physically compatible orbital shells in the presence of an arbitrary Earth geopotential, simplified formulas for estimating shell centerline geometry and width, and an assessment of gains to admissible shells from use of shell-stacking methods;
2. The definition of metrics for assessing shell design and shell stacking, analysis on how to apply orbit compatibility techniques to provide decision support, and development of stakeholder-assessed policy implementation pathways;
3. An application of adaptive management and governance techniques to orbital use management, along with a technical demonstration of model-supported adaptive governance; and
4. An assessment of reductions to conjunctions from the use of compatible large constellation orbits.

These contributions advance the field by translating a theoretical model for LEO slotting into a practical and implementable framework for coordinating and managing intensive orbital use in LEO. They enable future work on cross-operator orbit coordination, efficient orbital use in LEO, and adaptive governance of orbital capacity.

1.3 Organization

The thesis is divided into seven chapters. Chapter 1 frames the motivation and scope for the work of this thesis. Chapter 2 briefly reviews risk-based capacity quantification, flower

constellation (FC) theory, and pre-existing work on LEO orbital slotting. Chapter 3 presents a technical description of methods to generate mutually exclusive and self-safe orbital shells. It then applies these methods to planned congested overlaps in LEO. Next, it offers recommendations for technical measures to improve the density of shell use in LEO. The chapter quantifies the improvements to orbital density associated with these methods and derives simplified methods for estimating orbit shape in the altitude-geocentric latitude plane as a tool to facilitate orbit coordination and analysis. Chapter 4 applies work on slotting from this thesis and associated collaborations [21]–[24] to define metrics and methods for quantifying orbital slots and shell use. It then demonstrates how these can be applied to provide decision support around questions of efficiency of orbital use, opportunity cost quantification, and assessment of remaining intrinsic orbital capacity. It then presents a high-level description of potential pathways to orbit coordination and discusses key differences in their suitability for achieving objectives related to spaceflight safety, efficiency, and equitable access. Chapter 5 discusses how to apply adaptive management and governance philosophies to orbital capacity and provides a technical demonstration incorporating orbital capacity constraints based on both geometric compatibility and stochastic kinetic space safety considerations using the Massachusetts Institute of Technology (MIT) Orbital Capacity Assessment Tool (MOCAT). These philosophies can improve cooperative management of LEO orbital use, whether applied in a broader capacity context or constrained to only coordination for intrinsic capacity. Chapter 6 estimates benefits to orbit coordination for physical collision avoidance between large constellations using the Monte Carlo (MC) modeling approach within MOCAT. Chapter 7 summarizes the content of the thesis and discusses potential areas for future work.

Chapter 2

Literature Review

This chapter contains a literature review of three areas: techniques to quantify orbital risk and capacity, FC theory, and orbital slotting. Before beginning, it is important to distinguish and disambiguate between the notions of capacity underlying the first and third topics, as they are fundamentally different measures. **Risk-based** capacity estimation seeks to extrapolate the evolutionary growth of the space object population subject to a variety of different conditions characterized by both epistemic and aleatory uncertainty. Epistemic uncertainty concerns lacking but potentially knowable information, such as the nature of the statistical distribution of the variable(s) in question, while aleatory uncertainty concerns information that is not practically knowable, such as the stochastic future that will be obtained from a potential distribution. Slotted or **intrinsic** capacity seeks to answer how many actively controlled objects in what configurations can be placed into a particular volume of space in a structure that indefinitely admits no collision risk along a set of reference trajectories. Intrinsic capacity is significantly more restrictive in its assumptions but is useful for addressing the allocative and assignment aspects of space traffic coordination and management (STCM). Because intrinsic capacity cannot address questions such as risk associated with interactions between an optimal slotting structure and non-compliant spacecraft or debris objects, spacecraft initial conditions derived from intrinsic capacity methods must be combined with risk-based capacity estimation methods to understand risk-based capacity subject to certain slotting structures.

A broader review of space sustainability, space situational awareness, and STCM is beyond the scope of this literature review. I provided a brief review of these topics in my master's thesis, along with an in-depth analysis of potential designs for internationalized STCM systems [25]. Intrinsic capacity is distinct from, but connected to, each of these topics.

2.1 Risk-Based Capacity Quantification

Ever since Kessler and Cour-Palais's iconic paper describing the potential for runaway growth in the orbital debris population [26], there has been interest in predicting the evolution of the space environment and characterizing the sensitivity of that environment to various spacecraft quantities, mission concepts of operation, and remediation practices. The Iridium-

Cosmos collision, debris-generating anti-satellite (ASAT) missile testing by several nations, and proposed large constellations have all further increased interest and concern.

The highest-fidelity techniques to estimate these trends involve evolutionary MC models that propagate the space environment according to well-understood spacecraft dynamics and fragmentation probability distribution equations, as well as assumptions about future traffic, solar activity, and other relevant factors. Leading models that take this approach include NASA’s LEGEND [27], the European Space Agency (ESA)’s DELTA [28], and Aerospace Corporation’s ADEPT process [29]. These models have been used for a variety of purposes, including to generate conclusions about the levels of active debris removal (ADR) necessary to stabilize the space environment [30], [31] and the impact of large constellations [32]. Unfortunately, evolutionary MC models are slow, computationally expensive, sample only a small portion of high-dimension parameter spaces, and generally require new runs for differing initial conditions. These factors significantly limit their usefulness and accessibility. At the time the work in this thesis was conducted, there was no open-source implementations of evolutionary orbital MC modeling tools or even most major components.¹ This lack of open, platform-agnostic implementations and the computing power required to run these models limits their use to specialized staff at a small number of organizations and imposes substantial inertial barriers to researchers seeking to validate other models, operators seeking to optimize designs for space sustainability, and regulators trying to assess license applications.

As an alternative approach, authors have proposed criticality indexes, metrics, or other simplified heuristics to produce useful information about long-term orbital risk trends without explicitly simulating the entire evolution of the orbital environment. Risk is considered differently in various tools, particularly whether risk is defined solely in terms of collision probability or in terms of both collision probability and the severity of the consequences of a collision. Bombardelli et al. [34] offers a high-quality and detailed comparison of several criticality methods.

One major use of criticality indices has been to prioritize objects for active debris removal. The most authoritative study on this topic is one by McKnight et al. which aggregated multiple criticality approaches to generate a list of the highest-priority large derelict objects [35]. Previous studies include work by Pardini and Anselmo [36], [37], Keschull et al. [38], Uetzmann et al. [39], Yasaka [40], and Liou et al. [41].

Some of the most developed work on debris indices is the ESA’s Mission Index [42]–[44], which is now being implemented in a publicly available open-source platform [45] and includes trackability, collision-avoidance efficacy, empirically derived anticipated probability of explosion likelihood, and orbital capacity estimation. Other notable methods not yet mentioned include Rossi et al. [46], [47] and work specifically intended for application to large constellations, including Rossi et al. [48] and Anselmo and Pardini [49], [50].

No consensus yet exists on a definition or method for calculating orbital capacity, although it can be roughly expressed as quantifying the set or number of objects consistent with the stable long-term evolution of the orbital environment. This stability can be defined in many ways, including fragment counts, debris density, or a more abstracted quantification of acceptable level of total cumulative orbital risk. None of the known models have attempted to integrate a constraint on physical compatibility between satellite orbits as a limitation on

¹A model implemented by Jang et al. was released in December 2023 [33].

orbital capacity.

One major approach to quantifying orbital capacity has been through simplified sets of differential equations that capture long-term behavior, referred to as source-sink, predator-prey, or systems dynamics models. These techniques have been explored with varying system boundaries, levels of fidelity, and validation [51]–[60]. Of these approaches, Somma’s particle-in-a-box approach [56] has been influential and widely adopted in recent work on this topic, including Trozzi et al. [51] and Rao and Letizia [53]. Work is underway by a team within the MIT Astrodynamics, Space Robotics and Controls Laboratory (ARCLab) to develop risk models using this approach (described in more detail in Chapter 5), as well as a MC modeling capability [33], [61] for calibration, validation, and verification.

Multiple techniques and tools exist for the simpler subproblem of estimating long-term collision risk without attempting to model iterative consequences, including the method from Alfano and Oltrogge [62] implemented as the Number of Encounters Assessment Tool (NEAT), simple estimates based on the kinetic theory of gases [63], and traditional conjunction detection techniques [64], [65]. These methods generally ignore phasing and are therefore best suited for long-term analysis of isotropically distributed debris objects or uniform constellations. The cube method [66] is intended to improve fidelity using numerical simulations, but it requires impractically small step sizes to obtain accuracy for large constellations [67]. Reiland et al. [68] sought to evaluate two higher-fidelity methods [69] and [70], [71] to assess suitability against reference techniques by Öpik [64] and Wetherill [65]. Reiland et al. concluded that neither method was sensitive enough to properly account for a proposed set of subtle orbital shifts to mitigate intra-constellation conjunction risk and, instead, that efficient brute-force methods are required.

2.2 Flower Constellation Theory

FC theory is a general and powerful set of analytical methods to define satellite constellations. It is chosen as the analytical method for this work because it allows consideration of all potential uniform distributions of satellites in right ascension of the ascending node (RAAN) and mean anomaly. This generalization encompasses many other constellation design methods, including Walker constellations, which are among the most commonly used designs for large constellation shells.

FCs were first introduced by Mortari et al. [72] as constellations featuring 1) identical orbit shape, argument of perigee, altitude of perigee, and inclination; 2) satellites equally spaced across an arbitrary RAAN range; and 3) repeating ground tracks (RGTs) for some number of orbital periods. In subsequent work, the ground-track requirement has been generalized to any arbitrary fictitious frame rotating at a constant rate. Mortari and Wilkins [73] and Wilkins and Mortari [74] described the theory in greater detail, including an additional parameter for satellite phasing and ways to partially identify redundant parameterizations that describe equivalent constellations. Avendaño and Mortari [75] and Avendaño et al. [76] recast FC theory from a number theory perspective, introducing a new minimal parameterization referred to as two-dimensional lattice flower constellations (2D-LFCs). 2D-LFCs are more intuitive because they render the rotating frame as implicit rather than explicit and address equivalency and similarity concerns associated with the original formulation

while also including additional configurations. Arnas et al. [77] introduced a generalization of 2D-LFCs and other uniform constellation definition systems and provided proofs for existence, uniqueness, and quantification of available configurations. Arnas et al. [78] describes a method to generate constellations with varying semi-major axes that preserves a certain repeating dynamic and could be used to coordinate between shells or satellites at different altitudes.

Under the 2D-LFC parameterization, a constellation with a shared semi-major axis a , inclination i , eccentricity e , and argument of perigee ω can be defined in the RAAN (Ω_{ij}) and mean anomaly (M_{ij}) space based on three integer values: the number of orbital planes (N_o), the number of satellites per orbit (N_{so}), and the configuration number (N_c), which acts as a phasing parameter between orbital planes according to the following equation:

$$\begin{bmatrix} N_o & 0 \\ N_c & N_{so} \end{bmatrix} \begin{Bmatrix} \Omega_{ij} \\ M_{ij} \end{Bmatrix} = 2\pi \begin{Bmatrix} i - 1 \\ j - 1 \end{Bmatrix} \quad (2.1)$$

where $i \in [1, \dots, N_o]$, $j \in [1, \dots, N_{so}]$ names the j -th satellite on the i -th orbital plane of the constellation. The configuration number is defined in the range $N_c \in [0, N_o - 1]$ to avoid redundant configurations.

The 2D-LFC formulation allows the straightforward and discrete enumeration of all possible uniform satellite constellations, up to an arbitrary size subject to an arbitrary reference point in the Ω, M space. Figure 2.1 shows an example 2D-LFC in M - Ω and Cartesian space. Davis et al. [79] generalized 2D-LFCs to an additional dimension to allow variations in satellite argument of perigee for eccentric orbits while preserving the uniformity of the resulting constellations. Work has also been conducted to map Keplerian 2D-LFCs into initial osculating states resilient to orbital perturbations and that preserve quasi-periodicity. Casanova et al. [80] proposed modifying the osculating semi-major axis values to preserve identical rates of change for secular perturbations. Arnas [81] proposed a methodology to define orbits and satellite constellations in a set of relative trajectories that were closed under the effects of periodic orbital perturbations such as the Earth's gravitational potential. Later, Arnas and Casanova [82] extended this result to obtain a set of invariants in the satellite distribution that were preserved under these periodic perturbations.

Arnas et al. introduced the time distribution constellation formulation and described how to convert a 2D-LFC defined in terms of RAAN and either mean or true anomaly to a time distribution constellation defined relative to a seed trajectory using ground-track angle and time offsets [83]. Because orbits can evolve under an arbitrary propagation model in the time dimension, this allows the perturbations to be internalized to the constellation design and then allows osculating values of an arbitrary satellite to be found by reference to an initial seed satellite trajectory. However, the time distribution constellation formulation does not inherently assure stability of the resulting structure, requiring methods such as those by Arnas and Casanova [82] that analytically or numerically preserve periodicity in the presence of perturbations.

Work on lattice flower constellations has been extended to include non-uniform distributions. In work by Arnas et al. [84], [85], Necklace FCs, which describe subsets of admissible locations within a 2D-LFC, were introduced, with applications for satellite reconfiguration. Arnas and Linares [24] leveraged 2D-LFCs and Necklace FCs to derive a general theory of

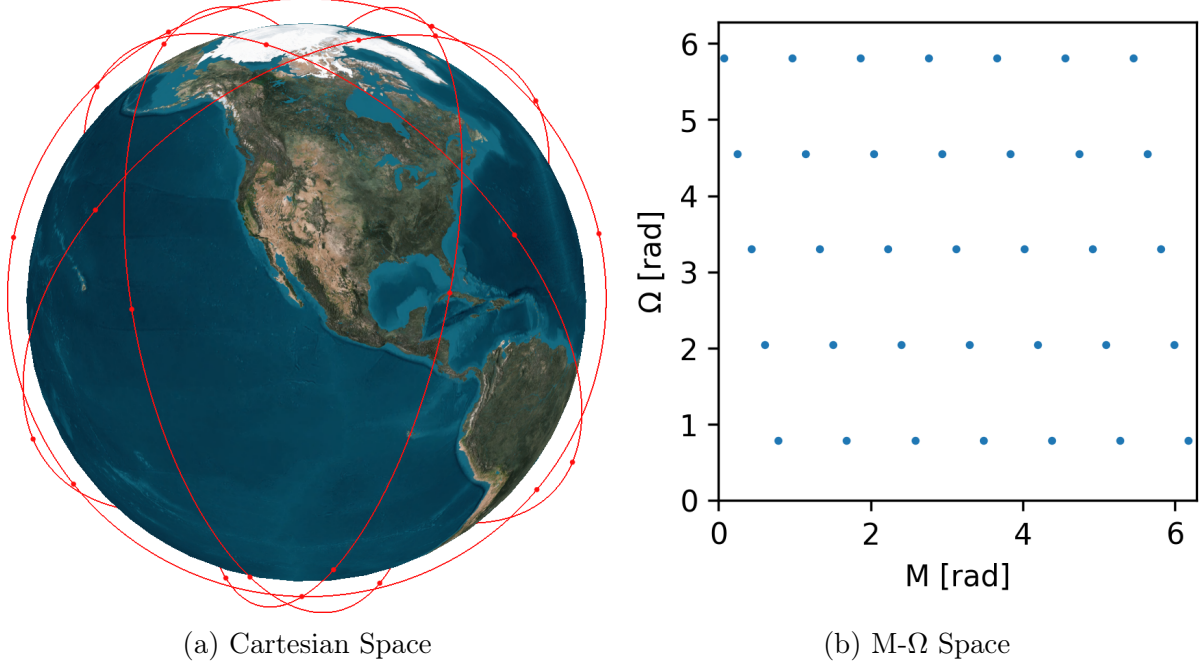


Figure 2.1: 2D-LFC with $N_o = 5$, $N_{so} = 7$, $N_c = 1$, and $a = 7000$ km, $i = 70^\circ$.

constellation reconfiguration with multiple methods for reconfiguration subject to different constraints.

Avendaño et al. [22] introduced an efficient implementation of an algorithm for computing the minimum separation distance between satellites in a Keplerian 2D-LFC and used this to compute empirical capacity and minimum separation distance relationships as a function of inclination to which trend lines were fit. According to Avendaño's formula, the minimum distance between any pair of satellites in circular Keplerian orbits can be obtained by using the following expression:

$$\rho_{\min} = \frac{1}{2} \left| A + D + \sqrt{(A - D)^2 + (B + C)^2} \right| \quad (2.2)$$

where:

$$A = \cos(\Delta\Omega) \cos(\Delta M) - \sin(\Delta\Omega) \cos(i_2) \sin(\Delta M)$$

$$B = -\cos(\Delta\Omega) \sin(\Delta M) - \sin(\Delta\Omega) \cos(i_2) \cos(\Delta M)$$

$$C = \cos(i_1) \sin(\Delta\Omega) \cos(\Delta M) + \cos(i_1) \cos(i_2) \cos(\Delta\Omega) \sin(\Delta M) + \sin(i_1) \sin(i_2) \sin(\Delta M)$$

$$D = -\cos(i_1) \sin(\Delta\Omega) \sin(\Delta M) + \cos(i_1) \cos(i_2) \cos(\Delta\Omega) \cos(\Delta M) + \sin(i_1) \sin(i_2) \cos(\Delta M)$$

and i_1 and i_2 are the inclinations of the two satellites. When combined with the inherent symmetry within an FC, the minimum distance calculations for a circular Keplerian 2D-LFC can be reduced from taking exponential time to linear time.

Arnas and Linares [23] use a special subset of 2D-LFCs with non-self intersecting (NSI) trajectories to derive an analytical bound for satellite capacity given a minimum separation distance between slots. These constellations represent a reasonable lower bound on capacity for the highest-capacity subset of constellations.

2.3 Orbital Slotting

The ITU acts as a de facto slotting authority for GEO based on the allocation of spectrum for satellite communications [13]. The process for gaining access to GEO slots is the subject of perennial international discussions and ongoing contention between established and emerging space nations for access to a finite number of useful GEO slots and the associated spectrum [25, Ch. 3]. No similar international physical slotting mechanism exists for non-GEO satellites, nor to the author’s knowledge has any state insisted on mutually deconflicted satellite slotting as a condition for licensure. There are several reasons for this. First, until now orbital densities were insufficient to motivate concerns about cross-constellation, active-on-active satellite conjunction risk as a major design driver. Instead, debris-on-debris and active-on-debris conjunctions dominate active-on-active conjunction risk [86]. Second, such deconfliction is significantly more complicated in LEO than in GEO due to the need to handle concentric constellations and intersecting orbital planes. Techniques for deconfliction in a generalized, constellation-agnostic way did not exist. Third, to the extent operators have tried to deconflict orbits, it has been handled on an ad hoc basis and largely outside of the public record.

Prior work has proposed LEO slotting in a context limited to Sun-synchronous orbits and has been technically focused. Such a coordination scheme was first proposed in Marshall et al. [87] for Sun-synchronous orbits and further developed by Weeden and Shortt [88] and Bilimoria and Krieger [89] and Master’s theses by Watson and Noyes [90], [91]. As seen in Figure 2.2, these orbits involve significant crowding and conjunctions near the poles, motivating potential orbit coordination.

Arnas et al. [21] proposed the use of 2D-LFCs to define nominal satellite positions or “slots” at nested altitudes that prevent overlaps between constellations. There are several benefits to this approach. First, slots can be used to coordinate in-shell satellite locations and provide robust assurances about non-conjunction between slotted spacecraft. Second, a slotting framework allows for the identification of alternative slotting arrangements and thus quantification of the relative efficiency of a design.

While not explicitly discussed in the context of slotting, Reiland et al. [68] and Bombardelli et al. [92] proposed the use of numerically frozen orbits to constrain satellite locations within a shell and limit the maximum radial displacement of a constellation as a function of latitude. These techniques are useful to optimize satellite trajectories but have limits for constellations with many orbital planes and lack the analytical benefits of an FC-based theoretical framework.

2.4 Literature Review Summary

Multiple techniques exist based on different simplifying assumptions and objectives. However, the connection between intrinsic and risk-based capacity is poorly understood and not well recognized.

A gap also exists in the literature concerning orbit coordination techniques that can generalize across LEO orbits. Previous work has been technically focused, to the exclusion of important non-technical dimensions of the problem. Past efforts have also been nar-

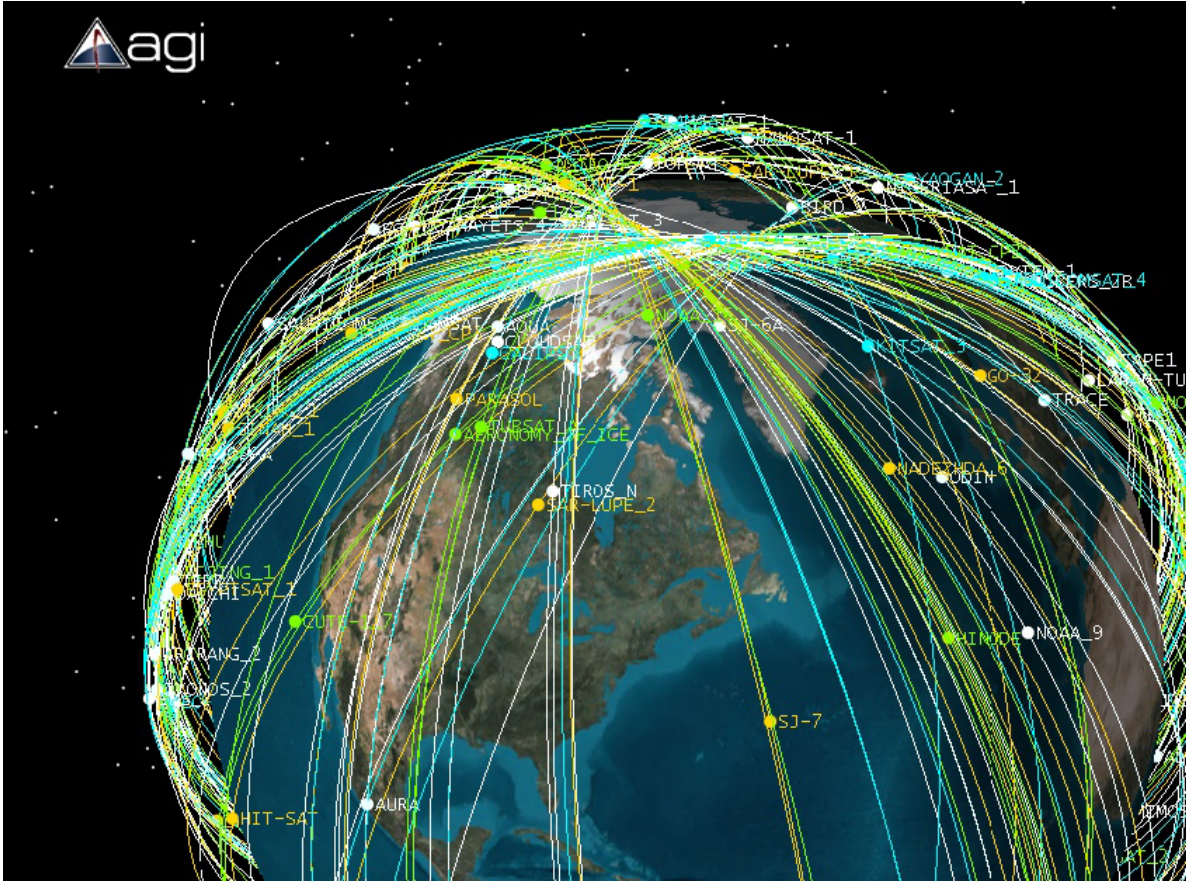


Figure 2.2: Sun-synchronous satellite orbit crossing at the North Pole, reproduced from Weeden and Shortt [88] with permission.

rowly focused on orbit coordination for non-inference rather than developing a generalizable framework to understand and improve orbital use. Existing shell-stacking techniques have technical limitations and lack analysis to identify and quantify design features that improve density. FC theory offers a promising tool to help address orbit coordination in a more generalizable way. Specifically, it provides a robust theoretical framework for LEO slotting, including helpful guarantees for enumeration of unique possibilities, efficient mechanisms for Keplerian minimum separation distance calculation, non-conjunction verification, and shell capacity estimation.

Simplicity is an important design criterion, as the benefits from orbit coordination have strong network effects and a more complicated theory is harder to adopt. Because the overwhelming majority of proposed large constellations use uniform circular or near-circular orbits, 2D-LFC theory represents an appropriate theoretical framework which is as simple as possible, but no simpler (to paraphrase Einstein). More elaborate orbit design schemes are possible, for instance, using three-dimensional lattice flower constellation (3D-LFC) theory to design elliptical constellations or four-dimensional lattice flower constellation (4D-LFC) theory to enforce compatibility across shells. However, these techniques are not strictly necessary to address the slotting problem, and they can invite additional complexity that risks undermining broad use. Generalized compatibility between elliptical shell-crossing orbits

and large constellations would be restrictive for orbit designs and would be better handled through ad hoc collision avoidance at current and expected levels of elliptical traffic. In some cases, more complicated design strategies can be represented as sets of 2D-LFCs, allowing for sophisticated designs for individual shells without requiring additional complexity for the overall orbit coordination scheme. For example, the use of 4D-LFC theory to design a set of compatible 2D-LFC shells (e.g., as part of a single multi-shell constellation) would not preclude consideration of those shells by an orbit coordination approach rooted in simpler 2D-LFC theory.

Chapter 3

A Method for Generating Closely Packed Orbital Shells and Implications for Orbital Capacity

This chapter contains content from Lifson et al. presented at the AIAA SciTech Forum 2023 [93] and that has been submitted for journal consideration. The chapter reorganizes this content for enhanced clarity.

3.1 Introduction

Satellite constellations with more than 100,000 satellites have been proposed for LEO. This order-of-magnitude increase—from thousands of satellites to tens of thousands or more—will necessitate numerous technical, operational, and policy changes to ensure the long-term sustainability of the space environment in the face of denser operations. Recent studies by Henning et al. [19] and Letizia et al. [18] have shown that many plausible future large constellation scenarios are not compatible with the long-term sustainable evolution of the space environment.

Figures 3.1 and 3.2 display the nominal altitudes for selected proposed LEO constellations. Constellations were chosen subjectively at the time of original analysis using multiple factors including publicly announced funding, launches to date, and the reputation of the parent entity. Constellations proposed using nanosatellites and microsatellites without propulsion were also excluded.

Worryingly, multiple large constellations have been proposed with limited orbital separation or overlapping nominal semi-major axes.¹ Large constellations with overlapping orbital

¹Because operator FCC filings claim large nominal orbital tolerances (± 10 km or even ± 30 km) to account for both operations and maneuvers, and because these filings frequently do not distinguish between mean and osculating semi-major axis or describe intended eccentricity vector maintenance information, it can be hard to understand actual intended nominal orbital variation for constellations based on FCC filings. Maintaining orbital shell separation accounting for the full range of orbital tolerances claimed by operators in FCC filings would be wasteful and prohibitively restrictive on orbital use. Even separation based simply on maximum and minimum osculating variation in semi-major axis would place significant limits on current and future capacity.

altitude have the potential to significantly increase both orbital conjunction risk and the operational burden associated with planning and coordinating collision-avoidance maneuvers for active spacecraft controlled by different operators. For this reason, best-practice compilations by organizations including the Space Safety Coalition² and the American Institute of Aeronautics and Astronautics³ have stressed the importance of altitude separation between large constellations. As seen in Figures 3.1⁴ and 3.2, and based on data from the ITU, FCC, and Jonathan’s Space Pages⁵, overlapping or closely spaced cross-operator shell pairs include:

- Galaxy Space (Yinhe), Hanwha Systems, and E-Space at 500 km;
- Galaxy Space (BLACKSPIDER) and SpaceX at 525 km;
- Changchun Institute of Optics, Fine Mechanics and Physics (CIOMP) Jilin, and SpaceX Starlink at 540 km;
- China SatNet and Amazon Kuiper (both at 590 km) and Galaxy Space (BLACKSPIDER) at 595 km;
- China SatNet, Globalstar, and E-Space at 600 km;
- SpaceX Starlink at 604 km and 614 km and Amazon Kuiper at 610 km;
- Inmarsat⁶ at 724 km and AST SpaceMobile at 727.5 km, both of which intend to operate small equatorial shells that could potentially be combined into a single equatorial shell;
- Rivada at 1050 km and Boeing at 1056 km⁷; and
- China SatNet at 1145 km and Hughes at 1150 km.

This thesis proposes a potential solution to impose safe segregation between orbital shells while improving the number of constellations that can be admitted in a region of space by relying on the use of frozen orbits and taking advantage of the approximate latitude-based altitude dependency that these shells exhibit. This effect has been previously noted in the literature. For example, Lara and Russell [94] described an automated way to design periodic orbits in the presence of a geopotential, with such orbits being almost circular except near the critical inclination. Bombardelli et al. [92] suggested using frozen orbits and specifically optimizing for minimum radial distance variation as a function of latitude in order to avoid cross-shell collision risk. Bombardelli et al. computed these orbits numerically

²<https://spacesafety.org/best-practices/>, accessed 2 June 2023.

³<https://www.ascend.events/outcomes/satellite-orbital-safety-best-practices-by-iridium-oneweb-space-x-aiaa/>, accessed 2 June 2023.

⁴E-Space’s shells would distort the scale of this graph and have been truncated.

⁵<https://www.planet4589.org/space/>, accessed 28 November 2022.

⁶The future of Inmarsat’s proposal is unclear, following its acquisition by Viasat, which withdrew a V-band application for the system.

⁷Boeing’s proposal was withdrawn in late 2023.

in the presence of zonal and tesseral harmonics, lunisolar third-body perturbations, solar radiation pressure, and atmospheric drag. The same frozen orbit technique was used to define satellite locations within a single shell in Reiland et al. [68] and shown to reduce intra-shell conjunction frequency.

While Bombardelli et al. proposed nesting sequential orbital planes in altitude to prevent conjunction, this work presents an alternative formulation that instead incorporates only the effects of the Earth’s geopotential, relying on station-keeping to reject other perturbations. In Lavezzi et al. [95], it is shown that reasonable station-keeping with electric propulsion, used by most large LEO constellations (LLCs), can maintain tight orbits at reasonable cost in the presence of these perturbations. Multiple orbital planes of a particular constellation shell can then be placed in an overlapping orbital volume while maintaining compatible phasing. This may lead to greater efficiency for constellation designs featuring large numbers of orbital planes with a limited number of satellites per plane⁸. Slots generated using these methods are agnostic to spacecraft physical parameters, enhancing flexibility within potential orbit coordination architectures.

A 2D-LFC-based formulation also connects the generated shells to previous theoretical results on 2D-LFCs [76] that allow estimation of intrinsic (or geometric) orbital capacity, reconfiguration, and optimization for minimum separation distances [21]–[24]. Previous work on orbital slotting using 2D-LFCs assumed Keplerian orbits, significantly limiting the fidelity with which analysis of separation between concentric shells could be carried out [21]. In this work, slotting is demonstrated using 2D-LFCs defined to include the effects of higher order and degree terms of the Earth’s gravity field. Specifically, two numerical orbit freezing methods are demonstrated to define 2D-LFCs that preserve quasi-periodicity in the presence of the Earth’s geopotential. These methods draw on previously published approaches for generating perturbed FCs [80]–[83]. Particularly, Arnas [81] proposed a methodology to define orbits and satellite constellations in a set of relative trajectories that were closed under the effects of periodic orbital perturbations such as the Earth’s gravitational potential. Later, Arnas and Casanova [82] extended this result to obtain a set of invariants in the satellite distribution that were preserved under these periodic perturbations. Finally, Arnas et al. [83] described the time distribution constellation formulation and how to convert a 2D-LFC defined in terms of RAAN and either mean or true anomaly to a time distribution constellation defined relative to a seed trajectory using a ground-track angle and time offset [96].

A key motivation of this chapter is understanding how choices for constellation shell design and placement influence the set of constellations that may be admitted to a particular orbital volume while preserving mutual non-conjunction indefinitely. This form of orbital capacity, coined as intrinsic capacity [78], [97] and related to the notion of “seat capacity” in other fields [98], is distinct from the definition of orbital capacity advanced by Krag, Letizia, Lemmens, and their co-authors [42]–[44], which is concerned with the long-term evolution of the space environment. Both concepts are important and may limit orbital use under differing circumstances. Work by D’Ambrosio, myself, and co-authors [99]–[101] has sought

⁸For instance, see Amazon Kuiper’s latest constellation design, https://licensing.fcc.gov/cgi-bin/ws.exe/prod/ib/forms/reports/swr031b.hts?q_set=V_SITE_ANTENNA_FREQ.file_numberC/File+Number/%3D/SATMOD2023022800043&prepare=&column=V_SITE_ANTENNA_FREQ.file_numberC/File+Number, accessed 15 October 2023, which features 289, 1292, and 782 orbital planes in its three shells.

to integrate consideration of both kinds of capacity constraints.

This work makes several new contributions. First, it develops methods for designing compatible sets of 2D-LFC shells that minimize latitude-dependent altitude variation while maintaining self-safe shell structure. This contribution includes the first large-scale demonstration of these techniques to such configurations under arbitrary geopotentials [82]. These methods are applied to mitigate proposed adjacent and overlapping constellation shells in LEO. Second, this work proposes that, for maximum orbital density, shells should be designed to be quasi-periodic and structured to nest radius-latitude curves (generally through sequential or at least similar inclinations among adjacent shells) and quantifies the benefits associated with efficient shell-nesting techniques. Third, it assesses performance of several simplified models of shell shape and determines that inclusion of J_2 short-period effects in these models is necessary for reasonable fidelity in analyzing the geometry of shell nesting.

This chapter is organized into the following sections. In Section 3.2, several necessary concepts are briefly summarized. In Section 3.3, two techniques are described to define osculating 2D-LFCs. The first technique accounts for only zonal terms in the Earth’s geopotential. An example is then presented comparing the in-shell minimum separation distance for a Keplerian 2D-LFC and its osculating analog. The second technique is then introduced, which accommodates zonal, sectoral, and tesseral effects through the use of RGT orbits. Next, an example is presented using this method for nearby shells in high LEO. In Section 3.4, a simplified method for estimating shell centerline geometry in the latitude-altitude plane is presented and demonstrated. The goal of this method is to provide insight on shell geometry by means of a simple analytical tool that does not require numerical propagation. In Section 3.5, a simplified method for estimating the width of a particular orbital shell from its orbital centerline is presented and then applied. Shell width, in combination with an additional chosen safety offset between shells, allows higher-fidelity estimation for density of orbital use than other approaches using fixed separation between shell centerline geometry. In Section 3.6, plotting in the latitude-altitude plane is used to demonstrate several conceptual results associated with the analysis in this chapter. This includes how relative inclination is a driving factor when designing consecutive shells in altitude, and how the use of frozen orbits allows shells to be stacked closer than the osculating variation in semi-major axis for a constellation. Finally, the chapter’s content and significance are summarized in Section 3.7.

3.2 Preliminaries

This section summarizes several concepts that are used in this chapter: 2D-LFCs, non-spherical Earth effects, classical orbit freezing analysis, the equinoctial element set, and various orbital perturbations relevant for LEO satellites. Additionally, it provides a graphic overview of how the different techniques can be used to perform shell design and analysis.

2D-LFCs are used to define and map between Keplerian and equivalent quasi-periodic osculating constellations. Classical and numerical orbit freezing techniques are used to define quasi-periodic orbits for these 2D-LFCs under perturbations. Equinoctial elements are used to avoid numerical issues associated with argument of perigee for near-circular orbits. When assessing the behavior of modeled orbits under high-fidelity numerical propagation, various

additional effects beyond the Earth’s geopotential are included. Several details regarding model assumptions are presented for reproducibility purposes and to clarify the intention associated with selected values or assumptions.

3.2.1 2D-LFCs

2D-LFCs [76] are a special type of FC that can represent all possible uniform distributions of satellites sharing values for same semi-major axis a , inclination i , eccentricity e , and argument of perigee ω [77]. In a 2D-LFC, admissible satellite slot locations are defined in terms of the relative RAAN ($\Delta\Omega_{ij}$) and mean anomaly (ΔM_{ij}) distribution of slots based on three integer values: the number of orbital planes (N_o), the number of satellites per orbit (N_{so}), and the configuration number (N_c), which acts as a phasing parameter between orbital planes according to the following equation:

$$\begin{bmatrix} N_o & 0 \\ N_c & N_{so} \end{bmatrix} \begin{Bmatrix} \Delta\Omega_{ij} \\ \Delta M_{ij} \end{Bmatrix} = 2\pi \begin{Bmatrix} i - 1 \\ j - 1 \end{Bmatrix} \quad (3.1)$$

where $i \in [1, \dots, N_o]$ and $j \in [1, \dots, N_{so}]$ name the j -th satellite on the i -th orbital plane of the constellation. The configuration number is defined in the range $N_c \in [0, N_o - 1]$ to avoid redundant configurations. The periodicity of 2D-LFCs provides useful assurances for collision avoidance and shell capacity evaluation [21].

3.2.2 Non-Spherical Earth Effects

The Earth’s geopotential is aspherical rather than perfectly uniform. These differences can be modeled using an infinite set of spherical harmonics:

$$U = \frac{\mu_{\oplus}}{r} \left[1 + \sum_{l=2}^{\infty} \sum_{m=0}^l \left(\frac{R_{\oplus}}{r} \right)^l P_{l,m}[\sin(\phi_{gc_{sat}})] \{C_{l,m} \cos(m\lambda_{sat}) + S_{l,m} \sin(m\lambda_{sat})\} \right] \quad (3.2)$$

where μ_{\oplus} is the standard gravitational parameter of the Earth, R_{\oplus} is the Earth’s equatorial radius, l is the degree of the geopotential, m is the order of the geopotential, $P_{l,m}$ is the associated Legendre polynomial of degree l and order m , $\phi_{gc_{sat}}$ is the geocentric latitude of the satellite, λ_{sat} is the geocentric longitude, and $C_{l,m}$ and $S_{l,m}$ are empirical constants provided by the chosen gravity field model. In practice, these are truncated based on the required fidelity in orbit propagation [102, Ch. 8.6]. In this chapter, the geopotential used to propagate a model is sometimes short-handed as J_l where all zonal and tesseral terms up to degree l are included. J_l refers to either a specific zonal harmonic constant, $J_l = -C_{l,0}$, or a zonal-only model including all zonal terms up to degree l , depending on context. Taking the gradient of Equation (3.2) provides us with perturbing accelerations, which may then be numerically integrated using Cowell’s formulation [102, p. 592]:

$$a_{non\text{spherical}} = \nabla \left(U - \frac{\mu_{\oplus}}{r} \right) \quad (3.3)$$

The Orekit space dynamics library is used to perform much of the numerical propagations in this chapter⁹. In Orekit, central body gravity forces are implemented based on the approach by Holmes and Featherstone [103].

⁹<https://www.orekit.org/>, accessed 2 June 2023.

3.2.3 Classical Orbit Freezing

Classical frozen orbit theory analysis considers only the J_2 and J_3 terms in the Earth's potential and seeks to find solutions to the Lagrange planetary equations that set the change to mean eccentricity, $\frac{d\bar{e}}{dt}$, and mean argument of perigee, $\frac{d\bar{\omega}}{dt}$, to zero [102] in Equations (3.4) and (3.5).

$$\frac{d\bar{e}}{dt} = -\frac{3}{2} \frac{\bar{n}}{(1-\bar{e}^2)^2} J_3 \left(\frac{R_\oplus}{\bar{a}} \right)^3 \sin \bar{i} \left(1 - \frac{5}{4} \sin^2 \bar{i} \right) \cos \bar{\omega} = 0 \quad (3.4)$$

In Equation (3.4), \bar{a} , \bar{e} , \bar{i} , $\bar{\omega}$, and \bar{n} are the mean values of the semi-major axis, eccentricity, inclination, argument of perigee, and mean motion, respectively.

$$\frac{d\bar{\omega}}{dt} = \frac{3\bar{n}}{(1-\bar{e}^2)^2} J_2 \left(\frac{R_\oplus}{\bar{a}} \right)^2 \left(1 - \frac{5}{4} \sin^2 \bar{i} \right) \left[1 + \frac{J_3}{2J_2} \left(\frac{R_\oplus}{\bar{a}} \right) \frac{1}{(1-\bar{e}^2)} \left(\frac{\sin^2 \bar{i} - \bar{e}^2 \cos^2 \bar{i}}{\sin \bar{i}} \right) \frac{\sin \bar{\omega}}{\bar{e}} \right] = 0 \quad (3.5)$$

Equation (3.5) is satisfied for $\bar{\omega} = \frac{\pi}{2}$ or $\bar{\omega} = \frac{3\pi}{2}$ radians (or at the critical inclination), meaning there will be no secular drift in mean argument of perigee. Equation (3.4) implies there will be no secular shift in mean eccentricity for an orbit with these values of $\bar{\omega}$ when:

$$\bar{e} = -\frac{1}{2} \frac{J_3}{J_2} \left(\frac{R_\oplus}{\bar{a}} \right) \left(\frac{1}{1-\bar{e}^2} \right) \left(\frac{\sin^2 \bar{i} - \bar{e} \cos^2 \bar{i}}{\sin \bar{i}} \right) \approx -\frac{1}{2} \frac{J_3}{J_2} \left(\frac{R_\oplus}{\bar{a}} \right) \sin \bar{i} \quad (3.6)$$

3.2.4 Equinoctial Elements

Equinoctial elements are a convenient way to represent near-circular and near-equatorial orbits, where some Keplerian elements suffer from ambiguity [104]. Given a set of Keplerian elements corresponding to a non-circular, non-equatorial orbit $(a, e, i, \omega, \Omega, \theta)$, equinoctial elements can be expressed as (following the naming conventions of the Orekit space dynamics library¹⁰):

$$a = a \quad (3.7a)$$

$$e_x = e \cos(\omega + \Omega) \quad (3.7b)$$

$$e_y = e \sin(\omega + \Omega) \quad (3.7c)$$

$$h_x = \tan\left(\frac{i}{2}\right) \cos(\Omega) \quad (3.7d)$$

$$h_y = \tan\left(\frac{i}{2}\right) \sin(\Omega) \quad (3.7e)$$

$$l_\theta = \theta + \omega + \Omega \quad (3.7f)$$

3.2.5 Other Perturbations

This section briefly describes the modeling of other relevant orbital perturbations. Where described in detail in the Orekit documentation, this description matches their conventions.

¹⁰<https://www.orekit.org/>, accessed 2 June 2023.

Where less information is provided, these descriptions follow Vallado [102]. In the full force model in this work, atmospheric drag is assumed to be isotropic and modeled as:

$$\vec{a}_{drag} = -\frac{1}{2}\rho v^2 \frac{S}{m} \vec{D} \quad (3.8)$$

where ρ is the atmospheric density provided by the chosen atmospheric model, v is the relative velocity between the spacecraft and the atmosphere, m is the mass of the spacecraft, S is the product of the drag coefficient and cross-sectional area, and \vec{D} is the drag coefficient vector. The value of ρ is computed using DTM2000 [105], a semi-empirical atmospheric model that depends on solar flux and geomagnetic data as well as atmospheric location and time. For this chapter, solar and geomagnetic data was sourced from Celestrak¹¹. Third body accelerations are modeled according to:

$$\vec{a}_{3rd} = -\frac{\mu_{\oplus} \vec{r}_{\oplus sat}}{r_{\oplus sat}^3} + \mu_3 \left(\frac{\vec{r}_{sat3}}{r_{sat3}^3} - \frac{\vec{r}_{\oplus 3}}{r_{\oplus 3}^3} \right) \quad (3.9)$$

where μ_{\oplus} is the Earth's gravitational constant, μ_3 is the gravitational constant of the third body, $\vec{r}_{\oplus sat}$ is a vector from the Earth to the satellite, \vec{r}_{sat3} is a vector from the satellite to the third body, and $\vec{r}_{\oplus 3}$ is a vector from the Earth to the third body [102, p. 574]. Lunar, Earth, and solar positions are derived from Jet Propulsion Laboratory's DE440 ephemerides.

Solar radiation pressure is modeled assuming a constant exposed area and coefficient of reflectivity using:

$$\vec{a}_{srp} = -\frac{p_{srp} c_R A_{\odot}}{m} \frac{\vec{r}_{sat\odot}}{\|\vec{r}_{sat\odot}\|} \quad (3.10)$$

where p_{srp} is the force of solar pressure per unit area, c_R is the coefficient of reflectivity of the spacecraft, A_{\odot} is the sun-exposed area of the spacecraft, and $\vec{r}_{sat\odot}$ is a vector from the satellite to the sun [102, p. 581].

Solid tides are modeled, including pole tides and third-body effects from the Sun and Moon. Following Orekit defaults, 12 points are used for tides field interpolation, with a time-step of 600 seconds. Because the equations are lengthy and the effect is small, these equations are not reproduced here.

3.2.6 Other Modeling Assumptions

In later examples in this chapter where the constellation is not specified, a 2D-LFC with parameters $N_o = 5$, $N_{so} = 5$, $N_c = 2$ is used with the indicated mean inclination and altitude. When satellites or slots are said to be propagated under a full force model, this includes a 21 by 21 geopotential using the EIGEN-6S gravity field model, solar radiation pressure (isotropic radiation, $c_r = 1$, $a_{srp} = 28$ m), atmospheric drag ($c_d = 2.2$, $a_{drag} = 15$ m, DTM2000 model using COMSPOC Corporation Center for Space Standards & Innovation space weather data), solar and lunar Earth solid tides, and lunar and solar third-body attraction (based on DE440 ephemerides [106]). All starting epochs are assumed to be January 1, 2022, 0:00:00.000 UTC.

¹¹<https://celestrak.com/SpaceData/>, accessed 2 July 2021.

Two larger examples are later demonstrated, drawing on proposed constellations from Amazon, SpaceX, Hughes, and China SatNet. These examples are chosen somewhat arbitrarily from examples of large constellations proposed at nearby altitudes. No statement is intended or should be inferred from the selection of a specific constellation pair for inclusion in this section.

Shell widths and the separation distance necessary between shells depend on multiple factors, including the chosen 2D-LFC used to generate the shell, satellite locations relative to the nominal center of each slot, orbital state estimation and control accuracy, desired additional safety margin, satellite physical properties, and the frequency of orbital station-keeping desired for the constellation.

3.2.7 Overview of the Proposed Techniques and Their Potential Use

To provide a better overview of all the techniques presented in this chapter and to clearly show their applicability to different problems, Figure 3.3 presents a flowchart containing the summary of these techniques and how they should be used to design and analyze different aspects of the orbital shell problem. Each technique is associated with its related section in this chapter to improve traceability of the methodologies presented.

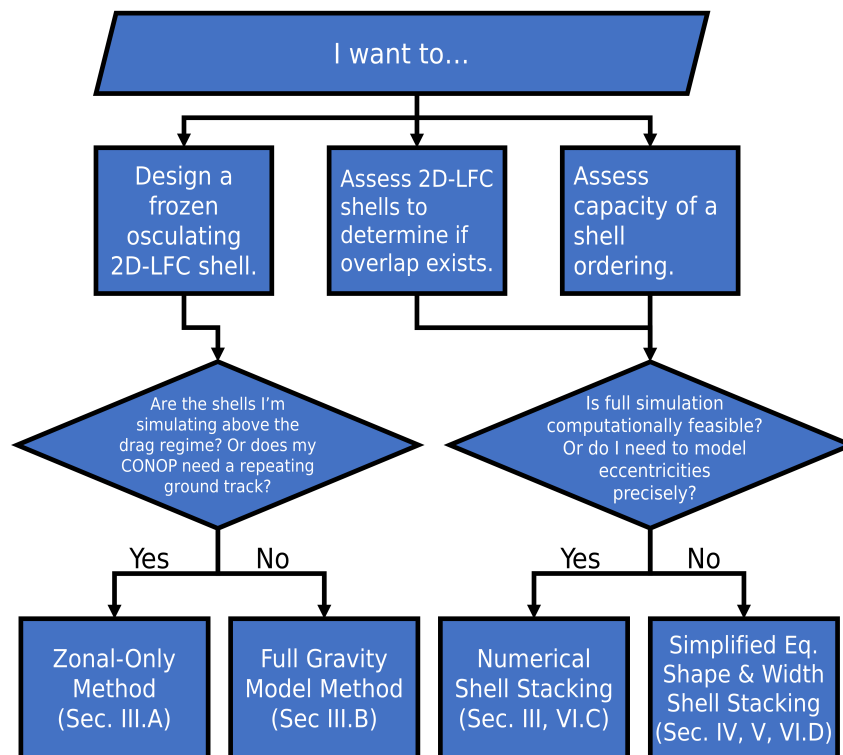
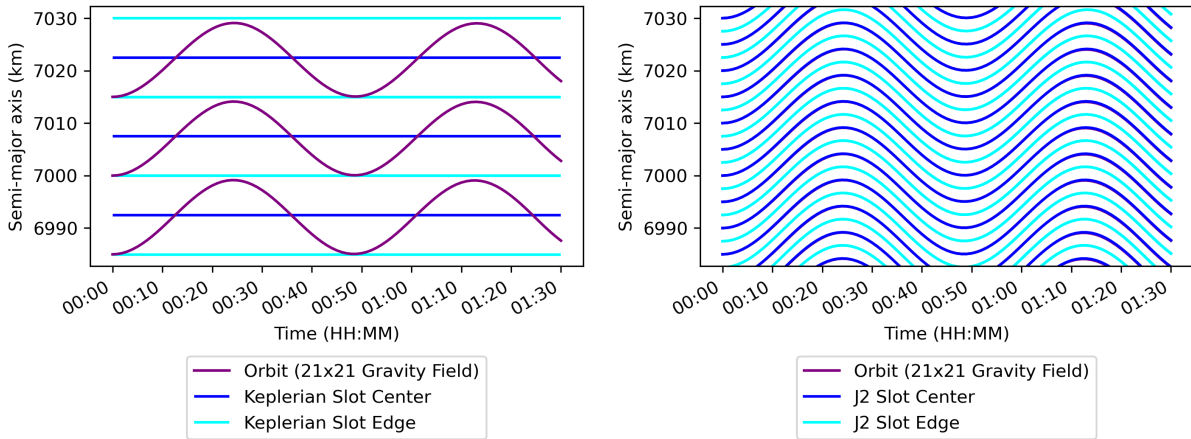


Figure 3.3: Flowchart for Applicability of the Introduced Techniques.

3.3 Definition of Osculating 2D-LFCs

This section describes two methods to define osculating 2D-LFCs. The first method to define osculating 2D-LFCs in the presence of the Earth’s geopotential assumes a zonal geopotential of arbitrary degree, while the second is applicable to a model with zonal, sectoral, and tesseral terms. While not a fundamental constraint of the underlying theory, the zonal-only technique is likely more relevant in lower regions of LEO, where atmospheric drag will necessitate frequent restoring maneuvers, while the second technique is potentially more interesting at higher altitudes, where longer-term stability may be desired.

In each, it is necessary to generate a numerically closed seed orbit, which is used to define slot locations using the time distribution constellation formulation [83]. As seen in Figure 3.4, the essential idea is that rather than defining orbital separation using fixed altitude bands, it is possible to define separation boundaries between shells accounting for the Earth’s geopotential and enabling close shell stacking without generating overlaps in the latitude and altitude between adjacent shells. In Figure 3.4b, J_2 shells are defined, but any geopotential could be used. Note that the J_2 shell height is chosen for illustration and is not a recommendation or fundamental size limit.



(a) 15 km Keplerian Slots ($i = 60^\circ$). (b) 5 km Geopotential-Aware Slots ($i = 60^\circ$).

Figure 3.4: Comparison of Sequential Constellation Shell Spacing Strategies.

Periodicity is a necessary condition to define a 2D-LFC. In the zonal-only method, periodicity is obtained over a single orbit through use of a genetic algorithm (GA) to find starting eccentricity conditions that minimize differences in the radial distance over the equator and shifts to the eccentricity vector. In the zonal, sectoral, and tesseral method, periodicity is obtained over an RGT cycle for the orbit using the method developed by Arnas and Casanova [82].

3.3.1 Definition of Osculating 2D-LFCs under a Zonal Geopotential

In this subsection, a 2D-LFC is mapped onto a zonal Earth geopotential of arbitrary degree. The approach exploits the fact that the gravity field is assumed to be invariant with latitude,

and thus periodicity only requires radial closure and a frozen eccentricity vector. This process has two steps. First, it is necessary to find a seed trajectory closed and frozen under the chosen zonal geopotential, $X_{0,0}$. Second, the 2D-LFC's RAAN and mean anomaly values can be mapped to ground-track offset angles, $\Delta\Gamma_{i,j}$, and propagation times, $\Delta t_{i,j}$, relative to $X_{0,0}$.

Each frozen seed trajectory is found using a GA (in this case, the differential evolution method within the SciPy library implementing work by Storn and Price [107]) with an objective function that seeks to preserve periodicity in the orbital radius and eccentricity vector over a single orbital period, which can be seen in Equation (3.11).¹² States are represented as initial osculating equinoctial orbits composed of a , e_x , e_y , h_x , h_y , and true longitude, l_θ , with the algorithm free to change e_x and e_y within generous bounds $[lb_e, ub_e] = [-0.02, 0.02]$.

$$\begin{aligned} \min \quad & \sqrt{\left(k_1|\vec{E}_f - \vec{E}_0|\right)^2 + \left(k_2(|r_f - r_0| + |r_f - r_m|)\right)^2} \\ \text{s.t.} \quad & e_x, e_y \in [lb_e, ub_e] \\ & \dot{\mathbf{X}} = f(\mathbf{X}(t)) \end{aligned} \tag{3.11}$$

where $\dot{\mathbf{X}} = \mathbf{f}(t, \mathbf{X})$ is the dynamics in the orbital element space, $k_1 = \frac{1}{ub_e}$, and $k_2 = \frac{1}{500} \frac{1}{2} \frac{1}{a}$. The coefficients k_1 and k_2 calibrate the relative importance of minimizing changes in the eccentricity vector and equatorial orbital radius over the orbital period. For a given conservative disturbing function, in this case $R = U - \mu_\oplus/r$, the Lagrange planetary equations [102, p. 628] can be expressed in a non-singular form as:

$$\begin{aligned} \frac{da}{dt} &= \frac{2}{na} \frac{\partial R}{\partial l_\theta} \\ \frac{de_y}{dt} &= \frac{B}{na^2} \frac{\partial R}{\partial e_x} - \frac{e_y B}{na^2(1+B)} \frac{\partial R}{\partial l_\theta} + \frac{e_x C}{2na^2 B} \left\{ h_y \frac{\partial R}{\partial h_y} + h_x \frac{\partial R}{\partial h_x} \right\} \\ \frac{de_x}{dt} &= -\frac{B}{na^2} \frac{\partial R}{\partial e_y} - \frac{e_x B}{na^2(1+B)} \frac{\partial R}{\partial l_\theta} - \frac{e_y C}{2na^2 B} \left\{ h_y \frac{\partial R}{\partial h_y} + h_x \frac{\partial R}{\partial h_x} \right\} \\ \frac{dh_y}{dt} &= -\frac{h_y C}{2na^2 B} \left\{ e_x \frac{\partial R}{\partial e_y} - e_y \frac{\partial R}{\partial e_x} + \frac{\partial R}{\partial l_\theta} \right\} + \frac{fC^2}{4na^2} \frac{\partial R}{\partial h_x} \\ \frac{dh_x}{dt} &= -\frac{h_x C}{2na^2 B} \left\{ e_x \frac{\partial R}{\partial e_y} - e_y \frac{\partial R}{\partial e_x} + \frac{\partial R}{\partial l_\theta} \right\} + \frac{fC^2}{4na^2} \frac{\partial R}{\partial h_y} \\ \frac{dl_\theta}{dt} &= n - \frac{2}{na} \frac{\partial R}{\partial a} + \frac{B}{na^2(1+B)} \left\{ e_y \frac{\partial R}{\partial e_y} + e_x \frac{\partial R}{\partial e_x} \right\} + \frac{C}{2na^2 B} \left\{ h_y \frac{\partial R}{\partial h_y} + h_x \frac{\partial R}{\partial h_x} \right\} \end{aligned} \tag{3.12}$$

where:

$$\begin{aligned} B &= \sqrt{1 - e_y^2 - e_x^2} \\ C &= 1 + h_y^2 + h_x^2 \end{aligned} \tag{3.13}$$

Equation (3.11) seeks to minimize the ℓ_2 norm of the difference in the norm of the eccentricity vector (not to be confused with e_x and e_y) at the start and end of the orbit

¹²This approach was selected for simplicity and ease of implementation, although analytical solutions for frozen orbit eccentricity and argument of perigee exist for an arbitrary zonal geopotential model [108].

and the differences between the final equatorial orbital radius and the starting and half-orbit orbital radius. The values of k_1 and k_2 were chosen arbitrarily to yield good results in both high and low LEO by scaling the two components in a way that corresponds closely to minimizing overall orbital radius. If ub_e is changed significantly, k_1 can be adjusted to maintain rough comparability in the magnitude of the two terms. The $\frac{1}{2}$ factor in k_2 is left to emphasize that two radius norms are being considered: 1) the difference between the mid-orbit radial distance over the equator and final radius, and 2) the difference between the beginning and final radial distance over the equator. Numerical simulations determined that in both low and high LEO, shell width across several examples was insensitive to moderate changes in the ratio between k_1 and k_2 , but that extreme shifts (several orders of magnitude) could lead to thicker, less stable shells or extend the time for GA convergence. To generate an optional starting guess, the mean J_2 - J_3 frozen orbit elements are converted to osculating elements using the method from Kwok [109], as presented by Vallado [102], treating them as if they were produced with a J_2 -only theory. This is not strictly true but is sufficient for the purpose of generating an initial approximate guess. An arbitrary 2D-LFC is then defined in terms of Keplerian elements using Equation (3.1) to populate the Ω, M space.

Once a seed orbit is defined, a rotation about the Earth's axis of rotation can be conducted for the first satellites in each orbital plane of the 2D-LFC. Under a zonal geopotential, this rotation does not change energy levels or orbital period, and thus no adjustment to the rotated osculating state is needed. This simplifies the resulting time distribution constellation. The nodal period of the numerically closed seed orbit, T_z , can be found by propagating the seed orbit from one ascending equatorial crossing to the next (or another equivalent period). The propagation time $t_{i,j}$ to the initial location for the j -th satellite in the i -th orbital plane from the starting epoch and state of $X_{0,0}$ can be found by the proportionality between the fraction of orbital period under the zonal model and mean anomaly for the Keplerian 2D-LFC:

$$t = \frac{M_k}{2\pi} T_z \quad (3.14)$$

Example: Zonal-Only Approach, Low Altitude

This subsection demonstrates the zonal method for a set of nearby orbital shells. Both Amazon and SpaceX have proposed expansions to their LLCs. As part of SpaceX's Gen2 Configuration 1 Proposal, it requested permissions to operate shells at 604 and 614 km [110]. Amazon has received approval for a shell at 610 km that would be expanded to have twice as many satellites [111]. In February 2023, Amazon modified its proposed constellation [112]. This work was completed using the pre-modification Amazon constellation design. Overlaps between these shells are particularly concerning because Amazon's shells are prograde while these two SpaceX shells are retrograde, meaning any collisions would likely occur at an especially high relative velocity in a very dense region of LEO (see Figure 3.5). This subsection demonstrates how the zonal approach described in this chapter could be used to maintain minimum separation between these shells. This analysis relies only on regulatory filings rather than SpaceX's as-flown orbits. No claim is made as to whether implementing this method would be feasible given the concept of operations and spacecraft capabilities of either company. The initial states of the seed trajectories used for the examples included in

this chapter are summarized in Appendix A.

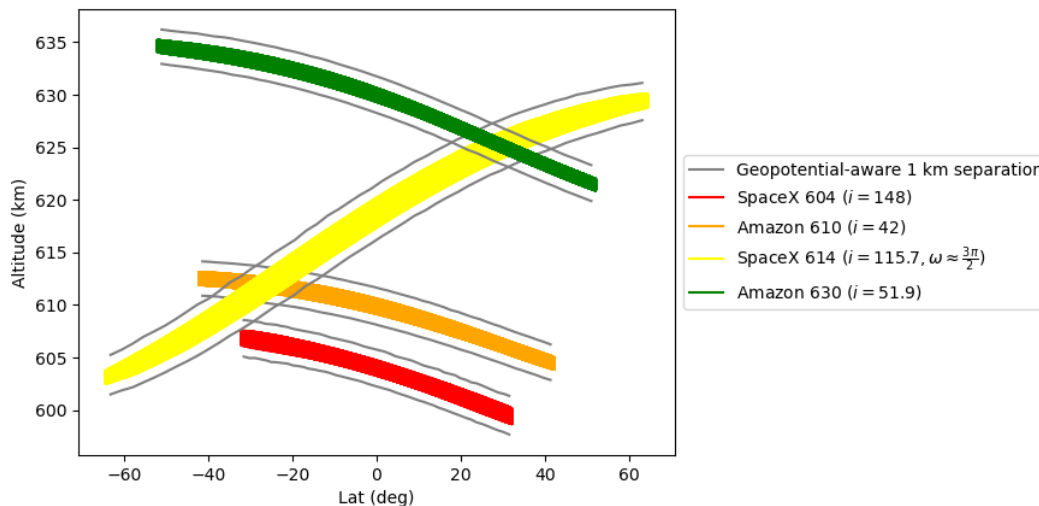


Figure 3.5: SpaceX and Amazon Shells (Unconstrained GA, 30-Day Propagation, Full Force Model). Uncoordinated eccentricity vectors lead to hazardous overlaps.

This example is a bit unusual because of the retrograde orbits proposed by SpaceX, one of which lies very near critical inclination, with consequences for frozen orbit stability. As discussed in Section 3.4.1, the direction of the slope of shells in the latitude-altitude space is dependent on the argument of perigee about which the curve is frozen. In this case, the GA prioritizes a frozen orbit for the SpaceX 614 km shell that slopes the opposite direction compared with the other two shells (associated with the frozen orbit nearer to $\omega = 3\pi/2$, for which the seed orbit has an initial osculating argument of perigee of 4.34 radians). This shell could be raised to a higher nominal altitude, although it would then overlap with a proposed Amazon Kuiper shell at 630 km. Alternatively, the GA can be constrained to use a solution nearer to $\omega = \frac{\pi}{2}$, for which the seed orbit has an initial osculating argument of perigee of 2.042 radians. In this case, the new solution is less stable but is compatible with the other two shells (see Figure 3.6). As seen in Table 3.1, the shell is initialized about 5 km higher than the reference altitude to leave ample separation from both of these shells and the proposed Amazon shell at 630 km. While the generated reference orbits do not incorporate non-gravitational effects, the propagation in Figures 3.5 and 3.6 incorporate these effects to show that, while doing so will break the intra-shell phasing between satellites, the shells still maintain mutual separation over the relevant time period.

Table 3.1: Zonal Example: Selected SpaceX and Amazon Shells. Data sourced from previously referenced FCC filings [110], [111].

Name	Nom. Altitude (km)	Inclination (deg)	N_{sat}	N_{o}	N_{so}	N_{c}
SpaceX Starlink Gen2 C1	604	148	144	12	12	5
Amazon Kuiper (Kuiper-V + Kuiper-Ka)	610	42	2592	36	72	35
SpaceX Starlink Gen2 C1	614	115.7	324	18	18	1
Amazon Kuiper (Kuiper-V + Kuiper-Ka)	630	51.9	2312	34	68	33

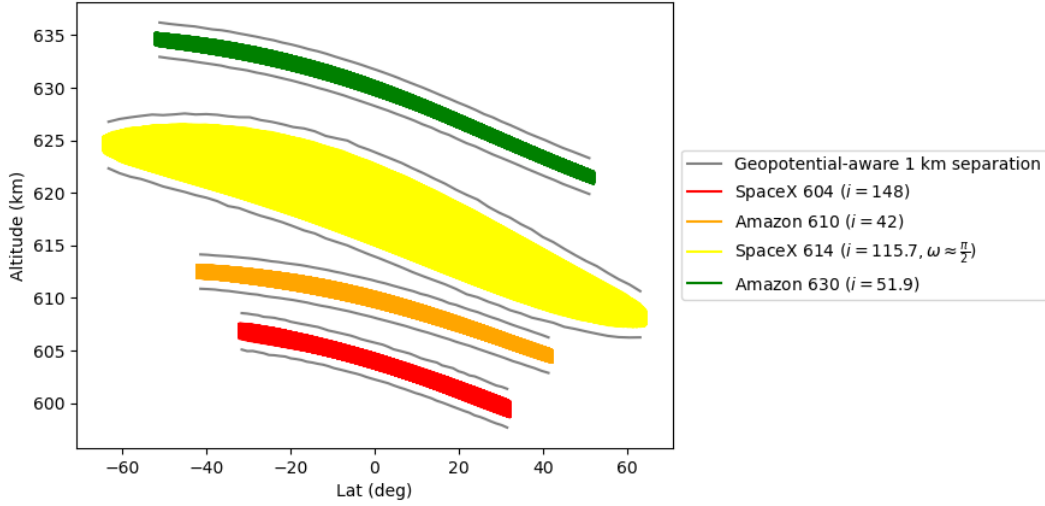


Figure 3.6: SpaceX and Amazon Shells (Constrained GA, 30-Day Propagation, Full Force Model). Coordinated eccentricity vectors prevent hazardous overlaps.

Minimum Distance Comparison between Keplerian and Osculating 2D-LFCs

To verify that the generated slots within a shell preserve collision avoidance, a constellation was chosen from a database of high-capacity 2D-LFCs and checked for conjunction events over a 30 day period, after being numerically propagated using the same J_{21} geopotential to define the adjusted 2D-LFC as the method in Section 3.3.1. The chosen constellation was placed at 600 km in altitude at an inclination of 60° and with 2D-LFC parameters $N_o = 19$, $N_{so} = 26$, $N_c = 6$. The elements Ω and M were set to 0 for the seed orbit. As calculated using the method from [22], this constellation has a Keplerian minimum separation distance of 1.408° . This corresponds to a separation of approximately 171.4 km (for this separation and altitude, the difference between arc length and cord length is minimal). A comparison was conducted between every pair of satellites every five seconds, based on the premise that even if two satellites moved directly toward one another for a five-second period at their orbital velocities, they would be unable to collide before the next screening time. The closest approach identified between slot centers is 130.556 km. This distance decreases by 352 meters over the course of a 30 day simulation, or about 0.27% of the initial separation distance.

This is not to say that minimum separation distance will always be similar between a Keplerian 2D-LFC and a periodic osculating analog. Even for a perfectly periodic shell, 2D-LFC minimum separation distance is not necessarily stable with respect to osculating variation in inclination and should be checked for the ranges obtained over the periodic orbit prior to use. Similarly, while Keplerian and perturbed constellations demonstrate fairly similar minimum separation distances, this relationship becomes increasingly noisy as the number of satellites increases.

3.3.2 Definition of Osculating 2D-LFCs under a Zonal, Sectoral, and Tesseral Geopotential

Under a geopotential model that no longer only considers zonal terms, the process is more complicated, as rotations change energy levels (meaning the rotated state may need slight adjustments to preserve an RGT for the same period) and a single orbital period is no longer sufficient to ensure periodicity. Instead, it is possible to use the process described in [82], which uses the fact that the Earth's geopotential is reasonably modeled as time invariant and thus trajectories closed in the Earth-centered Earth-fixed (ECEF) frame have approximate periodicity:

$$T_c = N_p T_\Omega = N_d T_{\Omega G} \quad (3.15)$$

A closed trajectory in the ECEF frame (i.e., an RGT trajectory) must satisfy Equation (3.15) where T_c is the cycle period of the closed trajectory, N_p is the number of orbital revolutions per cycle, N_d is the number of Earth sidereal days per cycle, T_Ω is the nodal period of the orbit, and $T_{\Omega G}$ is the nodal period of Greenwich [82].

The first step is to find an RGT at an altitude/semi-major axis within a user-specified tolerance of the user's desired altitude. J_2 -adjusted semi-major axis values can be calculated from N_d and N_p using the method by Arnas [81, Sec. 7.1]. The mean \bar{a} is obtained by solving Equation (3.16) using a Newton-Raphson solver, where ω_\oplus is the Earth's angular velocity:

$$\bar{a}^{7/2} - k_1 \bar{a}^2 - k_2 = 0 \quad (3.16)$$

$$k_1 = \frac{N_d \sqrt{\mu_\oplus}}{N_p \omega_\oplus} \quad (3.17)$$

$$k_2 = k_1 \frac{3J_2 R_\oplus^2}{4(1 - \bar{e}^2)^2} \left[(2 - 3 \sin^2(\bar{i})) \sqrt{1 - \bar{e}^2} + 4 - 5 \sin^2 \bar{i} - 2 \frac{N_p}{N_d} \cos \bar{i} \right] \quad (3.18)$$

The solver is initialized using the Keplerian semi-major axis:

$$\bar{a}_0 = \left[\left(\frac{N_d}{N_p} \right)^2 \frac{\mu_\oplus}{\omega_\oplus^2} \right]^{1/3} \quad (3.19)$$

and each successive update can be calculated using Eq. (3.19) until $|\bar{a}_{j+1} - \bar{a}_j| < tol$ for a user-defined tolerance ($1 * 10^{-9}$ meters was used in this work.):

$$\bar{a}_{j+1} = \bar{a}_j - \frac{\bar{a}_j^{7/2} - k_1 \bar{a}_j^2 - k_2}{\frac{7}{2} \bar{a}_j^{5/2} - 2k_1 \bar{a}_j} \quad (3.20)$$

Figure 3.7 shows altitudes for co-prime pairs of N_d and N_p that result in RGTs including J_2 for an inclination of 45° . Changes in inclination slightly adjust the altitude of N_d, N_p pairs due to changing the rate of J_2 -induced RAAN precession but do not impact the spacing of admissible altitudes, a result seen in the identical median shell spacing in Figure 3.8. As demonstrated in these figures, the RGT condition is not particularly onerous. This means that admissible altitudes can be made arbitrarily close by increasing N_d and finding corresponding N_p . For $N_d \leq 60$, shells can be found within a median distance of about 250 m from a given reference altitude.

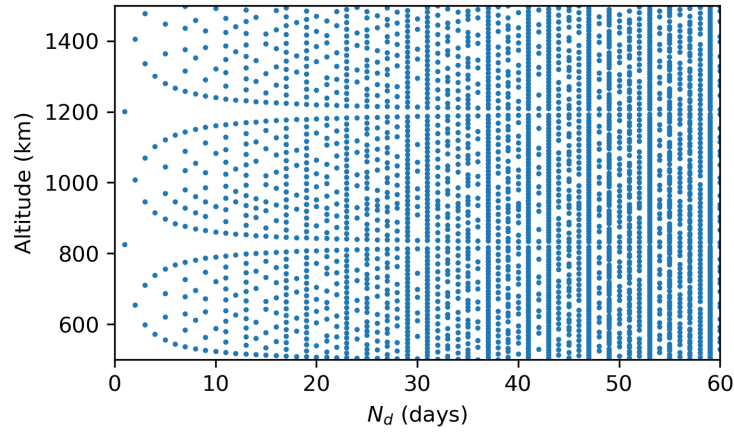


Figure 3.7: J_2 -Adjusted Approximate Admissible Mean Altitudes ($i = 45^\circ$). RGT orbits are widely available across LEO.

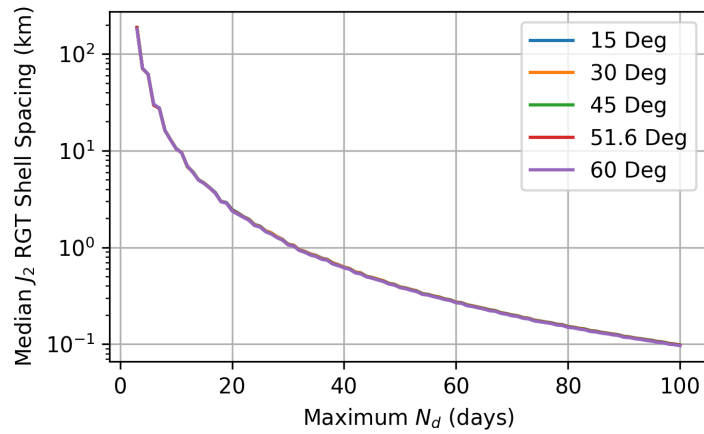


Figure 3.8: Median Distance between RGTs in Figure 3.7 under a Maximum Repetition Time. An altitude can generally be chosen to sub-kilometer precision.

Because the method in this subsection only closes orbits with respect to J_2 , a further correction must be performed to close the reference trajectory in the presence of the full geopotential model. Using chosen N_d and N_p values, the seed trajectory is propagated from its initial state (transformed from J_2 theory mean to osculating elements using the method from Kwok [109] presented by Vallado [102]) for the full cycle period (obtained by counting the number of equatorial crossings). The difference in initial and final longitude is used to find longitudinal drift. The initial osculating semi-major axis, a , is then iteratively modified using a secant method solver to close the relative trajectory under the chosen gravity model by bringing the longitudinal drift arbitrarily close to zero. This process can be combined with the previous frozen search in Subsection 3.3.1.

Because rotations in the presence of tesserals potentially change energy levels, it is required to find a seed trajectory for each different ground track in which the constellation is distributed. This means repeating the iterative process to find the conditions of semi-major axis that numerically close the ground track for each individual ground track of the space architecture. Once a seed trajectory is found, the actual cycle time, T_c , can be calculated by propagating the seed-relative trajectory for a full cycle. Arnas and Casanova [82] derived a method to transform 2D-LFCs into time distribution constellations using the time and angle offsets in Equations (3.21) and (3.22).

$$\Delta t_{ij} = \frac{T_c}{N_p} \left[\frac{j-1}{N_{so}} - \frac{N_c(i-1)}{N_o N_{so}} \right] \text{mod}(T_c) \quad (3.21)$$

$$\Delta \Gamma_{ij} = 2\pi \left[\left(1 - \frac{N_d}{N_p} \frac{N_c}{N_{so}} \right) \frac{i-1}{N_o} + \frac{N_d}{N_p} \frac{j-1}{N_{so}} \right] \text{mod}(2\pi) \quad (3.22)$$

This formulation is able to determine both the distribution on a given ground track as well as the different spacing between ground tracks in the constellation. Once this transformation is performed, the seed trajectories obtained previously can be used to generate the initial positions of all of the satellites of the constellation.

As an example of application, the techniques described in this subsection are applied to the China SatNet shells proposed for a nominal altitude of 1145 km and the Hughes shell proposed at 1150 km, contained in Table 3.2. Hughes is based on information from its FCC filing [113]. China SatNet is based on information from Jonathan’s Space Pages.¹³ RGT orbits are found at admissible altitudes to stack these 2D-LFCs into five concentric shells. Each shell is an RGT orbit seeded with a zonally frozen seed orbit. While these orbits are sufficient to avoid inter-shell conjunctions, phasing between orbital planes would need to be modified via a different N_c to eliminate intra-shell conjunctions at orbital crossings. The FCC filing from Hughes [113] indicates that “[t]o avoid collisions within the constellation, Hughes will make use of a moderate amount of altitude variation such that safe radial separations are maintained at plane intersections.” The fact that China SatNet’s proposal involves similar overlaps at orbital plane intersections implies that they will likely employ a similar method. While separating orbital planes in altitude does ensure safety and is more robust to failed satellites, it does so at the cost of reduced orbital density as compared to a properly phased and maintained shell. The China SatNet proposal features multiple co-altitude shells with

¹³<https://www.planet4589.org/space/con/conlist.html>, accessed 28 November 2022.

heterogeneous inclinations. In this example, no effort is made to control for the resulting differential RAAN precession.

Table 3.2: RGT Example: China SatNet and Hughes Shells.

Name	Nom. Altitude (km)	N_p	N_d	Adjusted Altitude (km)	Inclination (deg)	N_{sat}	N_o	N_{so}	N_c
China SatNet	1145	79	6	1123.205	30	1728	48	36	46
China SatNet	1145	408	31	1131.249	40	1728	48	36	46
China SatNet	1145	79	6	1137.326	50	1728	48	36	46
China SatNet	1145	79	6	1147.181	60	1728	48	36	46
Hughes	1150	105	8	1158.289	55	1440	36	40	18

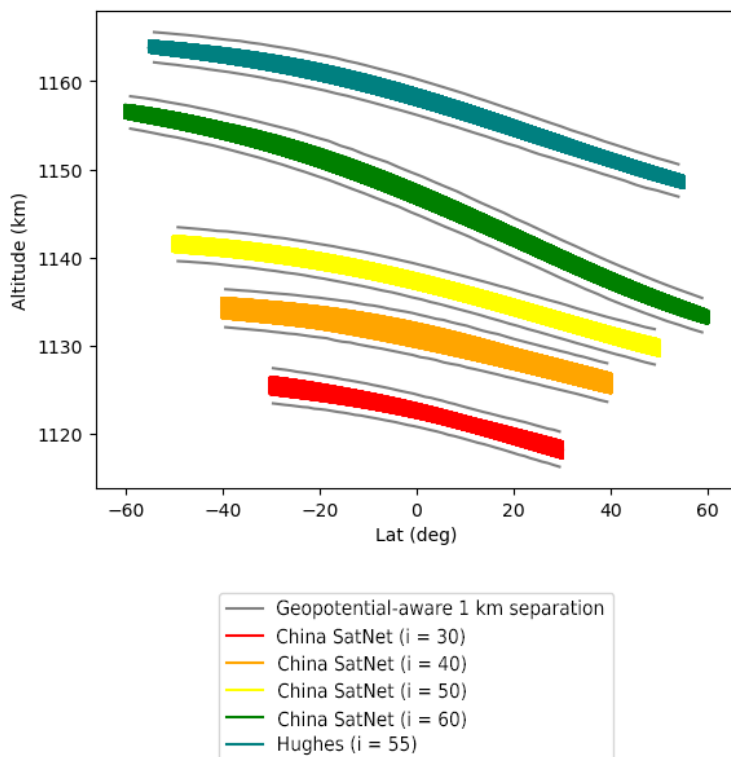


Figure 3.9: Hughes and China SatNet Shells Showing Separation. RGT orbits seeded with GA-generated zonal-frozen orbits, 60-day propagation, full force model.

As seen in Figure 3.9, the sequential ordering of China SatNet’s shells allowed for tighter tessellation between shells. Note that improved density could be achieved by nesting Hughes’ shell between the China SatNet 50° and 60° shells as compared to the order presented here. Separation distances are picked notionally. If eccentricity-vector restoring maneuvers were performed more frequently than every two months, shells could also be placed closer than demonstrated in Figure 3.9. No analysis is conducted concerning the accumulation of differential drift and phasing error between shells. Eventually this error will also force minor restoring maneuvers. The shells are presented in Table 3.2, where adjusted altitude refers to the arithmetic mean osculating equatorial altitude of the shell.

3.4 Simplified Shell Model

For optimization studies or initial compatibility checks, it can be desirable to understand the approximate shape of shells without fully defining a 2D-LFC and propagating each satellite. This section describes and evaluates several simplified shell models suitable for these purposes. While bar notation is not used, to avoid cluttering the equations, all orbital elements in this and the next section are mean rather than osculating elements, unless otherwise specified. Mean elements are defined in terms of a particular orbit theory and set of perturbations. In Subsection 3.4.1, a J_2 -only theory is used to find approximate shell centerlines in the geocentric latitude and altitude plane. In Subsection 3.4.2, the performance of the equation is assessed using mean values calculated from osculating ephemeris using a higher-degree, higher-order geopotential-only theory using Orekit's implementation of the Draper Semi-analytical Satellite Theory (DSST) [114]. This is not technically correct, as it ignores the differences between the two mean element theories, but is a reasonable approximation in the context of this work, which simply seems to assess closed-form equations for approximate shell shape in this section and shell width in Section 3.5.

3.4.1 Simplified Shell Model Method

The radial distance can be expressed as a function of the true anomaly, θ , using it as a geometry-independent variable that is related with time through Kepler's equation [102].

$$r(\theta) = \frac{a(1 - e^2)}{1 + e \cos(\theta)} \quad (3.23)$$

Note that under perturbed motion, the radial distance curve diverges from Equation (3.23). Therefore, this analysis considers radius as an osculating quantity that changes with the osculating orbital elements. It is possible to derive simplified expressions for the osculating radius using the mean elements as inputs. Note that Equation (3.23) is expressed in perifocal coordinates aligned with the eccentricity vector, and therefore its relation to an inertial frame will also be a function of $i(t)$, $\omega(t)$, and $\Omega(t)$.

In general, radial distance is a function of both latitude and longitude, but shell width is considered as a function of latitude only for this analysis. Radial distance can be made a function of geocentric latitude angle, ϕ , by noting that $\sin(\phi) = \sin(i) \sin(\theta + \omega)$. The radius of an osculating orbit can be expressed as a function of latitude angle using the following equation:

$$r(\phi) = \frac{a(1 - e^2)}{1 + e \cos\left(\omega - \arcsin\left(\frac{\sin(\phi)}{\sin(i)}\right)\right)} \quad (3.24)$$

Several important features are visible in Equation (3.24).. First, the variable ω has the effect of widening the curve $r(\phi)$ for values not equal to $\omega = \pi/2$ or $\omega = 3\pi/2$. Additionally, $\omega = \pi/2$ and $\omega = 3\pi/2$ produce curves that are identical after a reflection of ϕ . Under this simplified model, selecting $\omega = \pi/2$ or $\omega = 3\pi/2$ is preferred for maximizing orbital capacity (this condition is also used when designing $J_2 - J_3$ frozen orbits). Equation (3.24) can be

simplified by assuming $\omega = \pi/2$:

$$r(\phi) = \frac{a \sin(i) (1 - e^2)}{\sin(i) + e \sin(\phi)} = \frac{a(1 - e^2)}{1 + e \frac{\sin(\phi)}{\sin(i)}} \quad (3.25)$$

Second, note that when $\sin(\phi)$ is equal to $\sin(i)$ or $\sin(-i)$, the radial distance is $r(i) = a(1 + e) = r_a$ and $r(-i) = a(1 - e) = r_p$, respectively. Therefore, the curves have negative slope for $\omega = \pi/2$ and $0 < i < \pi/2$ and positive slope for $\omega = 3\pi/2$ and $0 < i < \pi/2$. For best alignment, nearby shells should use the same argument of perigee to align the slopes of their shells. Third, it can be easily seen that the average slope of the radius versus latitude curve is given by ae/i . Non-zero eccentricity creates sloped radius versus latitude curves where larger semi-major axis values increase the slope.

For greater fidelity, it is possible to avoid assuming the value of ω and to add the short period effect of J_2 on orbital radius by manipulating the following equation from Vallado [102, p. 709], introduced by Kwok [109]:

$$\Delta r_{sp} = -\frac{J_2 R_\oplus^2}{4p} \left((3 \cos^2(i) - 1) \left\{ \frac{2\sqrt{1-e^2}}{(1 + e \cos(\theta))^2} + \frac{e \cos(\theta)}{1 + \sqrt{1-e^2}} + 1 \right\} - \sin^2(i) \cos(2u) \right) \quad (3.26)$$

where p is the semiparameter and u is the argument of latitude. The following substitutions can then be made:

$$\begin{aligned} p &= a(1 - e^2) \\ u &= \arcsin\left(\frac{\sin(\phi)}{\sin(i)}\right) \\ \theta &= \arcsin\left(\frac{\sin(\phi)}{\sin(i)}\right) - \omega \end{aligned} \quad (3.27)$$

to yield:

$$\Delta r_{sp} = -\frac{J_2 R_\oplus^2}{4a(1 - e^2)} \left((3 \cos^2(i) - 1) \left\{ \frac{2\sqrt{1-e^2}}{\left(1 + e \cos\left(\arcsin\left(\frac{\sin(\phi)}{\sin(i)}\right) - \omega\right)\right)^2} + \frac{e \cos\left(\arcsin\left(\frac{\sin(\phi)}{\sin(i)}\right) - \omega\right)}{1 + \sqrt{1-e^2}} + 1 \right\} - \sin^2(i) \cos\left(2 \arcsin\left(\frac{\sin(\phi)}{\sin(i)}\right)\right) \right) \quad (3.28)$$

and a modified osculating radius formula:

$$r(\phi) = \frac{a(1 - e^2)}{1 + e \cos\left(\omega - \arcsin\left(\frac{\sin(\phi)}{\sin(i)}\right)\right)} + \Delta r_{sp} \quad (3.29)$$

3.4.2 Simplified Shell Model Results

In this subsection, the equations from Subsection 3.4 are assessed to determine how well they perform in modeling shell centerline behavior and to assess the sensitivity of shell shape produced by the simplified equations when mean eccentricity is accurately computed versus when $J_2 - J_3$ mean eccentricity is used as a substitute. This second assessment is

important because computing mean frozen eccentricities in the presence of a higher-fidelity gravity model can be computationally expensive using numerical methods, but assessment using $J_2 - J_3$ mean eccentricity can miss nuances relevant for shell-nesting analysis, including inclination-dependent effects for shell tessellation.

Assessment of Simplified Shell Model Equation Accuracy

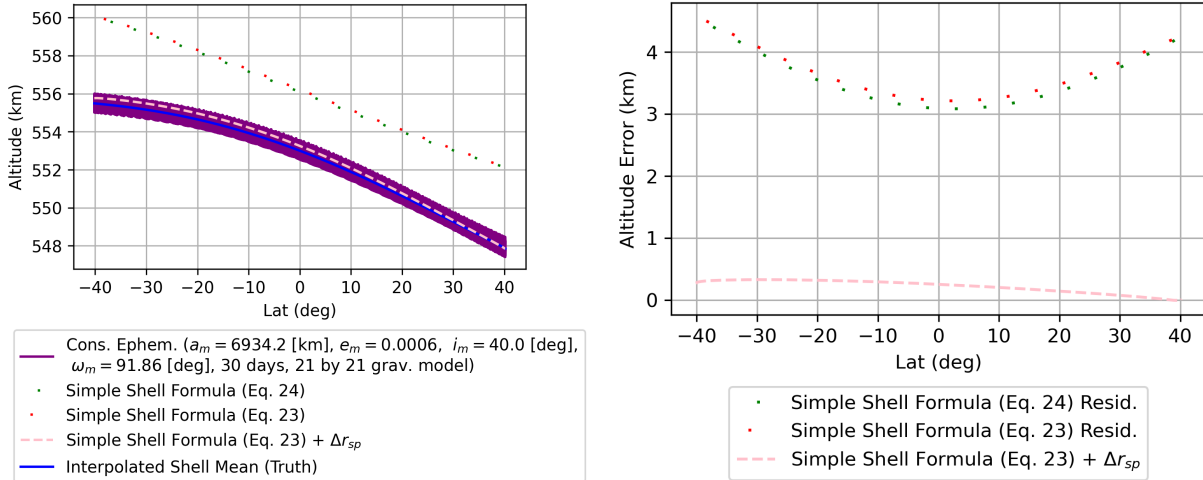
To assess the formulas in Section 3.4.1 for accuracy, Equations (3.24), (3.25), and (3.29) are implemented. While it is not necessary for this work, ω is potentially ambiguously defined for small eccentricities. To avoid this issue, Equation (3.29) can be recast into an alternative formulation using the u expression from Equation (3.27) and the following substitutions¹⁴:

$$e_x = e \cos(\omega) \quad (3.30)$$

$$e_y = e \sin(\omega) \quad (3.31)$$

$$e = \sqrt{e_x^2 + e_y^2} \quad (3.32)$$

$$\cos(v) = \frac{e_x}{\sqrt{1 + e \cos(v)}} \cos(u) + \frac{e_y}{\sqrt{1 + e \cos(v)}} \sin(u) \quad (3.33)$$



(a) Equation Fit.

(b) Fit Residuals.

Figure 3.10: Mean to Osculating Shell Geometry Comparison Example 1 ($i = 40^\circ$, $N_o = 5$, $N_{so} = 5$, $N_c = 2$). The Δr_{sp} correction is necessary to achieve centerline accuracy.

These equations are then evaluated for goodness of fit using the five constellations in Figure 3.20, although only two are shown in this chapter for conciseness. Mean element values were recovered from the initial osculating state of the seed trajectory using Orekit's implementation of the DSST for a model featuring only a 21 by 21 gravity model (mean

¹⁴As a first-order approximation of the mean values of the components e_x and e_y of the mean eccentricity vector, the osculating relations in Equations (3.30), (3.31), (3.32), and (3.33) are a reasonable representation to simplify the conversion between Keplerian and circular element sets.

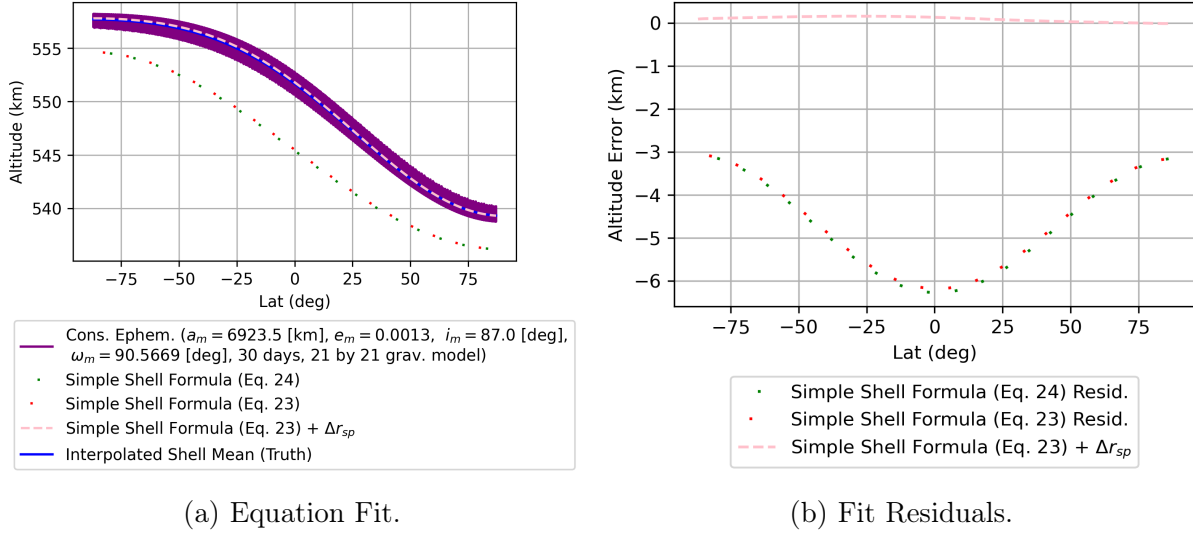


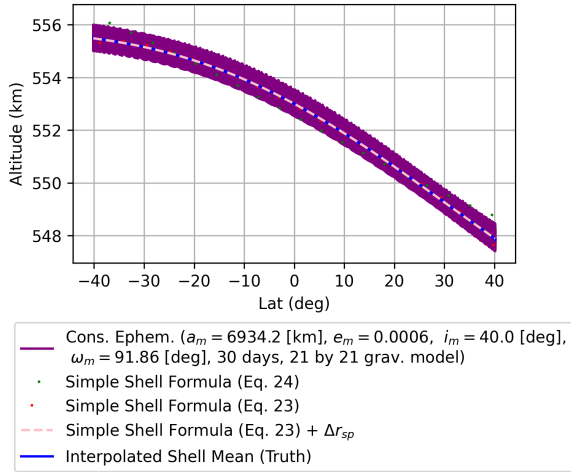
Figure 3.11: Mean to Osculating Shell Geometry Comparison Example 2 ($i = 87^\circ$, $N_o = 5$, $N_{so} = 5$, $N_c = 2$). The Δr_{sp} correction is necessary to achieve centerline accuracy.

elements as defined by DSST’s theory are different than the J_2 -only theory and method described earlier)[114]. These recovered mean values were used as inputs into each of the three equations. For each constellation, the osculating altitude-latitude relationships for all satellites were plotted and an interpolated function was generated for the mean of these curves using a 90 point interpolated quadratic spline. As seen in Figures 3.10 and 3.11, Equations (3.24) and (3.25) generate very similar results, with residuals of several kilometers and significant errors in shape, especially at more extreme latitudes. In contrast, Equation (3.29) performs much better, closely paralleling the actual empirical centerline.

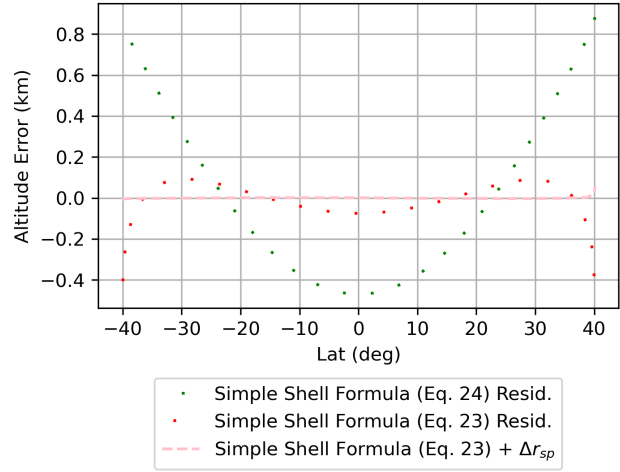
To rule out a difference in mean element generation methodology, this work uses a GA, allowing each run to adjust values for mean a , e , and ω (if the equation included it) to minimize root mean squared error between the interpolated shell mean and each of the shell geometry equations. This has no operational value but is intended simply to show that the chosen equations cannot fit the resulting curves for any set of parameters a , e , and ω . Inclination was assumed to remain fixed at the mean values calculated using DSST. As is evident in Figures 3.12 and 3.13, even allowing for arbitrary input parameters, Equations (3.23) and (3.24) have remaining residuals of hundreds of meters to just over a kilometer, while Equation (3.29) is able to almost perfectly match the reference curve. This indicates that Equation (3.29), which incorporates the Δr_{sp} correction term, appears necessary to properly model shell centerline conditions with accuracy sufficient for shell-nesting analysis. Equations (3.23) and (3.24) cannot generate accurate results for any possible input.

Error Associated with Using $J_2 - J_3$ Mean Eccentricity versus Numerically Computed Mean Eccentricity under Modeled Gravity Field in Simplified Shell Model

We now explore the impact on shell centerline geometry and residuals from using $J_2 - J_3$ classical frozen orbit eccentricity and argument of perigee values versus those calculated numerically. In this example, note that both options are evaluated for a single seed tra-

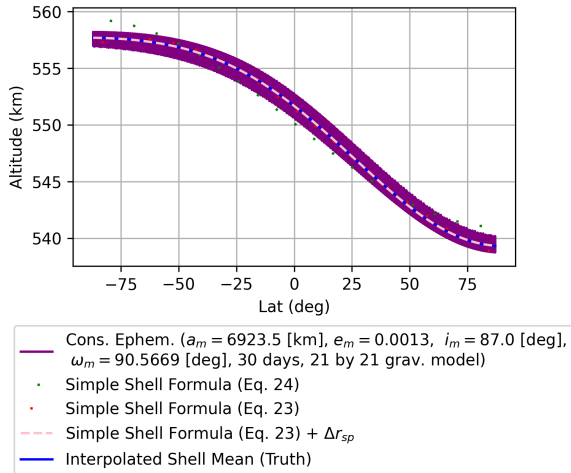


(a) Equation Fit.

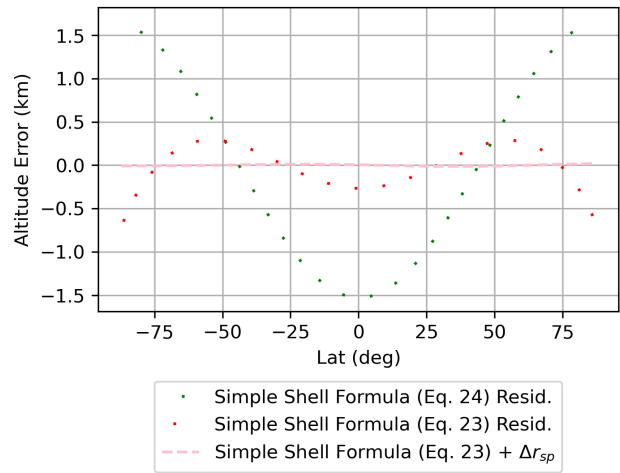


(b) Fit Residuals.

Figure 3.12: GA Geometry Comparison Example 1 ($i = 40^\circ, N_o = 5, N_{so} = 5, N_c = 2$). Equations 23 and 24 cannot fit the shell centerline, even for optimized inputs.



(a) Equation Fit.



(b) Fit Residuals.

Figure 3.13: GA Geometry Comparison Example 2 ($i = 87^\circ, N_o = 5, N_{so} = 5, N_c = 2$). Equations 23 and 24 cannot fit the shell centerline, even for optimized inputs.

jectory rather than for a full constellation. Errors for centerline curves are small for the low-inclination shells (tens of meters) but grow to nearly ± 1 km for the 87° shell in Figure 3.15.

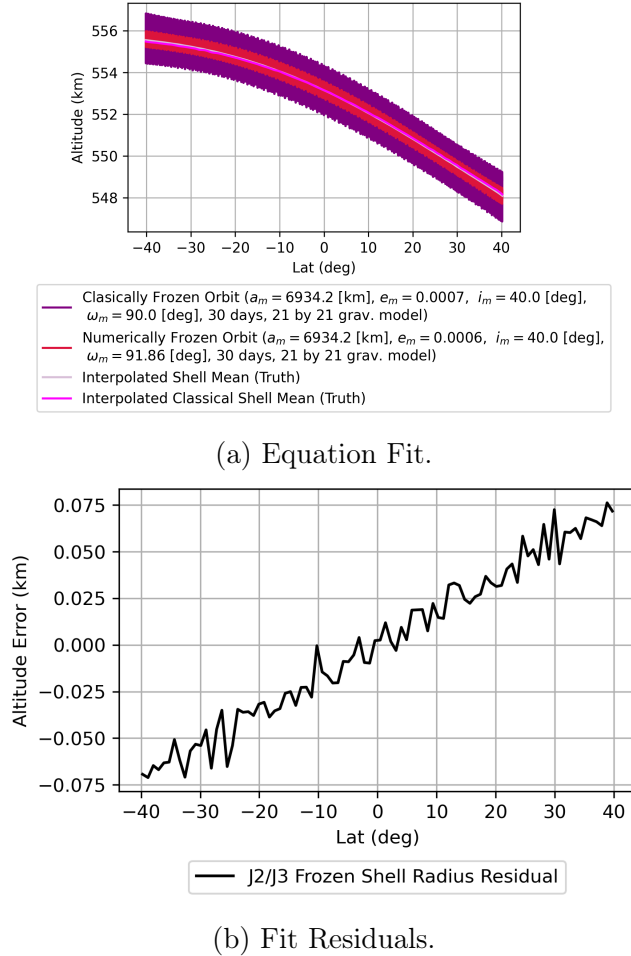


Figure 3.14: Classical versus Numerical Orbit Freezing Geometry Comparison for Example 1 ($i = 40^\circ$, $N_o = 5$, $N_{so} = 5$, $N_c = 2$). The numerically and classically frozen orbits are very similar.

Based on these results, it can be concluded that, for the purpose of shell geometry estimation, it is necessary to include the short-term periodic effects due to J_2 , and that doing so allows the reproduction of shell shape and altitude to an accuracy of hundreds of meters across several examples. When estimating shell shapes for stacking purposes, using frozen eccentricities incorporating higher-degree zonal effects improves accuracy as compared to J_2/J_3 frozen eccentricities. Nevertheless, the difference may be small enough to reasonably be ignored for estimating shell centerline geometry for some purposes. Incorporation of higher-fidelity orbit freezing is necessary for the stability of the resulting orbits, as is visible in Figures 3.14 and 3.15.

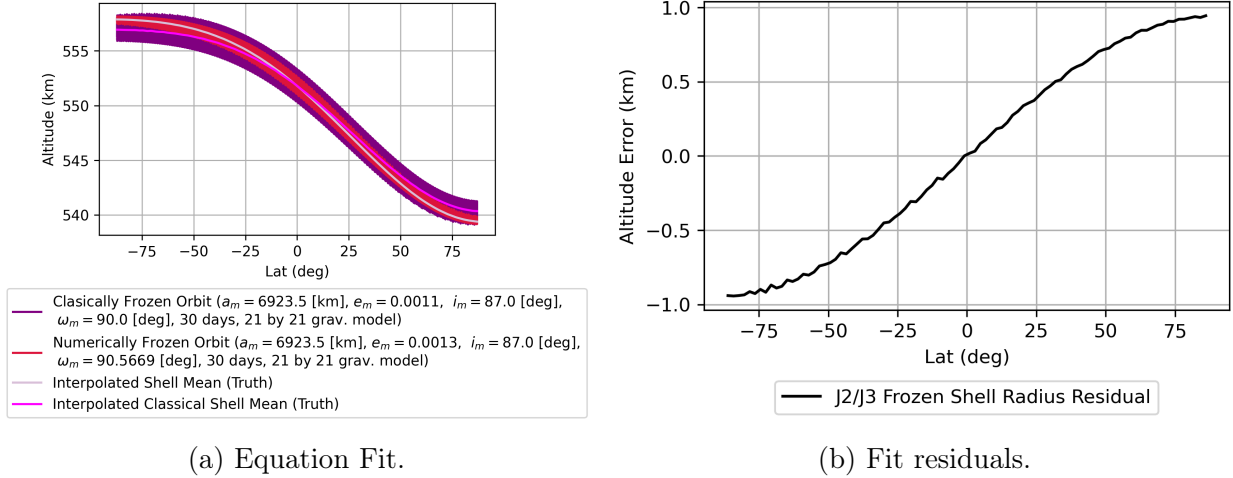


Figure 3.15: Classical versus Numerical Orbit Freezing Geometry Comparison for Example 2 ($i = 87^\circ$, $N_o = 5$, $N_{so} = 5$, $N_c = 2$). The numerically and classically frozen orbits diverge by ± 1 km.

3.5 Shell Width Estimation

The width of a shell about its centerline is not constant, with implications for how closely shells may be stacked, particularly for configurations seeking to maximize orbital density while preserving non-conjunction between adjacent shells. Therefore, this effect is studied in this section.

3.5.1 Shell Width Estimation Method

To investigate the effect of the time-varying orbital elements on the osculating $r(\phi)$, we compute a first-order linearization of the relationship in Equation (3.29). The linearized error propagation relationships are as follows:

$$\sigma_r^2 = \left| \frac{dr}{da} \right|^2 \sigma_a^2 + \left| \frac{dr}{de} \right|^2 \sigma_e^2 + \left| \frac{dr}{d\omega} \right|^2 \sigma_\omega^2 + \left| \frac{dr}{di} \right|^2 \sigma_i^2 \quad (3.34)$$

where the σ terms represent the error in the mean orbital elements and osculating radius parameters. Note that this expression assumes Gaussian errors in the mean orbital elements and translates these errors into Gaussian errors in osculating r . Therefore, the interpretation is that if we take the shell width to be given by $3\sigma_r$, then it should include 99.7% of all the errors due to J_2 variations. However, the full dynamic model includes higher-order terms over long propagation intervals that are neglected by Equation (3.29). A value of $6\sigma_r$ can reasonably account for these unmodeled effects (zonal terms higher than J_2 as well as sectoral and tesseral gravity terms) over a 30-day propagation period. Such a model can also be used to account for estimation and control errors and for a case that does not freeze the satellite orbit but rather controls the trajectory to achieve the desired shell width. This estimates the shell width at given altitudes based on assumed levels of mean element control or drift over the analysis time period.

The full expressions used for computing the shell width are shown in Appendix B, but we will examine the behavior of the radius as a function of latitude without the short-period terms to gain an intuitive understanding. Therefore, assuming $\omega = \pi/2$ and that $\Delta r_{sp} = 0$.¹⁵, we have the following:

$$\frac{dr}{da} = -\frac{\sin(i) (e^2 - 1)}{\sin(i) + e \sin(\phi)} = \begin{cases} 1 - e^2, & \text{with } \phi = 0 \\ 1 - e, & \text{with } \phi = i \end{cases} \quad (3.35)$$

$$\frac{dr}{de} = -\frac{a \sin(i) (\sin(\phi) e^2 + 2 \sin(i) e + \sin(\phi))}{(\sin(i) + e \sin(\phi))^2} = \begin{cases} -2ae, & \text{with } \phi = 0 \\ -a, & \text{with } \phi = i \end{cases} \quad (3.36)$$

$$\frac{dr}{d\omega} = -\frac{ae \sin(i)^2 (e^2 - 1) \sqrt{\frac{\sin(i)^2 - \sin(\phi)^2}{\sin(i)^2}}}{(\sin(i) + e \sin(\phi))^2} = \begin{cases} ae(1 - e^2), & \text{with } \phi = 0 \\ 0, & \text{with } \phi = i \end{cases} \quad (3.37)$$

$$\frac{dr}{di} = -\frac{ae \cos(i) \sin(\phi) (e^2 - 1)}{(\sin(i) + e \sin(\phi))^2} = \begin{cases} 0, & \text{with } \phi = 0 \\ ae \cot(i) \frac{e-1}{1+e}, & \text{with } \phi = i \end{cases} \quad (3.38)$$

Note that if we let $\phi = 0$, the derivative term for e is $-2ae$, and if we let $\phi = i$, the derivative term for e is $-a$. The effect of variations in the orbital elements can be taken into account using first-order relationships for small deviations. To consider the effect of e on the slope of the radius function, we take the derivative of r with respect to ϕ by substituting $\theta = \arcsin(\sin(\phi)/\sin(i))$. We compute the following:

$$\frac{dr}{d\phi} = \frac{ae \sin\left(w - \arcsin\left(\frac{\sin(\phi)}{\sin(i)}\right)\right) \cos(\phi) (e^2 - 1)}{\sin(i) \sqrt{1 - \frac{\sin(\phi)^2}{\sin(i)^2}} \left(e \cos\left(w - \arcsin\left(\frac{\sin(\phi)}{\sin(i)}\right)\right) + 1\right)^2} \quad (3.39)$$

or for $\omega = \pi/2$, we have the following simplification:

$$\frac{dr}{d\phi} = \frac{ae \cos(\phi) \sin(i) (e^2 - 1)}{(\sin(i) + e \sin(\phi))^2} \quad (3.40)$$

Note that if $e = 0$, then the slope of this curve is zero, as expected. It is evident that the slope scales with eccentricity and semi-major axis.

3.5.2 Shell Width Estimation Results

Figure 3.16 shows results of this width estimation approach for the seed satellite trajectory for the 40° and 87° shells used in the previous modeling examples, propagated for 30 days under a 21 by 21 gravity field model. A DSST mean element propagator was used to generate the mean elements for the propagated trajectory for the same satellite as inputs into the width equation.

¹⁵Note that this is just for Equations (3.35) through (3.38). We use the full expression in the shell width estimation numerical results

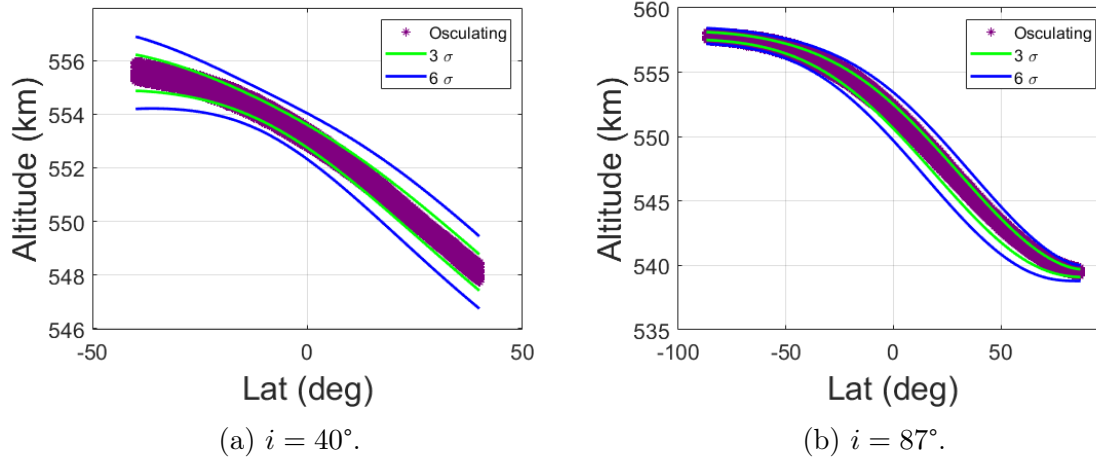


Figure 3.16: Estimated versus Actual Shell Widths for Sample Satellites. The width estimation formula obtains good results.

3.6 Shell Coordination, Number of Admissible Shells and Slots, and the Effect of Inclination Sequencing

This section explores how the use of the shell techniques influences the number of shells and satellite locations that can be placed in a particular orbital volume. This analysis is shown using separation of frozen shells in the latitude-altitude plane, as separation between shells in this space provides intuitive assurance that the shells will not intersect and do not pose an inter-shell conjunction hazard over the time period propagated.

First, two demonstrations are presented to visualize important concepts, then two experiments are conducted to quantify the influence of shell inclination ordering and shell separation distances on orbital density and intrinsic capacity.

3.6.1 Demonstration 1: J_2 - J_3 Shells Are Not Stable over Practical Time Periods

The goal of this demonstration is to show that shells defined using classical frozen orbit theory may not be sufficiently stable in the presence of a higher order and degree gravity model. A set of concentric orbital shells are generated using J_2 -/ J_3 -defined frozen orbits that are spaced to initially show orbital separation. These orbits are then propagated in the presence of a higher order and degree gravity model.

The shape of the shells is primarily a function of inclination and eccentricity. As seen in Figure 3.17 and demonstrated mathematically by Bombardelli et al. [92], shells generated to be classically frozen under a J_3 model are arbitrarily stable and thin, subject only to numerical error. These shells also show an inclination-dependent shape and tessellate well in an inclination-independent manner. As seen in Figure 3.18, J_2 - J_3 shells are not sufficiently stable when propagated under a more realistic geopotential and rapidly lose coherency over time, gaining shell width and occupying more area in the latitude-altitude plane.

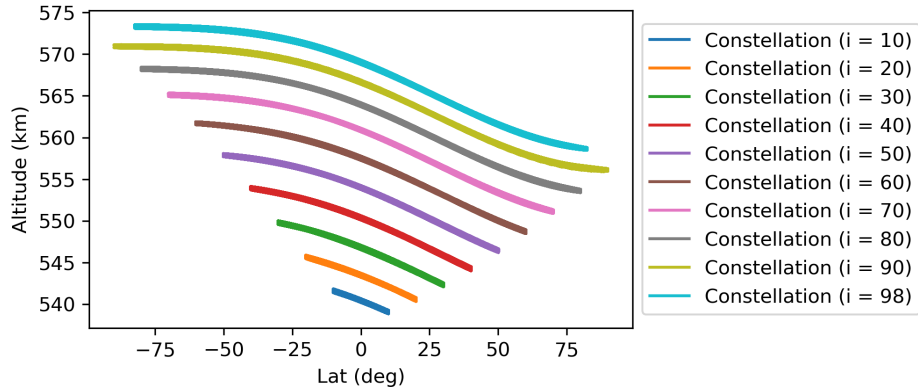


Figure 3.17: J_2 - J_3 Frozen Shells Propagated under a J_3 Model for 30 days. The shells stay compact over time and tessellate well for any inclination.

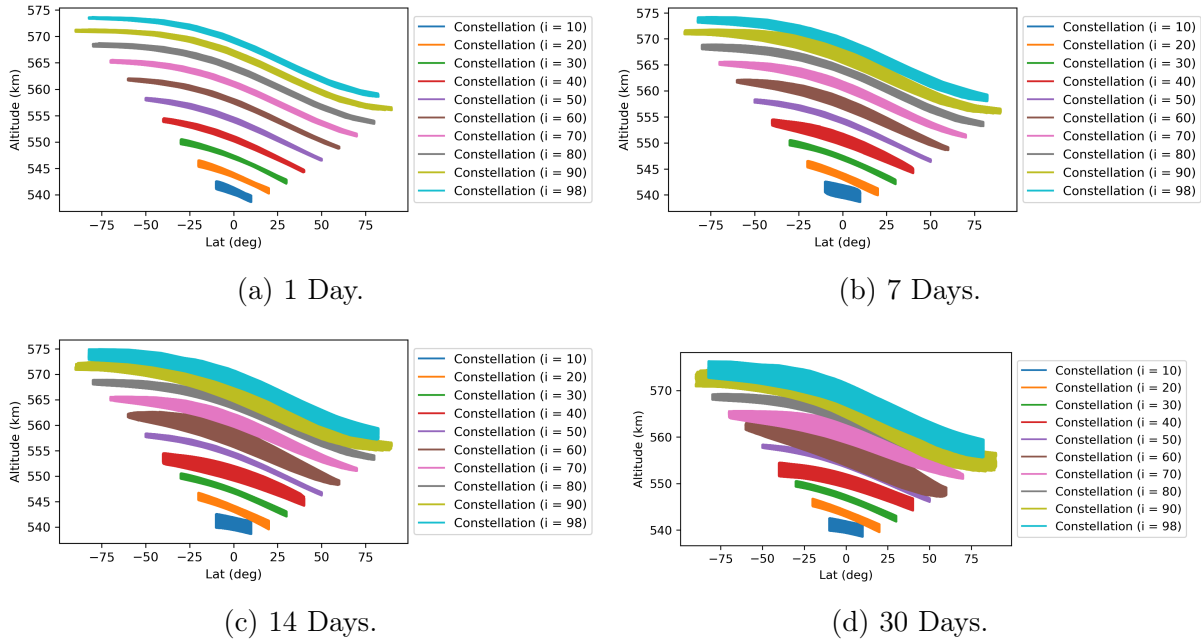


Figure 3.18: J_2 - J_3 Frozen Shells Propagated under a 21 by 21 Gravity Model. The shells blur over time and begin to overlap.

3.6.2 Demonstration 2: Coordinated Orbits Allow More Shells than Minimum-Maximum Altitude Separation, But Inclination Sequencing Matters

Shells can be defined to account for higher order or degree geopotentials, as described in Section 3.3, but this leads to additional shell thickness that increases with time and magnifies differences in shell shape as a result of inclination. This produces an important consequence for shell ordering. Shells generated to follow J_2 - J_3 reference orbits using frequent correcting

maneuvers may be placed in an inclination-agnostic ordering. However, shells generated using higher-fidelity gravity models experience an inclination-dependent slope that influences tessellation efficiency.

This demonstration will show how the use of frozen orbits allows for increased orbital density over non-frozen alternatives. It then explains why this density is influenced by the inclinations of adjacent shells. Two examples are demonstrated. In the first, a frozen orbit is presented, with its minimum and maximum altitudes highlighted. Two other shells are placed within that overlapping altitude range in a way that does not result in additional collisions. In the second, one of these shells is replaced by two shells that fit in the same orbital volume due to the use of sequential orbital inclinations.

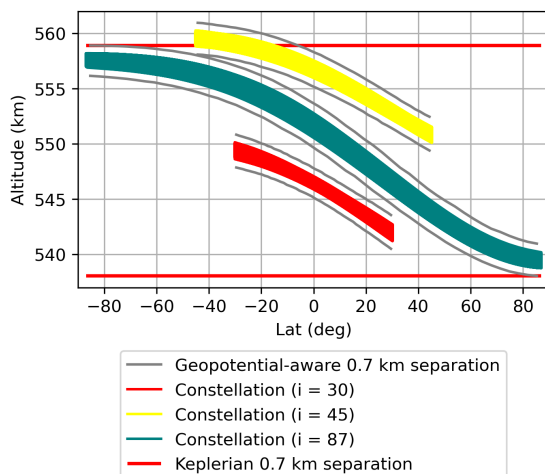
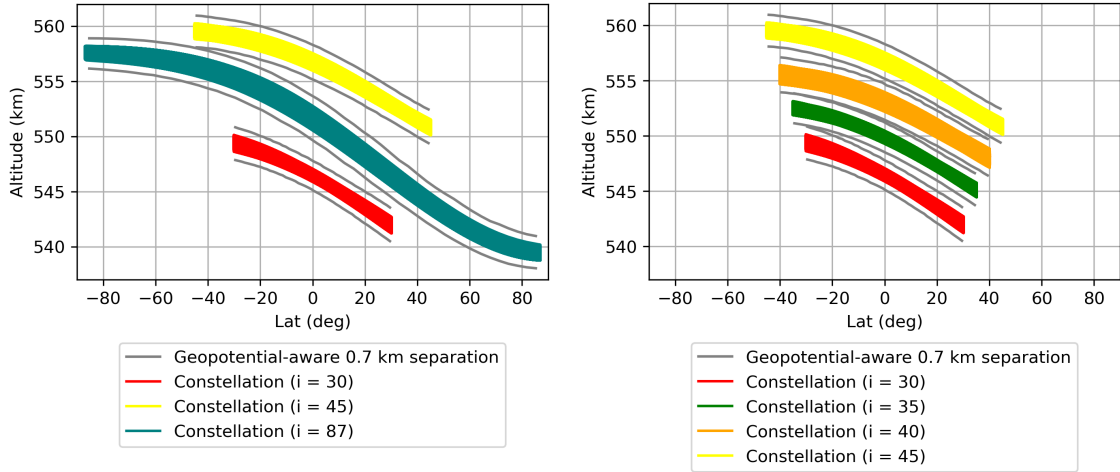


Figure 3.19: Compatible Geopotential-Aware Shell Placement within Keplerian Separation Distance (zonal freezing method, 30 day propagation, 21 by 21 gravity model).

In Figure 3.19, we can compare an orbital separation policy that relies on the maximum and minimum altitude that the orbit obtains plus a safety distance. Under this policy, no other shells could be placed such that they intersect the region delineated by the red lines in the figure. However, the orbit of a frozen shell does not occupy this entire altitude exclusion region at all latitudes. As a result, two other shells can be placed overlapping the exclusion region without producing conjunctions and still preserve the same safety exclusion region.

It is important to explain why inclination ordering matters for frozen shells generated using higher-fidelity gravity models, as shown in Figure 3.20. Because shell slope in the latitude-altitude plane is now inclination dependent, shells with different inclinations no longer nest cleanly in an altitude-agnostic way. In fact, as seen in Figure 3.20, two sequential shells can fit within the space occupied by a single shell with a very different inclination. This ordering is an important result and represents a trade-off for constellation operators where coordination could increase capacity, particularly in LEO regions characterized by significant demand for both Sun-synchronous and lower-inclination orbits.



(a) Non-Sequential Inclination Shells (same as in Figure 3.19).

(b) Sequential Inclination Shells.

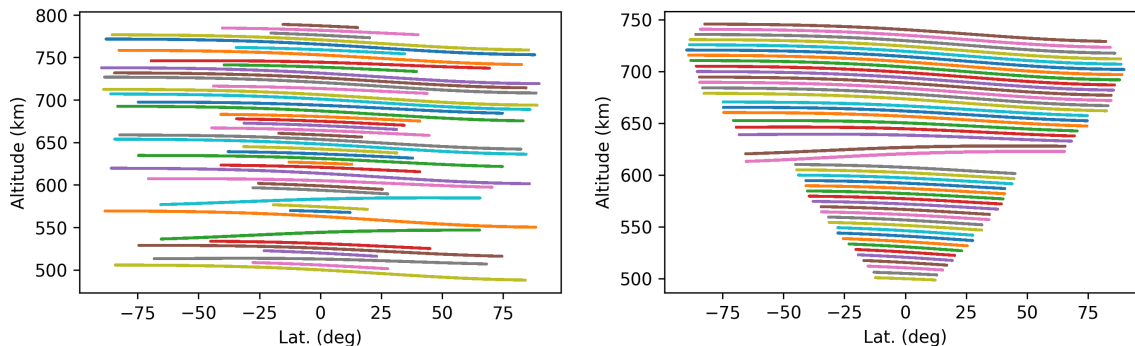
Figure 3.20: Shells Nesting Compared between Disparate and Similar Inclinations (zonal freezing method, 30 day propagation, 21 by 21 gravity model). Similar inclinations allow adjacent shells to tessellate better than disparate inclinations.

3.6.3 Experiment 1: Impact of Shell Coordination and Inclination Ordering on Number of Shells and Satellites

This subsection seeks to explore how orbit coordination and inclination ordering influence the number of satellites and shells that can compatibly coexist in a particular region of space. We make two hypotheses. First, we predict an increased number of admitted shells for a given minimum inter-shell separation distance when separation is based on actual separation in latitude-dependent altitude rather than the maximum and minimum altitude of a particular shell. Second, based on the inclination dependence seen in Demonstration 2, the number of admissible shells should be higher for inclination-ordered shells than for randomly ordered shell inclinations.

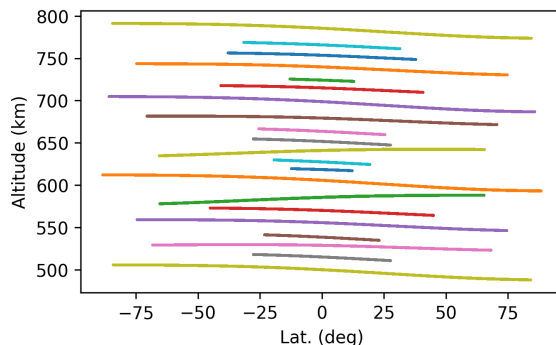
Three sets of shells are layered using the zonal geopotential-based approach: a set of randomly ordered inclinations, a sequentially ordered set of the same inclinations, and a set assuming separation between the maximum and minimum altitudes at any latitude. The random set of inclinations was selected ranging from from 10–100°, excluding inclinations between 60–65°, as optimum solutions tended to tessellate especially poorly given the nearby critical inclination at 63.4°, which skews GA results because periodicity no longer requires a specific small mean eccentricity value. Shells are spaced in altitude to preserve a 5 km separation between shells. In the randomly ordered and sequentially ordered inclination cases, this distance is calculated between interpolated shell centerlines, although the same calculation could easily be done for an interpolated maximum curve for the lower shell and an interpolated minimum curve for the upper shell. In the last case, the separation distance is measured from the highest value obtained by the shell centerline interpolation at any altitude to the minimum centerline value of the higher shell. This represents the naive case

where altitude-based separation uses the maximum osculating radial value of the shell to determine separation distances. The numbers of shells in each of the three cases were then transformed into representative counts for the number of aggregate satellites that could be fit as a function of the intra-shell minimum separation distance between satellites, using a method from Avendaño et al. [22] and Lifson et al. [97] that fits a power law to empirical results for Keplerian 2D-LFCs.



(a) Randomly Ordered Inclinations.

(b) Sequentially Ordered Inclinations.



(c) Random Inclinations, Separated based on Minimum and Maximum Osculating Shell Altitude.

Figure 3.21: A Comparison of Random and Sequential Inclination Shell-Layering Approaches using Equation (3.29). Latitude-based separation and ordered inclinations improve density.

As seen in Figure 3.21, examples are not necessarily *a priori* constrained to use curves aligned in the same direction on the latitude/altitude graph. In the example, the randomly ordered inclinations are able to fit 44 shells in the region from 500–800 km of equatorial altitude. The sequential ordering is able to fit this same set of shells in the region from approximately 500–740 km, a significant reduction in altitude range. Both strongly outperform the case based on maximum and minimum separation, where only 21 shells can be admitted to the same region.

In Figure 3.22, the three examples in Figure 3.21 are used to estimate aggregate numbers of admissible satellite locations based on the inclination, altitude, and minimum in-shell separation distance power law method in Avendaño et al. [22] and Lifson et al. [97]. Because the use of sorted geopotential-aware slots does not occupy the full orbital altitude range, these results are scaled based on the density of satellites in the occupied altitude range and presented as a fourth line in the figure.

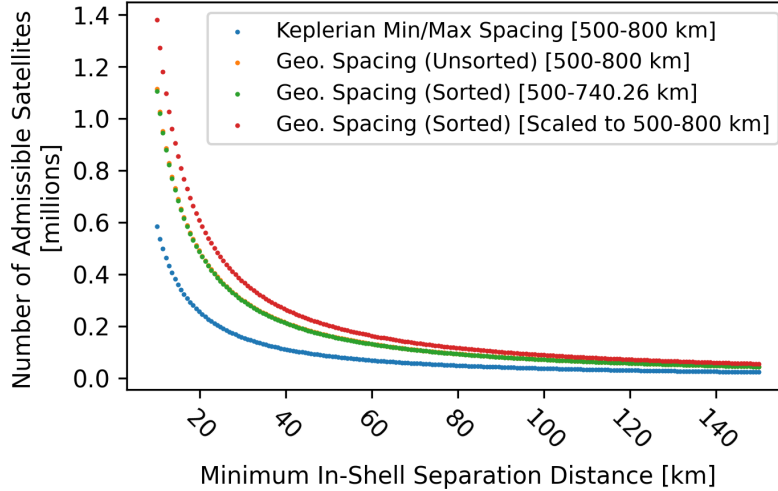


Figure 3.22: Admissible Satellite Locations for Various In-Shell Separation Distances.

3.6.4 Experiment 2: Impact of Shell Separation Distance on Number of Admissible Shells

This subsection seeks to explore the sensitivity of the number of admissible shells as a function of the separation distance between each shell. For maximum and minimum altitude separation, it is hypothesized that separation distance will weakly affect the number of admissible shells, but also that the effect will be larger for approaches that rely on actual latitude-based altitude separation between shells.

Explicitly simulating shell stacking for hundreds of different shell separation distances across several stacking techniques would be computationally burdensome. Instead, behavior is investigated using the simplified shell model across a wide range of shell separation distances ranging from 30 km to 100 m. The thickness of each shell is predicted by the shell estimation strategy. Shell inclinations are randomly sampled from the range $[10,100]$ degrees. Shell thicknesses are calculated using 3δ values for $d\omega = 1^\circ$, $de = 0.00002$, and $di = 0.1^\circ$. dA is computed as the lesser of one-third of the separation distance between shells or 2 km. Unlike in the numerical case, the GA is not run for each shell, and the true mean eccentricity is therefore unknown. To accommodate for this limitation, five shell-stacking strategies are investigated: $J_2 - J_3$ frozen shells stacked in random inclination order, $J_2 - J_3$ frozen shells stacked in sequential order of inclination, shells with a fixed mean eccentricity of 0.001 in random inclination order, shells with a fixed mean eccentricity of 0.001 in sequential inclination order, and shells separated based on an offset from the maximum altitude obtained at any inclination for each shell and its upper neighbor.

As seen in Figure 3.23, the simplified shell model shows significant gains to capacity from nesting of frozen inclinations (ordered or unordered), with the fixed mean eccentricity values in inclination order performing slightly worse. Randomly ordered fixed eccentricities still outperformed the worst-case altitude-based separation. Based on these modeling results, it appears that $J_2 - J_3$ stacking results tessellate better than numerical results for shells accounting for higher-order zonal terms, underestimating the benefits of inclination

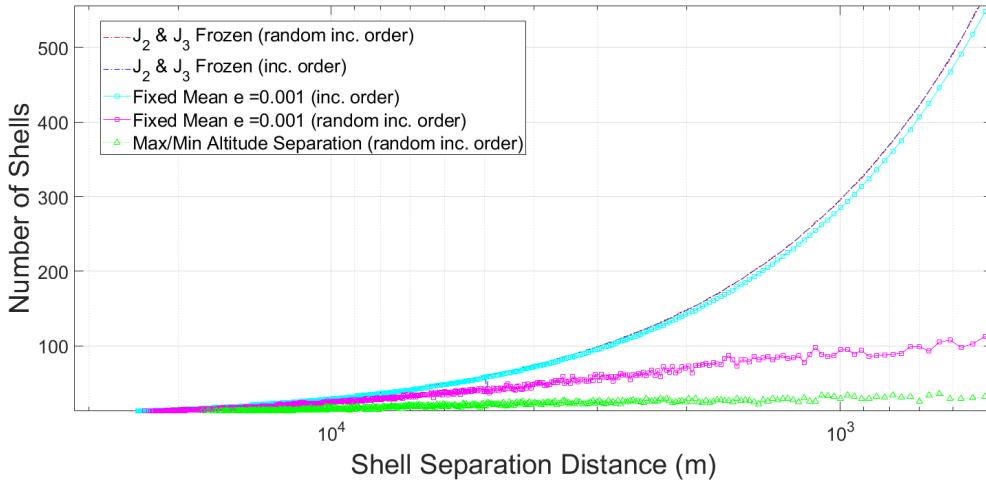


Figure 3.23: Admissible Shells for Various Shell Separation Distances.

coordination between nearby shells. Compared to the numerical results, the simplified shell model estimates approximately 57 shells for frozen eccentricity methods and 20 shells for the maximum and minimum altitude-based approach. This is a reasonable estimate for the maximum and minimum approach but an overestimate for the $J_2 - J_3$ numerical results, in part driven by the unaligned shells. According to the simplified modeling approach, for shell separation distances of approximately 7500 meters, shell-stacking techniques double the number of admissible shells versus the approach based on maximum and minimum altitude. This benefit, represented by the difference between the green and other lines in Figure 3.23, increases even further as shell separation distances become smaller.

3.7 Summary

This chapter introduces several techniques to design and analyze safe orbital shells to improve the sustainability of the space sector in congested regions. These techniques cover the definition of frozen osculating 2D-LFCs, the estimation of the shape and width of frozen shells in the latitude-altitude plane, and the assessment of orbital density under various shell ordering choices, including the explicit simulation of shells or the use of a simplified shell geometry estimation method. These techniques are applied to assess the performance and safety of different orbit designs for large constellations expected to be launched in the following years, with the goal of providing a set of tools to analyze and mitigate operational complexity, threats to space safety, and constraints to orbit placement associated with overlapping, non-coordinated large constellations.

Certain regions of LEO are oversubscribed with interested parties seeking to place more large constellations than can be accommodated using naive Keplerian spacing. Orbit design that takes advantage of the Earth’s geopotential can allow for closer stacking to more efficiently utilize orbital volume. The methods and results contained in this chapter demonstrate that the use of frozen orbits can be combined with geometric analysis in the altitude-latitude plane to ensure non-conjunction between shells. Such shells can be designed as 2D-LFCs

and therefore take advantage of considerable previous work on 2D-LFC design. The design burden associated with this technique is modest, as many operators will seek to freeze their orbits and maintain constant energy levels across satellites and orbits for their own station-keeping purposes.

Both capacity per shell and shell thickness influence aggregate intrinsic orbital capacity. Denser shell stacking will likely be the more critical driver as demand in LEO continues to increase. Previous work has demonstrated methods for estimating shell capacity and that large shell capacities are possible at reasonable orbital separation distances. Nevertheless, two factors constrain this result. First, our work to date limits shells to a single inclination due to concerns around differential RAAN precession. Second, while sharing a shell across multiple operators is fundamentally feasible, it has not yet been demonstrated on-orbit and would require extensive coordination among operators who have little incentive to do so if they are not required by either congestion of the space environment or a mandate.

As orbit demand increases, conversations between planned orbital neighbors will become increasingly important to ensure efficient and compatible orbits. Use of common constellation-agnostic methods and schema for discussing slotting and orbit coordination will be helpful to enable interoperability and prevent unsafe states. Such analysis would require information beyond that disclosed in most regulatory filings, including mean eccentricity and eccentricity vector information, intended station-keeping control box sizes (as opposed to general and overly expansive orbital tolerances), and greater precision in distinguishing between nominal, mean, and osculating numbers in orbit disclosures. If operators or regulators wish to adopt these or similar techniques, such sharing and explicit coordination can improve the efficiency with which operators make use of orbital volume.

Chapter 4

The LEO Packing Problem: Implications for Orbit Design and Policy

This chapter contains and expands on content from a conference paper I presented virtually at the 8th Annual Space Traffic Management Conference in Austin, Texas, in 2022. This chapter adds a discussion of reconfiguration and results from interviews with stakeholders regarding proposed adoption pathways [97].

4.1 Introduction

As the internationally shared LEO commons becomes more congested, there is a growing need to understand the implications of these proposals for aggregate orbital risk, develop smart ways to more efficiently make use of the finite orbital volume and risk budget, and understand the opportunity costs imposed by placing a particular constellation configuration at a given altitude.

The chief contribution of this chapter is an application of prior work on coordinated orbit design, or orbit packing, demonstrating how previous methods and theoretical results might be practically employed for orbit coordination and policy purposes. The chapter offers a high-level summary of our research on LEO orbit coordination and explains how these technical findings can contribute to understanding orbital constraints, encourage efficient use of orbital volume, and quantify what alternatives are foreclosed by a particular set of orbital uses. For detailed technical explanations of these techniques, interested readers are directed to the relevant papers [21], [22], [24], [93].

Before proceeding, it is important to distinguish between two related but separate definitions of orbital capacity. The first is *risk-based capacity*, which seeks to address the number and distribution of anthropogenic space objects (ASOs) consistent with a stable temporal evolution of the space environment. There is not yet consensus regarding criteria for constraints to risk-based capacity, but some potential examples include a stable or declining trend in the number of non-functional ASOs over time (either generally or in a particular altitude regime) and a background collision risk or anticipated collision avoidance maneuver frequency below some threshold value [101]. Risk-based capacity is characterized by significant uncertainty regarding the nature of the statistical distribution of inputs, potential

futures, and which specific future will actually be realized. Because of this, most attempts to measure risk-based capacity are either stochastic, seeking to extract information about the statistical moments of projected future distributions, or seek to evolve an average state as representative of the underlying distribution.

On the other hand, *intrinsic capacity* seeks to address the number and configuration of active ASOs that can be placed in a particular region of space in a manner that assures close approaches cannot generate collisions. In other domains, this is sometimes referred to as “seat” capacity [98]. In this work, we refer to this as both solving the orbit packing problem and as slotting. Intrinsic capacity is a much more restrictive problem framing: it considers only active spacecraft (since ensuring passive self-safety among debris objects is generally unfeasible) and requires trajectory definitions that do not admit collision risk. Nevertheless, it is highly relevant for the definition of large satellite constellations, where the high numbers of spacecraft involved mean that relaxing this self-safety requirement would produce vast numbers of conjunctions that elevate orbital risk and impose significant operational burden and complexity.

These two questions are separate but coupled measures of capacity. In an admittedly stretched metaphor, intrinsic capacity might ask how many cars can be transported across a given road network under nominal conditions and how this number compares to alternatives given other sets of potential roadway designs. Risk-based capacity would then ask what number of cars can be supported subject to anticipated weather distributions, road debris, and a requirement that the road network generate on average no more than a certain number of fatal crashes per year.

We emphasize that as used in this chapter, the orbit packing problem presents a theoretical framework to quantify efficiency but does not necessarily depend upon or presuppose a particular centralized authority to define and assign access to orbital slots or locations. Similarly, it is compatible with but does not require multiple operators to share orbital shells. Work on orbital separation between constellations is equally applicable for multi- and single-operator shells.

This chapter is divided into four sections. First, we describe our approach to the estimation of intrinsic capacity of active on-station spacecraft through slotting and quantify how to characterize the absolute and relative efficiency of a constellation configuration within a shell or a set of shells. Second, we describe potential pathways to implementation of LEO orbit coordination. Third, we offer recommendations for constellation design derived from our slotting research to date. Last, we conclude by summarizing the various roles orbit packing/slotting can play to help to advance space sustainability.

4.2 The Orbit Packing Problem

This section describes methodologies for construction of self-safe sets of constellation orbits and how to assess the efficiency with which particular shells or sets of shells make use of orbital volume. First, the fundamentals of the proposed orbit coordination mechanisms are explained. Then, methods to assess capacity of a single shell are explored. Questions are posed that quantify efficiency for various trade-offs. Three methods are described that can be used to estimate the capacity of a particular shell: direct enumeration, trend fitting using

power laws, and comparison to NSI orbits. Next, we explore intrinsic capacity in the context of potential reconfiguration of an orbital shell and explain various potential constraints on reconfigurations that can influence intrinsic capacity. Last, we discuss ways to assess the efficiency with which a particular set of shells makes use of orbital volume.

4.2.1 Preliminaries

In Arnas et al. [21], a proposed definition of the orbit packing problem is offered with three requirements that must be satisfied to generate a valid slotting solution. Solutions are said to consist of time-varying three-dimensional regions of space that meet the following criteria:

1. Each slot must maintain a certain specified minimum separation distance from all other slots at all times.
2. It must be feasible for a satellite to maintain a position within a slot. This does not require that slots exactly and passively follow the natural evolution of satellite trajectories, but simply that slots cannot require prohibitively large amounts of propulsion or infeasible state estimation and control. This criterion can be evaluated relative to either a known spacecraft’s capabilities or a baseline set of capabilities reasonably reflective of anticipated operator traffic.
3. A slotting scheme (but not necessarily a specific configuration) should be minimally burdensome. That is, it should be possible to accomplish a given mission under a slotted system using a similar number of satellites as under a non-slotted system.

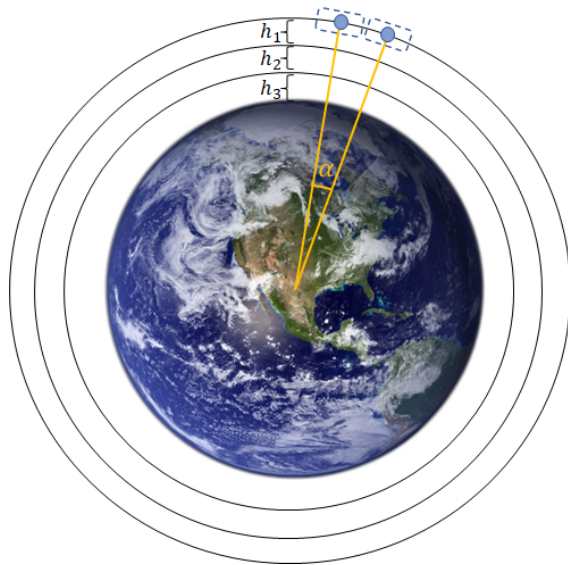


Figure 4.1: Self-Safe Shells Can Be Sequentially Nested.

Figure 4.1 demonstrates our proposed solution for near-circular orbits. Orbital volume can be divided into sets of concentric shells, with satellites placed within admissible locations on each shell surface that will maintain a certain minimum separation distance indefinitely

from one another. While this proposed solution is only applicable to circular and near-circular orbits, these orbits make up the overwhelming majority of proposed on-station spacecraft orbits, and highly eccentric orbits can still be handled by coordination and collision avoidance processes. Under the proposed system, orbital volume is divided into sets of concentric *shells* that constitute near-spherical surfaces of finite thickness, spaced such that no two shells overlap in volume. This means that orbital shells inherently maintain orbital separation from each other and that a satellite within one shell cannot ever pose a collision hazard against a satellite in another shell. Within each shell, *slots* are defined based on a uniform distribution of initial relative states known as a 2D-LFC. 2D-LFCs are defined by three integer constellation parameters: the number of orbits (N_o), number of satellites per orbit (N_{so}), and a configuration number that controls the way satellites in each orbit are phased relative to one another (N_c). Assuming that the Earth is a point-mass and that no other forces act upon satellites, a given 2D-LFC will follow Keplerian dynamics and all slot centers (or nominal satellite positions) will share a semi-major axis, eccentricity, inclination, and argument of perigee.

The minimum angular separation distance that occurs for a 2D-LFC is not known *a priori* from its configuration parameters and may be 0° . Avendaño et al. [22] proposed a method to efficiently determine the minimum separation distance between any pair of satellites within a circular Keplerian 2D-LFC. Using this formula and the inherent symmetries of these constellations allows for the efficient calculation of minimum separation distance for a 2D-LFC in linear time. This allows for screening of Keplerian separation distance between slots very quickly without any propagation. The methodology can thus be used to exhaustively search all circular Keplerian 2D-LFCs up to an arbitrary size to calculate solutions that are self-safe and identify the solutions that maintain the largest minimum separation distances for a certain number of satellites and inclination.

Lifson et al. [93] described methods to adjust the orbital states for a 2D-LFC to maintain quasi-stable and periodic orbits in the presence of a more realistic aspherical Earth gravity field. Under this model, shells can be coordinated so that while slot altitudes vary, they do so in a coordinated manner which ensures that adjacent shells preserve minimum separation from one another even accounting for these shifts. Figure 4.2 shows three shells generated using the zonal freezing technique from [93]. As can be seen in the figure, the shells can nest closer than the osculating variation in semi-major axis for each shell and still maintain coherency and safety. This can be seen in Figure 4.2, where the yellow and red shells are placed overlapping the altitude range of the aqua shell, but do so in a way that ensures the shells still maintain separation at all times. While minimum separation distances do not map perfectly from Keplerian 2D-LFCs to those defined in the presence of higher-fidelity gravity, they are close enough for Keplerian-based minimum separation distance to still be useful as an initial screening metric, which can be subsequently verified with standard conjunction screening methods. Lavezzi et al. [95] explored the ability of satellites with electric propulsion to maintain these orbits and estimated the number of shells and slots that could be admitted for various levels of caution in orbital separation. While electric propulsion systems in LEO can face atomic oxygen corrosion and aging issues, their widespread adoption implies that these issues are manageable.

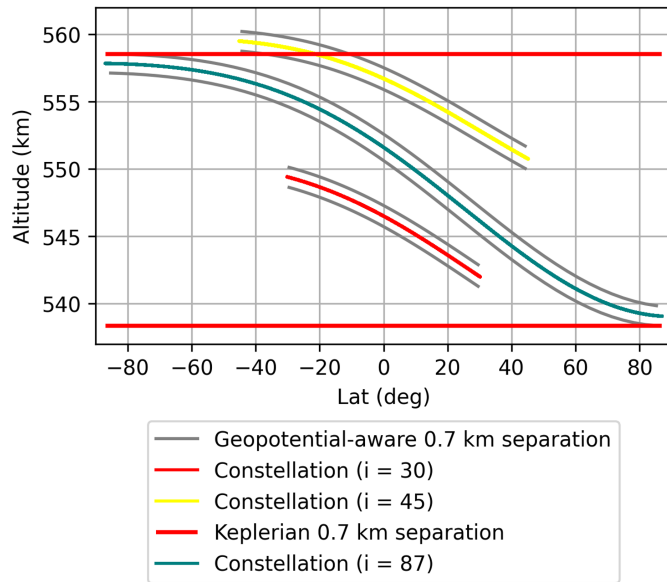


Figure 4.2: Nested Quasi-Periodic 2D-LFC Shells.

4.2.2 Capacity per Shell

This subsection describes how to use shell capacity as a tool to assess efficiency of orbital use. First, several potential framings for capacity evaluation are presented. Different framings are useful for different contexts, namely whether capacity should be compared against alternatives for a particular operator’s constellation or competing uses for the same orbital region. Another relevant consideration is whether calculated capacities should consider opportunities for compatible use by others sharing the shell. Three methods are then presented to calculate the actual capacity of a shell: direct (exhaustive) enumeration of possibilities, the use of trend lines to fit empirical capacity data, and the use of NSI orbits to estimate trends with greater fidelity. Relevant considerations for reconfiguration problems are described, and several examples of efficiency calculation are demonstrated.

Benchmarking Context

There are multiple ways in which capacity can be understood using metrics. At the simplest level, the number of satellites per shell is an absolute capacity metric. Shell capacity can also be understood in relative terms to understand opportunity cost versus potential alternative scenarios. For relative benchmarking, a given constellation design can be compared to alternatives that are equal to or improving in number of satellites and minimum separation distance. Alternatively, the design may be compared against designs that exceed a particular minimum separation distance. Such a distance might be chosen using analysis to estimate the smallest value that either the proposed constellation or a hypothetical benchmark satellite will be able to maintain based on factors such as control strategy, state estimation quality, and anticipated orbital perturbations—chiefly solar activity and the resulting impact on atmospheric density.

There are several useful questions that can be asked regarding shell capacity:

1. How does the number of slots under the chosen configuration compare to alternative configurations at the *same* inclination?

- Are there larger numbers of satellites than could be admitted relative to the reference minimum separation distance (either the notional constellation design or the chosen minimum separation distance)?
- Can a larger separation distance be achieved for the same or a greater number of satellites?

This question basically examines whether an alternative constellation design could include more satellites for the same minimum separation distance or based on the minimum separation distance that constellation satellites can maintain. There may be good reasons for a suboptimal configuration (e.g., coverage), but this form of analysis helps answer what else could have been placed as an alternative by the same operator at the same inclination.

2. How does the number of slots under the chosen configuration compare to alternative configurations at *different* inclinations for either the same number of satellites or the same minimum separation distance?

- Are there larger numbers of satellites than could be admitted for the reference minimum separation distance at any inclination (either the notional constellation design or the chosen minimum separation distance)?
- Can a larger separation distance be achieved for the same or a greater number of satellites at any inclination?

This question looks at what else could have been placed in the same shell with fewer restrictions, more closely approximating use by another operator with potentially different mission requirements.

3. What is the maximum number of satellites that can be admitted given feasible reconfigurations of the proposed constellation and the reference minimum separation distance? How does this compare against a clean-sheet capacity estimate that does not require compatibility with the original constellation?

For questions 1 and 2, the only relevant consideration is how many satellites the chosen configuration supports. This limitation arises since the operator's choice is assumed to be exclusive of other operators when evaluating alternatives. In this category, the operator's choice is not assumed to be exclusive, but rather as imposing an inclination and compatibility constraint on subsequent users seeking to also use the same shell. In this approach, comparison is most meaningful when based on the minimum separation distance technically achievable by that operator or anticipated co-tenants of the shell, whichever is more restrictive. Armed with this information, it is generally possible to compute potential reconfigurations (either strictly preserving the original slot locations or allowing small changes) using methods from Arnas and Linares [24].

The following three subsections describe methods to estimate the minimum separation distance of a particular 2D-LFC. Direct enumeration leverages a precomputed database of 2D-LFCs subject to a two-body circular orbit assumption. Trend fitting extracts power-law fits based on the database, trading fidelity for a simpler but reasonably accurate approximation that can also (carefully) be extended beyond the region of consideration in a computed database. The third method relies on the observation that a particular class of orbits, known as NSI orbits, is a reasonable proxy for a lower bound for high-capacity 2D-LFC solutions. This approach internalizes some of the structure of the problem not considered by the power-law approach. Fourth, intrinsic capacity is evaluated factoring in potential reconfiguration subject to different assumptions about feasible expansions. The total number of admissible slots after reconfiguration is used to identify remaining unconsumed intrinsic capacity.

Direct Enumeration and Database

This is the most direct method to estimate shell capacity. To answer the first two questions, 2D-LFCs are exhaustively enumerated and compiled. The chosen configuration can be compared against this database to examine capacity at the same minimum separation distance and inclination (question 1) or across all inclinations for either number of satellites or minimum separation distance (question 2).

A database has been constructed based on the largest angular separation distance for a particular inclination and number of satellites (N_{sat}) pairs. The 10 best 2D-LFCs for each N_{sat} from 1 to 15000 satellites were calculated for a 0.1° discretization of inclination from $0-90^\circ$. The inclusion of multiple near-optimal solutions is intended to enable searches that cross-reference capacity with reconfiguration, coverage optimizations, or other factors, recognizing that some of the highest-capacity solutions produce non-uniform Earth coverage or may have other undesirable properties.

Minimum angular separation distance is independent of altitude under a Keplerian model, meaning the database only needs to be constructed once. Accounting for the Earth’s oblateness introduces an altitude dependency that means the database must be recomputed as a function of mean altitude. Naturally, coverage is also an altitude-dependent quality.

We now demonstrate this approach with an example by applying it to a 60° 2D-LFC flower constellation with 1722 slots with parameters ($N_o = 246$, $N_{so} = 7$, $N_c = 224$). The configuration is plotted over the Earth in Figure 4.3 and has a minimum angular separation distance of 1.013° . In this example, the first two questions will be evaluated relative to the original constellation for simplicity, but the calculations can be performed relative to a reference minimum separation distance (e.g., 1°) using the same methodologies. No attempt is made to assess these orbits for coverage properties (which are important but mission specific).

Direct Database Example: We compare this constellation against the database of the best 10 2D-LFCs by minimum angular distance for every N_{sat} with 0.1° discretization in inclination. These results can be seen in Figure 4.4 for the same inclination as the original 2D-LFC. The gray improving region of the figure contains constellations that have a greater separation distance for a certain number of satellites, number of satellites for a certain separation distance, or both. For this particular inclination, we find that this constellation ($N_o = 246$, $N_{so} = 7$, $N_c = 224$, $\alpha = 1.013$) is the best capacity constellation for 1722

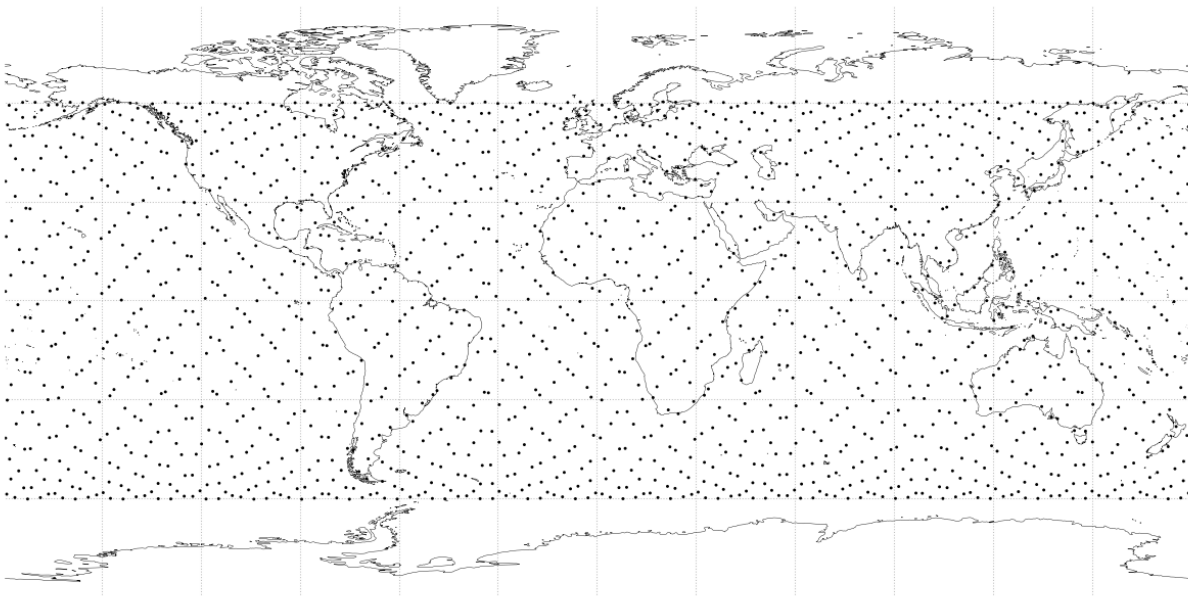


Figure 4.3: Distribution of a 2D-LFC ($i = 60^\circ$, $N_o = 246$, $N_{so} = 7$, $N_c = 224$). The constellation is self-safe.

satellites. For the same N_{sat} , the second-best constellation is ($N_o = 861$, $N_{so} = 2$, $N_c = 746$, $\alpha = 0.873$), although it is evident that slight changes in N_{sat} would yield better solutions than this alternative. There are several larger solutions that have smaller minimum separation distances. These are: ($N_o = 1758$, $N_{so} = 1$, $N_c = 1136$, $\alpha = 1.030$), ($N_o = 1765$, $N_{so} = 1$, $N_c = 629$, $\alpha = 1.021$), and ($N_o = 1803$, $N_{so} = 1$, $N_c = 701$, $\alpha = 1.126$). Comparing to the database, the original constellation has the greatest minimum separation distance for 1722 satellites at 60° inclination, but it would be possible to increase minimum separation distance by 11.1% and capacity by 4.7% with ($N_o = 1803$, $N_{so} = 1$, $N_c = 701$, $\alpha = 1.126$).

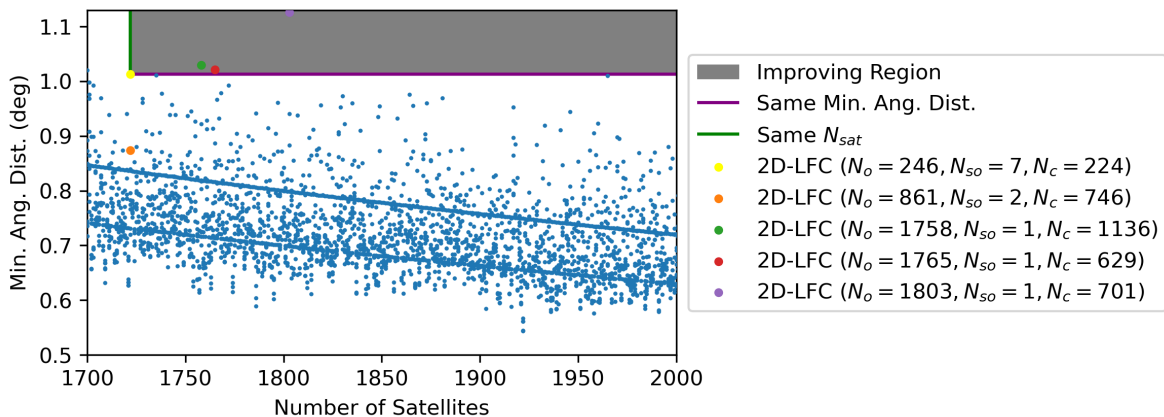


Figure 4.4: Direct Database Capacity Results ($i = 60^\circ$). The gray region improves separation distance or number of satellites at the same inclination.

We next examine capacity assuming no constraint to inclination. As seen in Figure 4.5, there are many solutions that have better minimum angular distance or number of satellites relative to the original constellation. In particular, the best minimum angular distance is achieved for ($i = 50.6^\circ$, $N_o = 866$, $N_{so} = 2$, $N_c = 643$, $\alpha = 1.19321$) and the best number of satellites is achieved for ($i = 56.9^\circ$, $N_o = 2056$, $N_{so} = 1$, $N_c = 1082$, $\alpha = 1.023738$), although there are also many other solutions in the improving region. These two constellations achieve improvements in minimum angular distance and N_{sat} of 17.8% and 19.4%.

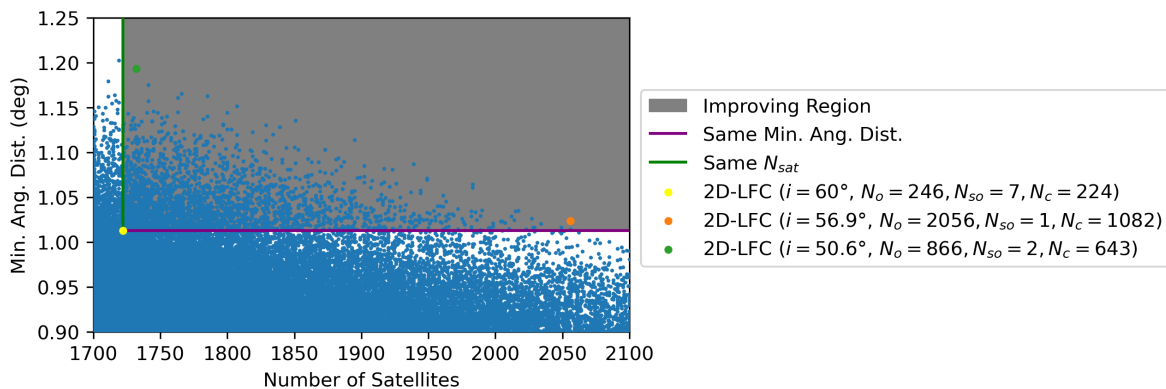


Figure 4.5: Direct Database Capacity Results (any Inclination). The gray region improves separation distance or number of satellites.

Trend Fitting

Results from Subsection 4.2.2 can be used to fit empirical trend lines. Specifically, power laws can approximate the relationship between minimum angular distance and number of satellites, with equations fit to various inclinations and assessed for accuracy in Avendaño et al. [22].

While results were only reported for these inclinations in Avendaño et al. [22], this process can easily be repeated for any discretization in inclination and capacity region of interest. This technique has the advantage of being extremely fast to use once fits are calculated and does not require direct use of large databases. Nevertheless, it adds error, as it cannot capture the variance in capacity/angular separation relationships that is not included in general capacity trends. Particular caution is necessary when power laws are extrapolated to N_{sat} values far from the fitted data. We now demonstrate the trend-fitting approach with the same example as the previous section.

Trend-Fitting Example: We can compare the value against the trendlines using the approach in Avendaño et al. [22]. To avoid skewing the curve, only the best solution per N_{sat} is used for fitting. Using the results for $i = 60^\circ$ in Table 4.1 predicts a minimum separation distance of 0.896° . This is an under-prediction of 11.5%. Alternatively, we can predict the number of satellites based on the minimum separation distance. Here we get 1487 satellites, rounding to the nearest integer, an under-prediction of 13.6%.

To compare against values for other inclinations using this method, a new set of power laws is computed with 0.1° discretization. To do this, the log of N_{sat} and angular distance

Table 4.1: Best Fit Power Laws for $angdist[deg] = c \cdot N_{sat}^b$ and Goodness of Fit. Reproduced from [22].

incl	c	b	R^2
10°	155.21	-0.7321	0.9955
20°	368.85	-0.8129	0.9948
30°	458.86	-0.8295	0.9944
40°	482.97	-0.8329	0.9933
50°	484.94	-0.8360	0.9918
60°	447.34	-0.8338	0.9909
70°	392.54	-0.8317	0.9890
80°	350.94	-0.8419	0.9884
90°	360.99	-1.0004	0.9996

data are taken for each inclination and a linear fit is performed in loglog space before being transformed back into linear space. To minimize the effect of values far from the region of interest ($N_{sat} \approx 1700$), fits were performed using data for $500 \leq N_{sat} \leq 2000$, a range chosen based on an examination of fitting residuals. This reduces R^2 values compared to fitting with a longer window simply because there is more variance in this region that is not explained by the power law.¹ The fit for $i = 60^\circ$ can be seen in Figure 4.6, and residuals can be seen in Figure 4.7.

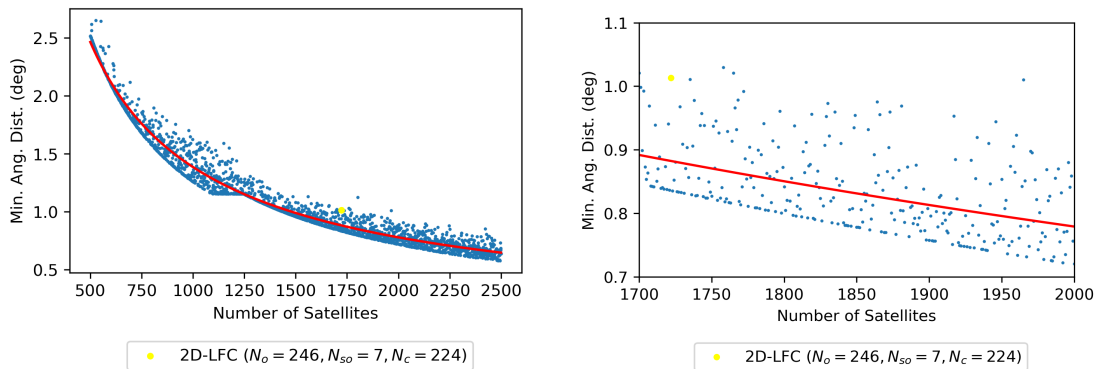
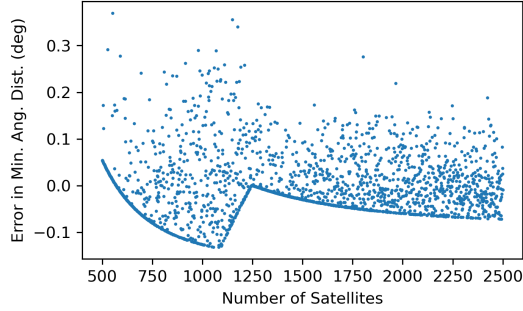


Figure 4.6: Power Law Fit ($c = 429.811$, $b = -0.8305$, $R^2 = 0.97661$). The power law reasonably models the relationship between number of satellites and minimum separation distance for the fit region.

While the power laws do a reasonably good job in capturing the general relationships, they do not capture the full pattern of the data, as seen in Figure 4.7. As a result, it is not possible to extract meaningful exact optimization values, particularly for higher inclinations. This is demonstrated visually in Figure 4.8.

¹The selected fitting domain depends on the domain of interest for analysis, with more localized fits outperforming global fitting because local fits tend to cross fewer of the jumps associated with transitions between different capacity-dominant sets of NSI cycle periods. This is described further in Subsection 4.2.2.



(a) Residual Error from Power Law Fit.

Figure 4.7: Angular Distance to N_{sat} relationship for $i = 60^\circ$. Not all structure of the data is captured by a power law.

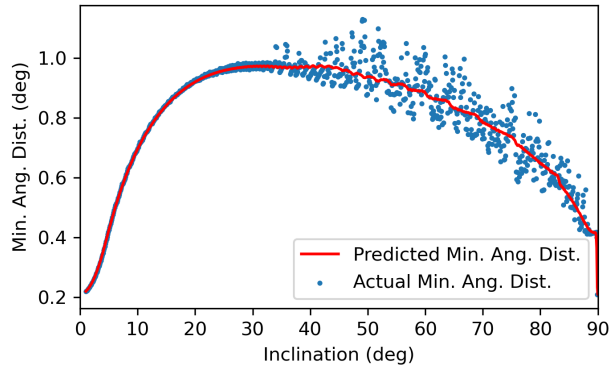
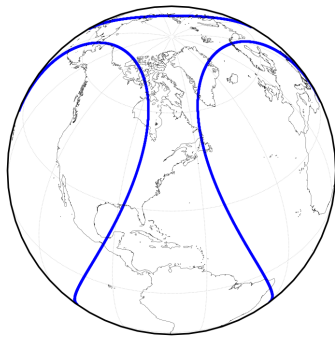


Figure 4.8: Power Law Angular Distance Predictions and Actual Values for $N_{sat} = 1722$. Data dispersion varies with inclination.

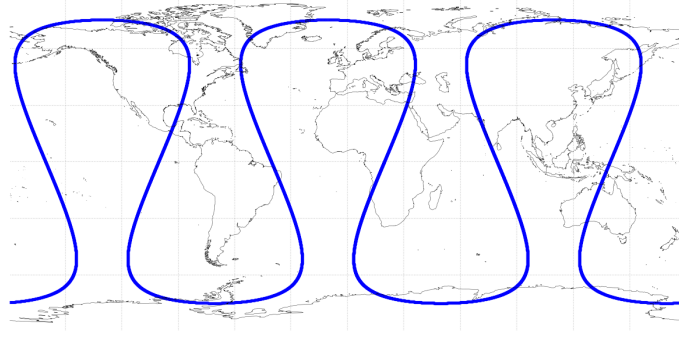
NSI Orbits

The capacity metrics in the previous two subsections were generated empirically; however, Arnas and Linares [23] propose a method that uses a subset of 2D-LFCs known as NSI relative trajectories to define a capacity bound. As seen in Figure 4.9, these constellations appear as a single closed trajectory with no overlaps when viewed in the appropriate rotating frame. These constellations tend to be significantly more stable and reconfigurable than constellations distributed over self-intersecting relative trajectories and appear to define a lower bound for minimum distance among near-optimal solutions that can be used as a reasonable metric for orbital capacity. Unfortunately, NSI trajectories tend to have time-varying coverage properties that make them less attractive for global telecommunication applications unless layered with synchronized orbital precession, a method described in Arnas et al. [78]. This subsection now demonstrates the NSI orbit comparison approach for the example from the prior two sections.

NSI Orbits Example: We can compare capacity against a piece-wise capacity curve composed of the maximum angular separation distance of an NSI trajectory for each N_{sat} . As seen in Figures 4.10 and 4.11, this curve forms a lower bound for the best 2D-LFCs in terms of minimum angular distance and number of satellites. Note that while the power



(a) Three-Dimensional View.



(b) Two-Dimensional View.

Figure 4.9: An Example of an NSI Trajectory ($N_d = 2, N_p = 3$). NSI trajectories act as a lower bound on high-capacity 2D-LFC solutions.

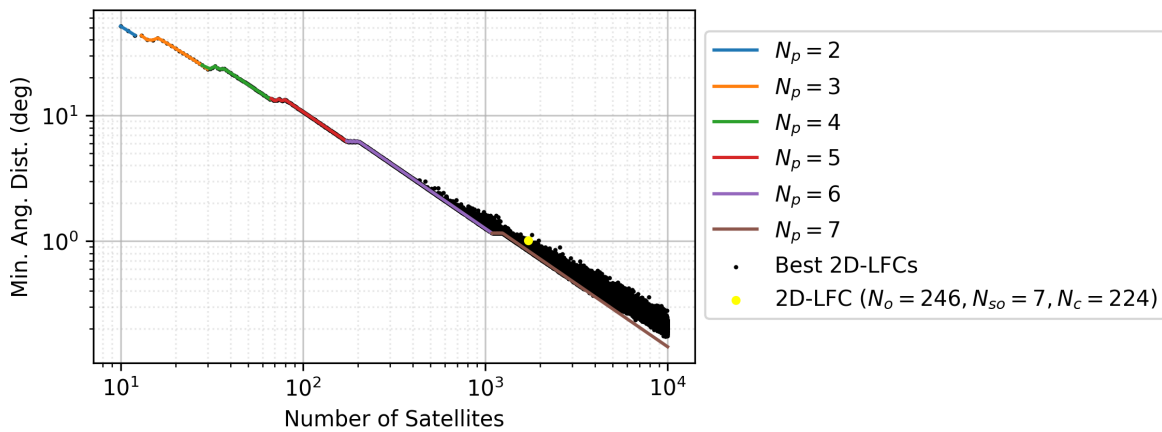


Figure 4.10: NSI Capacity Curve ($i = 60^\circ$). Adapted from [23]. The NSI constellations are a reasonable lower bound for high-capacity 2D-LFCs.

law in Figure 4.6 follows the middle of the distribution, NSI orbits instead provide a lower bound to capacity here. This bound can serve as a precise reference value for efficiency, as compared to power laws, and is not skewed in the same way by the sample range chosen to fit the curve. As seen in Figure 4.12, the NSI method performs very well for constellations of up to about 500 satellites, at which point it becomes a conservative lower bound for capacity that underpredicts the minimum separation distance by up to 50% for some of the optimal constellations by the end of the region examined.

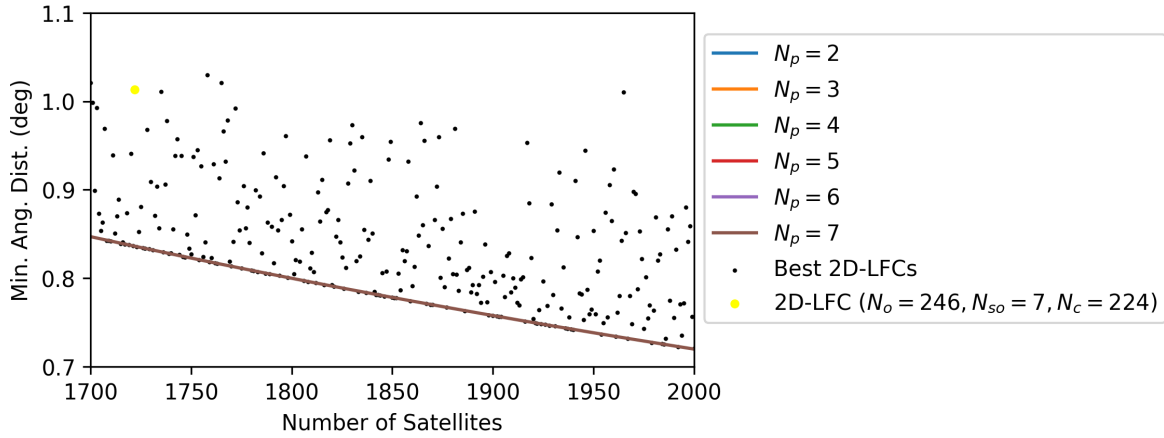


Figure 4.11: NSI Capacity Curve ($i = 60^\circ$). Unlike the power law, the NSI orbits are a lower bound.

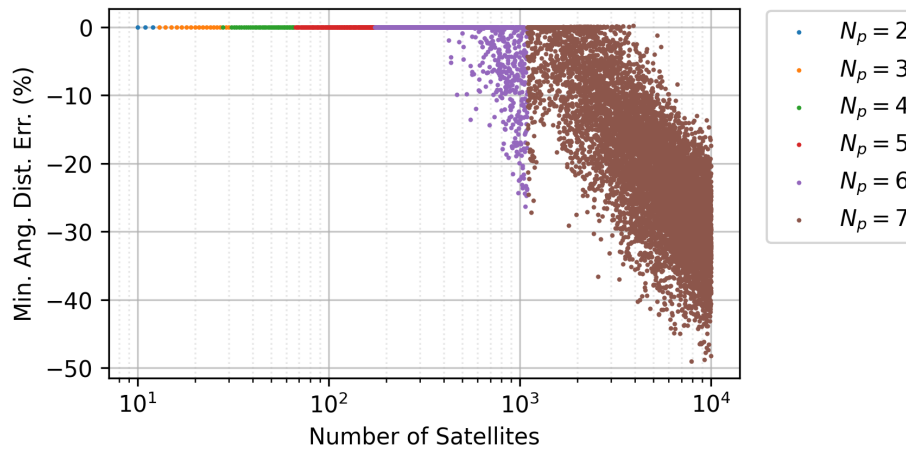


Figure 4.12: NSI Prediction Error vs. Best 2D-LFCs ($i = 60^\circ$). Error for the NSI approach increases with the number of satellites.

Reconfiguration

Arnas and Linares [24] describe several ways to potentially reconfigure sets of slots within a shell based on various different design constraints set by the operator(s) intending to occupy the shell. These include:

1. Shall the centers of the original slots be maintained exactly or shall minor adjustments to orbital plane and RAAN be allowed?
2. If minor adjustments are allowed, shall they be permitted in only the orbital plane, in RAAN, or both?
3. Shall the larger reconfiguration maintain uniformity or is a non-uniform distribution permissible?

Reconfigurations can be designed starting from either the initial constellation and optimizing the final constellation, starting from the final constellation and optimizing the initial constellation, or through a bi-directional search. Because the original satellites impose limits on admissible orbit structures arising from the reconfiguration process, reconfigured results may underperform when compared to initial or final orbit configurations optimized for capacity without this constraint. This penalty takes the form of a smaller minimum separation distance for a given number of satellites, as compared to more optimal alternatives identified using one of the previous three methods. The more restrictive the assumptions (e.g., exact maintenance of the original slots or an exact number of final slots after reconfiguration), the larger the penalty tends to be.

Figure 4.13 presents an example of calculating future potential reconfiguration possibilities. The large blue circles correspond to the original slot locations. The green dots represent an exact expansion corresponding to the requirement that slot centers be maintained exactly. The cyan dots represent a reconfiguration allowing minor adjustments in orbital plane. The magenta dots correspond to a constellation allowing adjustment in both orbital plane and RAAN.

Future Potential Reconfiguration Possibilities Example: We now suppose that the 2D-LFC with parameters ($N_o = 246$, $N_{so} = 7$, $N_c = 224$, $\alpha = 1.013$) has been placed into orbit in a particular shell. To aid users curious about how these reconfigurations are performed, this example is chosen to follow the examples provided in Arnas and Linares [24]. As with previous examples, these are computed using analytical minimum separation distance formulas for Keplerian orbits that would need to be checked numerically for osculating equivalent constellations at the altitude of interest.

We assume the 2D-LFC is placed at a particular altitude that is in high demand and that there is another operator who would like to deploy satellites at the same altitude in a compatible manner. What is more, we assume that while the original constellation design preserves a minimum 1° of separation, the satellites themselves are capable of maintaining position within a 0.2° control box.

Based on this control box size, it is possible to calculate the remaining number of slots that may be placed in a manner compatible with the original constellation to generate a utilization percentage for the shell. This number is sensitive to the restrictions on slot center adjustment and uniformity. For the purpose of this analysis, we assume that only uniform expansions are desirable. In practice, a non-uniform expansion leveraging necklace constellations [77], [84], [96], [115] may be more useful for designing compatibility between two known constellation designs, particularly if one or both constellations are non-uniform.

If the centers of the original slots must be maintained exactly, the best solution is ($N_o = 984$, $N_{so} = 7$, $N_c = 470$, $\alpha = 0.206$). Because this constellation contains 6888 satellites, the original constellation has utilized 25% of the intrinsic capacity of this shell. This highly restrictive condition is often unnecessary, as slight deviations to slot centers can admit additional solutions, either with acceptable but minor rephasing by the original constellation or without requiring modification to the reference trajectories of the original constellation (because the changes are still encompassed in the size of the original slots).

More solutions are possible if we further assume that the original constellation is willing to slightly relocate satellites in mean anomaly and RAAN to accommodate orbit sharing with an expanded structure. If reconfiguration of in-track location is permitted, but not

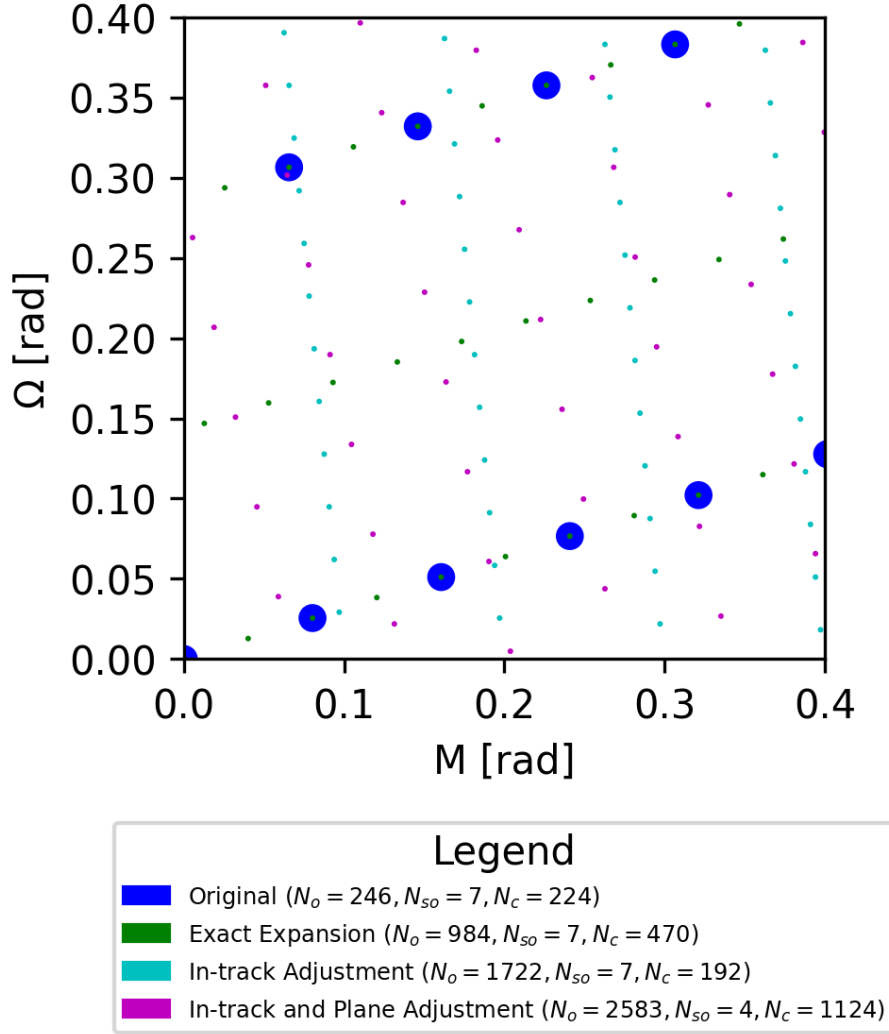
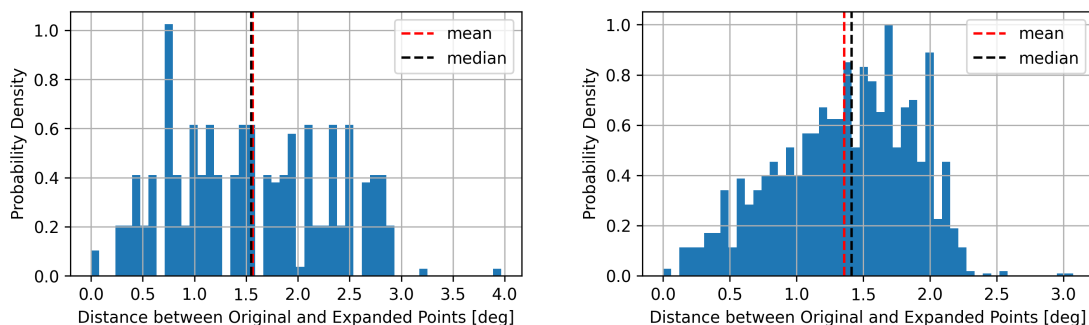


Figure 4.13: Original and Reconfigured Shells (Partial View). Fewer constraints allow higher-capacity expansions to the original set of slots.

reconfiguration in orbital plane, the best solution is is ($N_o = 1722$, $N_{so} = 7$, $N_c = 192$, $\alpha = 0.204$), meaning that only 14.3% of capacity has been used. If the original constellation (or decision authority) is able to accept modification in both in-track and cross-track slot locations, this admits other solutions. In this case, allowing adjustments to the orbital planes does not improve on the constant-plane solution. Nevertheless, other solutions, such as ($N_o = 2583$, $N_{so} = 4$, $N_c = 1124$, $\alpha = 0.208$), do exist and could be preferable for some other technical or operational reason. This solution would involve shifting the original orbital planes by 0.0348° , significantly less than the diameter of the original or new slots.

While not demonstrated here, it is also possible to constrain the magnitude of in-plane and in-track reconfiguration such that the reconfigured slots do not exceed the bounds of the original unexpanded constellation, minimizing the impact on the original constellation [24]. Such a constraint further limits admissible expansions and tends to work better if the original

constellation and expansion are jointly determined in advance, as constellations with similar coverage and performance sometimes have very different suitability for expansion. Additionally, in this example we do not consider solutions that involve slight adjustments to the nominal inclination of the chosen slotting structure, but such adjustments can also increase capacity further by admitting more possibilities, potentially without requiring changes to the original reference constellation.



(a) (In-Track Modifications $N_o = 1722$, $N_{so} = 7$, $N_c = 192$, $\alpha = 0.204$) (b) In-Track and Plane Modifications ($N_o = 2583$, $N_{so} = 4$, $N_c = 1124$, $\alpha = 0.208$)

Figure 4.14: Histogram of Slot Center Adjustments from Expansion. The in-track only modification is higher capacity but results in slightly large relocations than a solution with both in-track and plane adjustments.

A view of a partial subset of these distributions in the mean anomaly and RAAN space is presented in Figure 4.13, with slots sized to reflect their on-orbit diameters. The distribution of distances between original and reconfigured slots for the cases requiring shifts to the original constellation is presented in Figure 4.14.

4.2.3 Number of Shells in LEO

The previous subsection dealt with quantifying the efficiency with which a particular shell makes use of orbital volume based on the number of admissible slots. This section describes ways to quantify the efficiency with which a set and ordering of shells makes use of orbital volume. Because methods are explicitly described with examples in Chapter 3, these examples are not repeated here. Rather, we draw on analysis from that chapter to provide qualitative methods to assess efficiency of a given configuration of compatible orbital shells.

There are numerous large constellations planned in LEO, with several shells proposed for either the same or overlapping adjacent altitudes, especially in the 450–650 km altitude range. Large constellations with overlapping altitudes pose an ongoing collision hazard to one another, significantly increasing orbital risk and the operational and coordination burden associated with collision avoidance maneuvers. The inherent osculating radial variation experienced by Earth-orbiting satellites complicates orbital compatibility. While a satellite’s orbital radius is constant in an unperturbed two-body model, even an orbit with zero mean eccentricity vector experiences variations due to the Earth’s asphericity, chiefly the Earth’s oblateness. This range is largely inclination dependent and on the order of 8–10 km in LEO

(but more for higher-inclination orbits) [102, p. 663]. In general, more shells in an altitude range indicate denser, more efficient use of orbital volume (although the number of satellites per shell also strongly influences density).

Quantifying Shell Efficiency

There are multiple potential ways to quantify the efficiency with which operators make use of LEO orbital volume. Shell width is largely (but not entirely) independent of constellation size. In Figure 4.15², three metrics for shell-stacking efficiency are described. Under a realistic Earth geopotential, shells experience some amount of vertical variability about the centerline curve, with other orbital perturbations adding further variation between restoring maneuvers. For an individual shell, the most relevant parameter is the maximum shell width across all latitudes of the shell (first proposed in Bombardelli et al. [92]) and seen as the black arrow in Figure 4.15. For a set of several shells, one can consider the number of shells that may be admitted in the orbital region from the minimum to maximum altitude reached by any shell (sky blue), assuming a minimum separation between shells of at least a certain safety distance (pink). Efficiency in this metric is driven largely by the extent of shell tessellation in latitude-altitude space. Because shell widths are largely invariant to the specific proposed slotting configuration within the shell, inclination is the major design driver, as it dictates the quasi-periodic eccentricity, argument of perigee, and shell shape. Shell configurations should be assessed for both their individual widths and the efficiency of shell tessellation. Less separation distance between shells, given sufficient separation and margin to still ensure non-intersection, also improves density of orbital use.

As seen in Figure 4.16, because frozen eccentricity is a function of inclination and a major determiner of shell shape, nearby shells can pack more tightly if adjacent shells use similar inclinations, particularly if inclinations can be “laddered” across successive sets of shells. Thus, Figure 4.16b can be said to be more efficient than Figure 4.16a. A sequential ladder of orbital shells with relatively tight discretization of inclinations (e.g., 5° or 10°) constitutes a reasonable reference scenario against which to benchmark other solutions.

To ensure reasonable reference shell width, these shells should be generated using numerical orbit freezing methods, standardized assumptions for additional safety margins between shells, and an assumed duration between restoring maneuvers (e.g., 30 days). Operators with good space situational awareness and intending to use electric propulsion or frequent station-keeping could naturally reduce shell widths relative to this reference scenario and maintain tighter spacing between shells [95].

It may be desirable to leave empty “road” shells between shells for phasing and contingency maneuvers, a concept first mentioned in Arnas et al. [21]. Whether these actions should occur in the safety margin between shells and the gray safety margins shown or in empty space outside of these safety margins is a topic that should be discussed among operators and may vary for different LEO regions and shell densities.

²For clarity, the shells in this figure and Figure 4.16 are designed to be thinner than similar figures in Chapter 3.

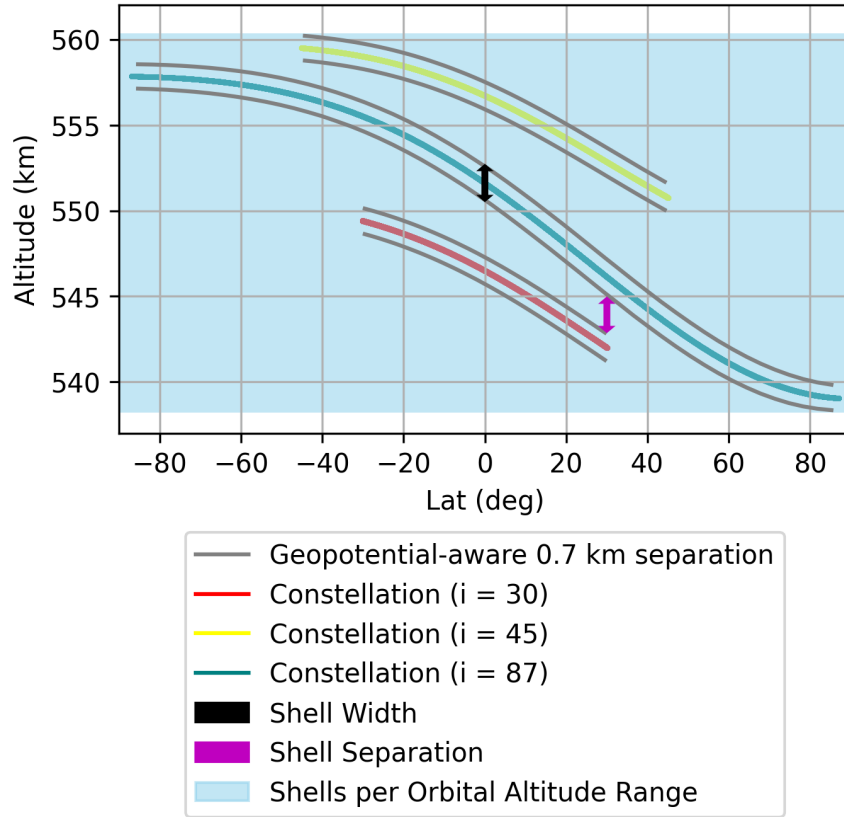


Figure 4.15: Metrics for Shell-Stacking Efficiency. This figure is a modified and annotated version of Figure 3.19 assuming propagation under a zonal gravity model.

4.3 Pathways to Implementation for Orbit Coordination

There are several distinct aspects of this work with policy implications. First, these techniques provide a way to define a reference scenario and assess the efficiency of a proposed shell or shells and associated slotting configurations. Current discussions for orbital capacity and efficiency are largely qualitative and subjective. Efficiency analysis can help inform mission authorization workflows by regulators concerned about orbital efficiency of the constellations they authorize. Similarly, clear, objective technical criteria can help lend additional regulatory clarity and certainty to operators on both how to design efficient constellations and how such designs might be assessed.

Secondly, examination of satellite reconfiguration options, as proposed in Section 4.2.2, helps identify remaining intrinsic orbital capacity within particular shells (albeit premised on a multi-operator shell sharing model). Regulators may have related but distinct interests in ensuring both efficient use of available orbital volume and stewardship of finite orbital volume. Understanding remaining orbital capacity may also help inform authorization conditions (e.g., maximum acceptable orbital tolerances or technical requirements for ability to safely operate at a given minimum separation distance) and authorization decisions.

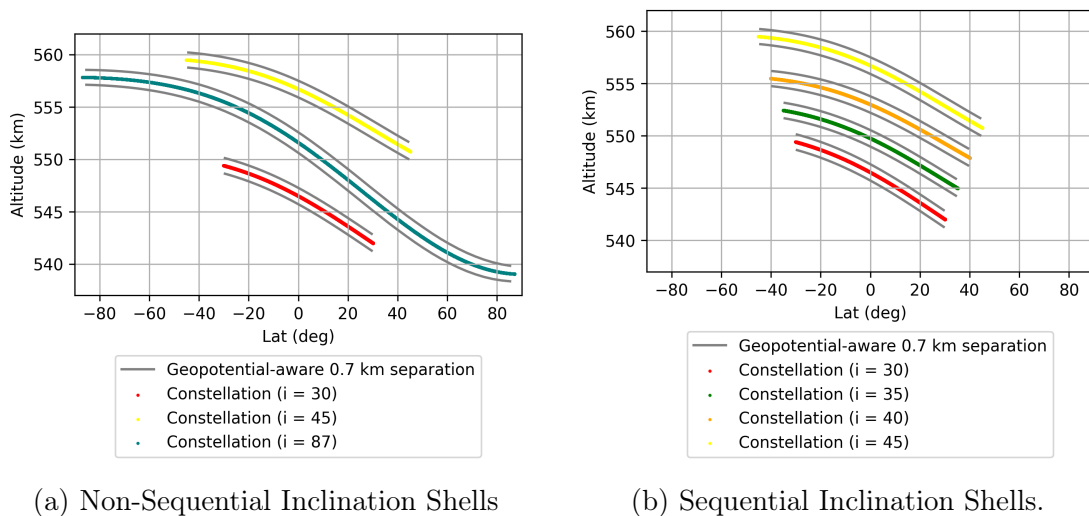


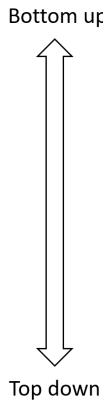
Figure 4.16: Shell Tessellation for Sequential and Non-Sequential Inclinations. Similar adjacent inclinations improve capacity. This figure is a modified version of Figure 3.20 assuming propagation under a zonal gravity model.

Third, it is useful to discuss potential pathways that could lead to the adoption of cross-operator coordination through use of slots and shells as envisioned in this work. At its core, orbit coordination through slotting is a commons-management technique, applied to a technically complex international commons with unfettered national access guaranteed by international law. Four potential pathways are described in Figure 4.17. Potential adoption pathways are distinguished largely by three questions:

1. What, if any, mechanisms exist to enforce an orbit coordination/slotting system?
2. Who gets to choose which shells and slotting configurations should be defined in different regions of LEO?
3. Who decides what operator or operators are able to use a particular slot or slots in a given shell?

These mechanisms span the gamut from purely voluntary coordination between operators to a binding system managed by an international organization similar to the process for GEO. LEO access demands similar balancing to achieve “rational, equitable, efficient and economical” outcomes as described in the ITU’s mission. Choices regarding shell and slot configuration designs could be handled in a way analogous to spectrum: an allocation process that sets aside frequencies or orbits for certain purposes with various rules and coordination requirements and an assignment process that provides operators with permission to use a particular allocation. Four concepts are briefly defined in turn:

Norms-based: Under this concept, one or more operators would announce their intention to use a slotted orbit framework and request that others intending to use nearby altitudes do so in a way that is compatible with their proposed slotting system. The process



Approach	Enforcement	Shell/Slot Allocation	Shell/Slot Assignment
Norms-Based	None	First mover	First come
Inter-operator negotiated legal coordination mechanism	Contracts	Contract parties	Negotiated agreement (not binding on others)
	State regulator	Involved operators (approved by state regulator)	Only binding on those under state regulator jurisdiction
Launching state authorization conditions	State regulator	State regulator	State regulator
Internationally coordinated shell design and/or allocation & assignment framework	States	Agreement between states through international entity	States through process at international entity (first come vs. planning issues like GEO?)

Figure 4.17: Potential Implementation Pathways for LEO Orbit Coordination and Key Differences.

of announcing and requesting is what distinguishes this process from an operator simply deploying a uniform constellation. An operator taking this approach could do so in a manner that is premised on exclusive shell allocations, such that the coordination aspect only involves the definition of neighboring shells, or regarding permissible satellite locations within an operational shell. At the risk of encouraging confusion, an operator could potentially seek something in the middle, encouraging other users to not deploy at its altitude but requesting that those who do so anyway use defined slots and deploy spacecraft with sufficient technical ability to station keep within slots of a certain size. Under such a system, the operator announcing an intention to slot has no way to compel others to adhere to the request. To encourage voluntary compliance, an operator could indicate that it would not oppose regulatory filings from those who complied with the request, or it could seek to encourage compliance with appropriate Coasian side-payments (where one party will voluntarily agree to pay the other to compensate for the harm associated with compliance or deviation from the slotting system). Nevertheless, these are weak tools and carry significant potential downsides. Under this model, the operator announcing slotting has full control over both its shell (although maybe not neighboring shells) and slot designs. It also de facto controls assignment to either the full shell, or whatever portions it claims, limited only by the need for mission authorization by its launching state.

Inter-operator negotiated legal coordination mechanism: This model envisions a legal enforcement mechanism, either on a bilateral basis between operators through contract law or through membership in a shared third-party membership organization. Legal protections may help reduce perceptions of risk associated with coordination, particularly if an operator intends to make significant concessions to a competitor as part of slotting negotiations. Contracts can also clearly specify responsibilities, standards for technical interchange and coordination, penalties for non-compliance, and intellectual property or proprietary information protections. In an alternative framework, slotting mechanisms could be similarly agreed upon between two or more operators and then presented to a launching

state's regulator with a request that it enforces the proposed slotting scheme as a condition for authorization of subsequent missions. Both of these approaches leave the definition of slotting structure, allocation, and other details in the hands of operators but provide additional assurances regarding behaviors on the part of relevant stakeholders. Neither of these mechanisms would be binding on all potential space users. A contract would only apply to signatories, and a launching state can only control those under its jurisdiction.

Launching-state authorization conditions: Under this model, a state regulator chooses to mandate or encourage some form of slotting. This is differentiated from the previous model where the onus is on operators who propose a system to a regulator. Under this model, a state might require constellations above a certain size or in a certain region of LEO to slot their orbits for compatibility. Under such a system, the state regulator has a much more involved role in both shell design and assignment, even if it chooses to do so in response to petitions from operators. Like both of the previous two models, actions by the state would only be binding on missions it authorized. For a major space-faring nation, this could perhaps be augmented by requirements to slot as a market-access condition. While operators have leveraged market access conditions to insist upon space sustainability measures, it is far from clear that a regulator would choose to leverage market access to encourage slotting.

Internationally coordinated shell design and/or allocation and assignment framework: This model envisions national regulators acting on behalf of operators through an internationally coordinated process at one or more international intergovernmental organizations. This could, for instance, occur as an extension of the existing process used by the ITU for GEO. Such a system would have significantly broader authority than national or private systems and encourage the most inclusive discussions about allocation and assignment processes. It would, however, need to overcome significant history regarding the imperfect compromises that characterize GEO slot allocation and assignment and a general trend of reluctance over the last several decades toward the development of new binding legal aspects of international space law and governance. The legitimacy of such a system might also be diminished in the eyes of late-comers by the significant amounts of LEO orbital volume already claimed by various operators under the current processes.

It is important to note that while coordination could arise through multiple methods, these methods are not all equally suited to accomplishing different slotting objectives. Norms-based methods may be adequate to achieve separation, but they may be less suited to achieving efficient resource use. Likewise, it is hard to imagine any structure other than an international intergovernmental coordination process being able to adequately address concerns about equity in access to LEO and orbital use.

In the short term, we view voluntary cross-operator coordination for mutual shell de-confliction as the most likely avenue for slotting implementation. Operators already have incentives to generate efficient slot configurations within shells. Prospective authorization of large overlapping shells by regulators offers a powerful incentive for operators to coordinate to avoid these conjunctions, both to protect their own investments and to prevent these concerns from delaying, derailing, or descopeing sought regulatory authorizations. Gradual voluntary adoption by operators can help establish best practices and norms, build technical capabilities across the industry, and build organic support for action by industry bodies or national regulators.

One potential escalation pathway to national or international coordination is if voluntary coordination fails to prevent uncoordinated overlapping large constellations. Authorization of such constellations may motivate operators to push for either national policies to prevent future such assignments or to push their states to develop coordination processes at the international level to again provide further regulatory certainty and protection from such physical interference.

As with any regulatory intervention for commons allocation, it is likely that operators may seek to exploit a potential slotting regime as a tool to exclude rivals, particularly later-filing operators. While the slotting work we have conducted could fundamentally support multi-operator co-habitation in different slots of a shared shell, there is significant coordination and technical interchange that would be necessary to safely enable such coordination in practice, with a particular focus on sharing of state information, control boxes and control strategies, common reference frames and models, and coordination pathways to address potential contingency events. Unless faced with a real threat of another large constellation being authorized to operate at overlapping altitudes in an uncoordinated manner, it is hard to imagine an operator voluntarily agreeing to share an otherwise exclusive shell, particularly if it intends to potentially modify or expand its own constellation in that shell.

International work to establish an LEO regime similar to GEO is probably the most unlikely of these pathways. Indeed, given the pace at which international space diplomacy occurs, it is hard to imagine such a system being enacted before the next decade of spacecraft has launched. Once operational, constellation operators that achieve sustainable profitability are likely to prefer to continuously upgrade and expand their constellations in subsequent generations rather than accept new limitations or changed orbits. One potential factor that could challenge this narrative and motivate rapid international coordination is if failed coordination between two or more operators results in a major debris-generating accident, particularly at a high altitude or one that significantly increases risk to human spaceflight. Changes to disclosures and coordination mechanisms to better support coordination for mutual deconfliction of adjacent orbital shells are possible and more likely than a binding regime in the near term.

One major factor that could delay, although not eliminate, the need for slotting is if the current wave of interest in LLCs collapses similar to the wave in the 1990s. While not all proposed LEO constellations will be built, and the economics of these proposals are quite uncertain at best, slotting would be necessary to accommodate even a significant fraction of current demand. In the long run, the number of active spacecraft will continue to grow and eventually produce these same concerns.

4.3.1 Verification of Slotting Implementation Pathways with Operators

In order to verify the analysis and pathways in this section, a series of interviews were conducted with satellite operators. Outreach was conducted to current or planned operators of LLCs involving outreach via phone, email, and professional social media networks. Interviews were ultimately conducted with four representatives from three LEO satellite operators. Interviews were approximately 45 minutes long and were conducted using a semi-structured

interview format, with interview questions shared with interviewees in advance. The interview questions touched on the practices interviewees considered most important to ensure space sustainability and kinetic space safety, operator kinetic space safety practices, views on cross-operator orbit coordination, and opinions on the slotting implementation pathways and orbital capacity. The full set of baseline interview questions is reproduced in Appendix C. The list of interviewees is contained in Table 2 in Appendix D.

Overall, interviews provided strong support for the analysis in this section. All three constellations use or intend to use frozen near-circular orbits for their constellations with self-safe constellation designs. The interviewed individuals mentioned the use of separation in the latitude-altitude plane as a planned or potential coordination mechanism. All three supported a general operational concept of operators using reference trajectories with safe-by-design separation between satellite control boxes and with separation between neighboring large constellations. One interviewee expressed confidence in their company’s ability to coexist with other constellations without compatible designs, but expressed concern about the ability to perform collision avoidance during the period of time between orbital injection and when objects are cataloged, particularly without active coordination between the involved operators.

While representatives at all three companies felt that there was good coordination between Western operators with adjacent constellations, there was concern about the lack of ability to effectively coordinate with Chinese operators and planned constellations. Two interviewees lamented the lack of standardized formats to share orbit design information with sufficient precision to enable orbit design for mutual separation and noted that existing FCC and ITU filings are inadequate for these purposes.

All three operators were already convinced of the utility of using orbit coordination methods such as those presented in this thesis to avoid the potential between close approaches between operators, without necessarily needing further analysis to be persuaded. Each had also come to similar conclusions internally as part of their own design processes. One interviewee suggested that quantifying the number of conjunction events avoided by cross-operator coordination could help persuade others of the value of such a system.³ Another interviewee felt that coordination as proposed in this thesis did not go far enough. That interviewee suggested a need to have operators also 1) demonstrate that their satellite covariances are both realistic and remain constrained within their chosen orbit control boxes, and 2) conduct probability of collision screening to show that the probability of collision between their satellites and neighbors is below an actionable threshold on both a per-satellite and per-shell basis. To ensure operational compatibility, that interviewee suggested that orbital neighbors should conduct testing to certify compatibility of their flight dynamics systems on a bilateral basis to ensure that they are able to properly interpret data products from the other and that mutual slotting separation is implemented correctly. That interviewee noted that closer orbital separation distances would require more intensive certification work.

Two interviewees felt that the pathways presented in Figure 4.17 covered all major possibilities. A representative from one of the operators recommended another pathway that focused on the adoption of voluntary norms through mutually agreed international arbitration between operators. This scheme was somewhat of a hybrid of the norms-based and

³A version of this analysis is conducted in Chapter 6.

international pathways, with bottom-up processes using international institutions to create and enforce norms over time. One interviewee preferred a coordination process led by a non-governmental organization, one preferred a norms-based process with explicit international coordination, and the third preferred a norms-based process that emphasized international arbitration. Two interviewees from different operators insisted that a slotting system should not preclude novel orbits and missions that are not compatible but could help coordinate near-circular orbit traffic where feasible. Two interviewees from different operators expressed concern that orbit coordination mechanisms could become too restrictive if implemented in a manner that leads to overregulation.

Interviewees did not agree on distances for separation between shells, noting that many engineering parameters can influence reasonable separation distances. Two interviewees from different operators expressed desires for small orbital tolerances to maximize the availability of the space environment, while one preferred compact but flexible orbits that allowed its constellation to adapt in altitudes and parameters as part of an iterative process.

One interviewee expressed skepticism about the usefulness of orbital capacity as a concept, mentioning concern that it would be invariably weaponized by competitors to limit innovation. The other interviewees recognized constraints associated with long-term sustainability, operational collision avoidance, and non-interference between operators. No interviewee wished to provide specific technical guidance on assumptions that should inform orbital capacity modeling.

Overall, the interviews help indicate that the proposed concept of operations for orbit coordination and implementation pathways appear sound. The strength of this result is undermined by the limited number of interviews and operators consulted. This was the result of many operators declining to be interviewed or not responding to repeated requests. In addition to the formal interviews conducted for this work, the slotting structure and implementation pathways discussed in this work have been discussed with several additional LEO operators as part of informal engagements for other purposes with similar results to those obtained in the interviews for this project.

4.4 Recommendations

Based on our work to date, we offer several recommendations:

1. **Uncoordinated LLCs should not overlap in orbital volume.**

We generally agree with the rationale that led Maclay et al. to caution that “Large constellations should not overlap in altitude” [1] but believe a nuanced definition is necessary to clarify what overlapping in orbital volume means. As shown in Chapter 3, it is insufficient to characterize large constellations by a single nominal altitude, and it is possible with careful orbit design to design shells that overlap in osculating semi-major axis without posing cross-shell collision risk. Similarly, it is fundamentally possible to design sets of slots that are passively self-safe, but more work is necessary to develop the technical interchange and operational concepts to do so safely. The set of recommendations compiled under the aegis of the American Institute of Aeronautics

and Astronautics by OneWeb, Iridium, and SpaceX offer similar but more specific recommendations [2].

2. LLCs should be designed to be self-safe.

A large constellation that is not designed with self-compatible orbital phasing faces significantly increased self-conjunction risk, but such risk is easily avoidable by proper phasing selection. Many high LEO constellations avoid the need to maintain compatible phasing across orbital planes by separating orbital planes in altitude. This move enhances passive safety but makes significantly less-efficient use of orbital volume and altitude. While constellations will have propulsion capacity and could in principle conduct collision avoidance maneuvers to avoid hazardous intra-constellation close approaches, this comes at significant operational burden and reduces overall system safety. Collision avoidance capabilities are still needed as part of a multi-layered safety system, even with orbital coordination, but their scope is reduced to addressing satellite-on-debris conjunctions that cannot be readily avoided through slotting and off-nominal satellites that fail to maintain safe slotted orbits (e.g., due to malfunction or during shell transits due to orbit-raising or de-orbiting).

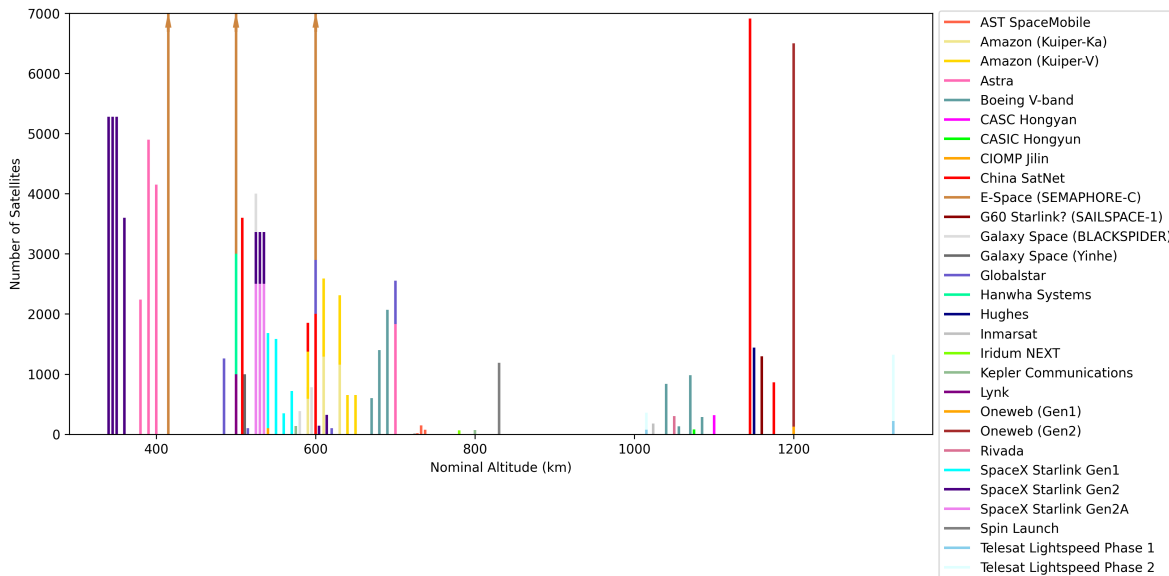


Figure 4.18: Selected Proposed LLCs. This figure is similar to Figures 3.1 and 3.2 but contains a different altitude range.

3. **To enable efficient orbital use, large constellation operators with near-circular orbits should use frozen quasi-periodic reference orbits. Where possible, these shells should be stacked in order of inclination with compatible arguments of perigee. Similarly, operators should maintain judicious orbital tolerances to limit the orbital volume required for their nominal operations.**

With more than 30 shells already proposed for low LEO as visualized in Figure 4.18, several conclusions become clear. First, tight shell radii and the use of frozen orbits

sequenced for mutual collision avoidance as proposed in Bombardelli et al. [92] and Chapter 3 are necessary to avoid significantly increased conjunction risk from cross-operator, cross-shell conjunctions. The alternative is significantly increased operational complexity and orbital risk that manifests as reduced risk-based orbital capacity, or a significant reduction in the amount of traffic that can be accommodated relative to present and future proposals and demand. Second, the number of available orbital shells and their placement will likely become an issue significantly before individual shell saturation. While we do not know the intended capabilities and operational concepts of most proposed constellations, it is possible to design shells that preserve technically reasonable minimum separation distances while exceeding today’s largest constellation proposals. In contrast, orbital altitude is constrained for several reasons: because orbital shells generally need to accommodate only a single inclination, because shell shape imposes geometric constraints for adjacent shells, and because shell distribution is scaled across a single radial dimension, whereas shell surface area increases with radius squared.

4. **Operators should share design and operations information sufficient to coordinate orbital separation with orbital neighbors and to enable subsequent constellations to design for compatibility with their constellations.**

Such disclosures include differentiating between altitude ranges intended for nominal operations and those that may be used rarely for contingency operations, as well as disclosing intended osculating reference trajectories and control box sizes (and associated reference frames, models, and other information sufficient for interoperability). Operators intending to use frozen orbits should disclose how these orbits are defined and the trace of their constellation in the latitude-altitude plane. Unfortunately, regulatory filings typically are insufficiently detailed for this purpose, containing two-body classical elements and overly generous altitude tolerances sized to accommodate all potential contingency operations.

5. **Operators intending to reconfigure or expand slots should plan for reconfiguration in advance of launching.**

Work is still ongoing to assess the performance of slotting reconfiguration schemes. Nevertheless, it is clear that reconfiguration, particularly reconfiguration with significant restrictions on reconfiguration methods, limits the set of admissible options relative to the full set of valid 2D-LFCs at relevant sizes and inclinations. If an operator intends to expand their constellation, it makes sense to conduct this optimization before finalizing either their initial or final design to allow cross-optimization for both states. If operators begin to share shells, understanding the minimum separation distance that is technically achievable for a given constellation’s spacecraft can inform potential co-shell slot placements for other users.

4.5 Summary

The purpose of this chapter is to summarize and apply previous results on intrinsic capacity, demonstrating how they can be practically used to inform orbit use decisions. We presented the orbit packing problem and described relevant intrinsic capacity metrics and estimation methods. Three methods have been described to estimate the capacity of an orbital shell: direct enumeration of Keplerian 2D-LFC analogs, power law trend fitting based on direct enumeration results, and comparison to relevant NSI orbits. Ways to calculate remaining possible future expansions from a particular 2D-LFC were described and depend on the constraints to acceptable expansions. Similarly, three mechanisms are described by which the efficiency of shell layering can be assessed: shell width, shell separation, and shells per orbital altitude range. Several potential paths forward to implement orbit coordination mechanisms based on intrinsic capacity have been discussed and contrasted, with major differences for enforcement, allocation, and assignment. Recommendations have been offered based on the results of relevant intrinsic capacity research.

LEO orbit coordination has the potential to serve a variety of important roles to help safely facilitate significant increases to LEO orbital density. Operationally, it can improve kinetic space safety, expanding risk-based orbital capacity while reducing operational burden on spaceflight operators. At a theoretical level, slotting provides useful ways to explicitly understand the opportunity costs of particular shell designs and slotting configurations and optimize these designs and configurations for safe density. At a policy level, in addition to encouraging efficiency, slotting also provides a framework to support quantitative conversations about equity and other values in coordination, allocation, and assignment of orbital volume.

In our view, multiple levels of coordination will be necessary to achieve different policy objectives. These forms of coordination can be pursued concurrently through a meet-in-the-middle approach, similar to broader efforts for STCM. Coordination is most likely, and has begun, on an operator-to-operator basis with a focus on achieving constellation separation and non-interference. Higher levels of coordination are desirable to achieve efficient and rational orbital use but will be challenging to achieve. Concerns about equity of orbital use will be most challenging to address and most likely require a level of international coordination and compromise well beyond current discussions on LEO orbital use.

Chapter 5

Space Environmental Governance and Decision Support Using Source-Sink Evolutionary Environmental Models

This chapter contains a paper I presented at the 2023 Advanced Maui Optical and Space Surveillance Technologies Conference [101]. It has been edited to conform to the style and formatting of the thesis.

5.1 Introduction

Existing U.S. orbital debris rules largely focus on imposing certain minimum technical standards and disclosure requirements on operators. Such rules are fairly simple and are derived at least in part from expert advice informed by high-fidelity, if sometimes dated, modeling. The benefits of such an approach are clear: rules are easy for operators to understand and give regulators a clear yardstick against which to measure behavior. Because for many years it was only irresponsible orbital use that threatened to exceed the capacity of the orbital environment, regulating to enforce responsible use was an adequate solution.

However, driven by new technology and economics, continuously increasing levels of traffic may begin to raise sustainability concerns—even if new operators comply with norms of responsible behavior at higher rates than legacy traffic [18], [19]. Faced with a credible supposition, but not definitive evidence, that this claim is true, stakeholders are left with an uncomfortable vacuum where the previous approach is potentially inadequate but the alternative is not necessarily clear.

In this chapter, we argue that a logical solution is to explicitly incorporate environmental modeling into decision-making on orbital use by individual stakeholders, multi-stakeholder coordination groups, and regulators. Such modeling has, of course, always informed expert comments to regulatory organizations and discussions within the U.S. government interagency process. What is different, and we argue necessary, is bringing that modeling capability more directly and accessibly into stakeholder discussions and decision-making in an iterative and responsible way that exceeds the cadence feasible under a model predicated on expert studies that occur over months to advise rulemaking processes that take years.

A conceptual process is described, discussing how accessible environmental models could be integrated into workflows for decision-making about orbital use as a decision-support tool. For concreteness, key steps in the process are demonstrated using a relatively simple and low-to-moderate-fidelity modeling tool called the MOCAT Source-Sink Evolutionary Model (MOCAT-SSEM). While this specific model is used to demonstrate the approach, the discussion about the role of models in space environment management is intended to be largely agnostic to the chosen model(s). It is important that any model is accessible to, usable by, and trusted among stakeholders. Stakeholders should drive the appropriate level of fidelity, complexity, accuracy, and precision for modeling, rather than a model-first approach that dictates what questions stakeholders can ask.

The process of incorporating such modeling tools is described, referencing learning from terrestrial resource management and mistakes made in previous U.S. attempts to manage natural resource systems (see, for instance, the discussion of scientific management in Brunner et al. [116]). Rather than transition from fixed rules to a centralized, expert-driven process of scientific management with adversarial dispute resolution, we recommend the adoption of adaptive management and governance philosophies shown to yield fairer, more efficient, more stable, and wiser outcomes [117, p. 145]. This chapter makes three main contributions to the literature:

1. It seeks to provide the most comprehensive description to date about how adaptive management and governance concepts could be applied in the space environment management context.
2. It advances the notion of orbital capacity as a constrained optimization across multiple distinct stakeholder-defined constraints.
3. It provides a demonstration of the use of an SSEM model to consider multiple kinetic safety constraints to orbital use.

The rest of this section briefly describes the SSEM approach used in this chapter and introduces adaptive management and adaptive governance concepts.

5.1.1 SSEMs

SSEMs are a low-to-medium-fidelity space environment modeling approach that make several simplifying assumptions. By making these assumptions, it is possible for even a laptop computer to be able to simulate the evolution of the space environment over hundreds of years in seconds or minutes. Accordingly, they permit a level of iterative exploration in near real time that is impossible with higher-fidelity evolutionary modeling approaches that require supercomputers and hours or days of computational time to complete a simulation. Because they abstract away much of the detail contained in the real world, they are simpler to understand and use. They can often simulate diverse analysis problems with relatively minor modifications compared with higher-fidelity modeling approaches that need to simulate phenomena in greater detail to understand effects.

SSEMs work by representing shifts in populations of various species of objects through sets of coupled ordinary differential equations (ODEs). SSEMs have long been used to provide rough modeling of the evolution of the space environment, with key papers including

Talent [118], Lewis et al. [59], and Somma et al. [119]. Higher-fidelity space environment evolutionary models typically semi-analytically propagate individual space objects, perform conjunction screening, and simulate collisions using a break-up model, where SSEMs aggregate objects into common species with set physical properties and interaction rates. Preliminary work has been done to investigate calibrating SSEM models [59], [120] against higher-fidelity three-dimensional MC models, but more work will be needed to develop SSEMs with generalized correlation that retain accuracy and fidelity across diverse modeling conditions. Such calibration is likely necessary for the models to obtain stakeholder acceptance to support the use cases demonstrated in this chapter.

Several SSEMs have been developed as part of MOCAT, incorporating various phenomena and analysis methods, including system-wide optimization, non-trackable debris, mass-binned species, and orbit-raising and de-orbiting [99], [100], [121]–[125]. In Lifson et al. [126], a new modeling framework called MOCAT-SSEM is described, which is used to integrate the various analysis methods and features from previous individual models while providing an object-oriented interface and automatic equation compilation. Compared with higher-fidelity models, these SSEM models within MOCAT make several significant simplifying assumptions: all objects are placed in concentric circular orbits, collision and break-up fragments are deposited into the circular altitude bin of the parent objects, and collisions are assumed to occur at rates derived from an analogy to the kinetic theory of gases rather than a higher-fidelity method that accounts for the physical details of object orbits (which are not modeled in the SSEM). These simplifying assumptions are generally acceptable for most analysis but struggle to represent the interactions of rocket bodies (which typically exist in elliptical orbits) and to accurately calculate collision flux changes from specific fragmentation events. We believe that some of the shortcomings of these modeling assumptions could be addressed in future work while retaining the computational benefits of this approach.

The equations that describe the population quantities and flows for a set of object species in MOCAT-SSEM are defined using a system of ODEs:

$$\dot{\mathbf{P}} = \mathbf{\Lambda} + \dot{\mathbf{C}}_{PMD} + \dot{\mathbf{F}} + \dot{\mathbf{C}} \quad (5.1)$$

where the change in the population of each species, \mathbf{P} , is a function of launch rate, $\mathbf{\Lambda}$, post-mission disposal, $\dot{\mathbf{C}}_{PMD}$, atmospheric drag, $\dot{\mathbf{F}}$, and collisions, $\dot{\mathbf{C}}$. Each of these terms is a time-varying quantity associated with each of a set of consecutive fixed-width interacting concentric orbital altitude bins. In this chapter specifically, $\mathbf{\Lambda}$ is defined as a linear interpolation of exogenously determined altitude-binned object launches divided across various species.

$\dot{\mathbf{C}}_{PMD}$ is modeled as:

$$\dot{\mathbf{C}}_{PMD} = -\frac{Q_i}{\Delta t} \quad (5.2)$$

for each active satellite species, simulating a certain portion of satellites being de-orbited from each altitude bin at each time based on the assumed orbital lifetime, Δt . For a debris species corresponding to each active satellite species, a percentage failure in post-mission disposal is modeled as occurring at each time step according to:

$$\dot{C}_{PMD} = \frac{1 - P_M}{\Delta t} Q_i \quad (5.3)$$

Atmospheric drag is modeled as in previous work, with inactive objects and active objects without propulsion experiencing drag according to:

$$\dot{\mathbf{F}} = \left[\dot{F}_{d,Q_1}, \dots, \dot{F}_{d,Q_N} \right] \quad (5.4)$$

where Q refers to the species in the system. $\dot{F}_{d,Q}$ is written for species with drag:

$$\dot{F}_{d,Q} = -\frac{Q_+ v_+}{d} + \frac{Qv}{d} \quad (5.5)$$

In Equation 5.5, d is the thickness of an altitude bin, the subscript “+” indicates quantities related to the bin immediately above the current one, and v is the rate of change of the semi-major axis, expressed as:

$$v = -\rho B \sqrt{\mu R} \quad (5.6)$$

where $B = c_D \frac{A}{m}$, defaulting to a flat-plate drag coefficient of $c_D = 2.2$ [56]. A is the drag area of the object, and m is the mass of the object. Atmospheric density ρ can be computed using either a static exponential model based on CIRA-72 [102, p. 537] or as a time-varying dynamic atmospheric density based on interpolation and down-sampling of the Jacchia-Bowman 2008 model (JB-2008) [127] following the approach described in [123]. In this case, ρ lacks a closed-form expression but can still be integrated using standard numerical ODE solvers.

Collisions are modeled according to the approach in [126], where the NASA Standard Break-Up Model (SBM) [128], [129] is used to estimate the number and mass of fragments created as a result of a collision between any two species across the set of debris species included in the model. These fragments are then binned across the model’s debris species.

The two colliding objects are decremented according to

$$\dot{C}_i = \Gamma_{ij} \phi_{ij} Q_i Q_j \quad (5.7)$$

$$\dot{C}_j = \Gamma_{ji} \phi_{ji} Q_j Q_i \quad (5.8)$$

where the collision modifier Γ_{ij} is -1, augmented by collision avoidance terms α_i (for collisions versus an inactive object j) or $\alpha_{active_i} \alpha_{active_j}$ (for collisions between two active objects). For collisions between two objects subject to coordinated mutually exclusive orbits, an additional factor $(1 - \zeta)$ based on slotting effectiveness factor ζ is applied, following the approach in [100].

Following Somma et al. [56] and others, the kinetic theory of gases is used to estimate intrinsic collision frequency, ϕ_{ij} , between species i and j , modeled as:

$$\phi_{ij} = \pi \frac{v_r(h) \sigma_{ij}}{V(h)} \quad (5.9)$$

where $v_r(h)$ represents the relative impact velocity, assumed as 10 km/s. While not used in this work, MOCAT-SSEM has the ability to set $v_r(h)$ for each altitude bin. $V(h)$ is the volume of the altitude bin, and σ_{ij} is the impact parameter for species i and j :

$$\sigma_{ij} = (r_i + r_j)^2 \quad (5.10)$$

Specifically, for a set of one or more debris species, the k -th debris species N_k is incremented by:

$$\dot{C}_{N_k} = w_k \Gamma_{ij} \phi_{ij} Q_i Q_j \quad (5.11)$$

where the Γ_{ij} term incorporates reductions to collision probability associated with the species i and j . Note that Γ_{ij} is assumed to be symmetric and equivalent to Γ_{ji} , since no meaningful distinction is modeled by one object being considered the primary versus the secondary. Weighting factor w_k is computed from the fragment mass distribution produced by the NASA SBM via the nearest-neighbor method.

5.1.2 Adaptive Management and Adaptive Governance

Describing the concepts of adaptive management and governance concisely and with precision is tremendously challenging. Both terms are used by multiple authors in different contexts to mean different things [130]. Brunner et al. caution, “adaptive governance is a pattern of practices [that] cannot be reduced to any one thing without serious distortion” [116, p. 19]. This subsection seeks to briefly describe both concepts, as well as the management context in which they were developed, with an emphasis on factors relevant to the application to space governance discussed in Section 5.2. Readers desiring a more comprehensive treatment should consult Steelman [130], Chaffin et al. [131], Brunner and Lynch [132], and Brunner et al. [116].

Avoiding the Trap of Scientific Management

Scientific management is a technocratic approach to centralized planning of resource management decision-making that delegates objective definition and management to a small set of experts. At first glance, this may seem like a reasonable way to incorporate environmental modeling into decision-making: trust the experts to rise above parochial interests and politics and make the “right” choices. Indeed, the approach dominated the United States’ national resource management for the first half of the twentieth century. Resource management, it promises, can be depoliticized by delegating management authority to scientific experts. Those experts will then craft an impartial objective against which changes to the natural environment will be assessed to guide decision-making to ensure the most rational, efficient outcome.

Unfortunately, this appealing technocratic ideal fails in several ways when implemented in practice [116, Ch. 1.], [132], [133], [130]. Centralized management excludes non-scientific stakeholders and their sources of practical knowledge. The selected management indicator is often reductive since it must be amenable to modeling. Technical experts fail to understand and incorporate stakeholder objectives and priorities and may fail to identify, much less

make reasonable trades, when multiple stakeholder interests conflict. Management goals may become less relevant to stakeholders over time (if they were even relevant in the first place).

Because scientific management regimes frequently lack systems for internal adaptation, stakeholder dissatisfaction undermines the legitimacy of the management system and encourages stakeholder recourse to legal or political processes that harm the stability and effectiveness of the management regime. Worse still, the U.S. approach to resource governance tends to pair scientific management regimes with dispute resolution through adversarial legal processes, encouraging ideologically short-term, zero-sum thinking at the expense of long-term cooperation, while simultaneously imposing large negotiation costs, side payments, and regulatory uncertainty [116, ch. 7] [134] [117, ch. 21] [135].

Adaptive Management

Adaptive management emerged in response to the failures of scientific management. It stresses inclusive decision-making processes, multiple stakeholder objectives, and iterative learning from experimentation in management actions. Adaptive management strategies recognize the existence of limited knowledge and irreducible uncertainty across multiple factors relevant to the management of a natural resource system, including the ecological dynamics of the system under management and future behavior and resource use by stakeholders. Adaptive management seeks to achieve robust, resilient outcomes in the presence of uncertainty. It does so through a flexible management philosophy featuring cyclical learning and periodic adjustments to management actions based on observations of environmental response and improvements to supporting models and parameters. Adaptive management is particularly suitable when stakeholders broadly agree on management goals but not necessarily on means to achieve those outcomes [117, p. 5]. While there is no consensus on a single set of steps for adaptive management, one possible diagrammatic breakdown is presented in Figure 5.1.

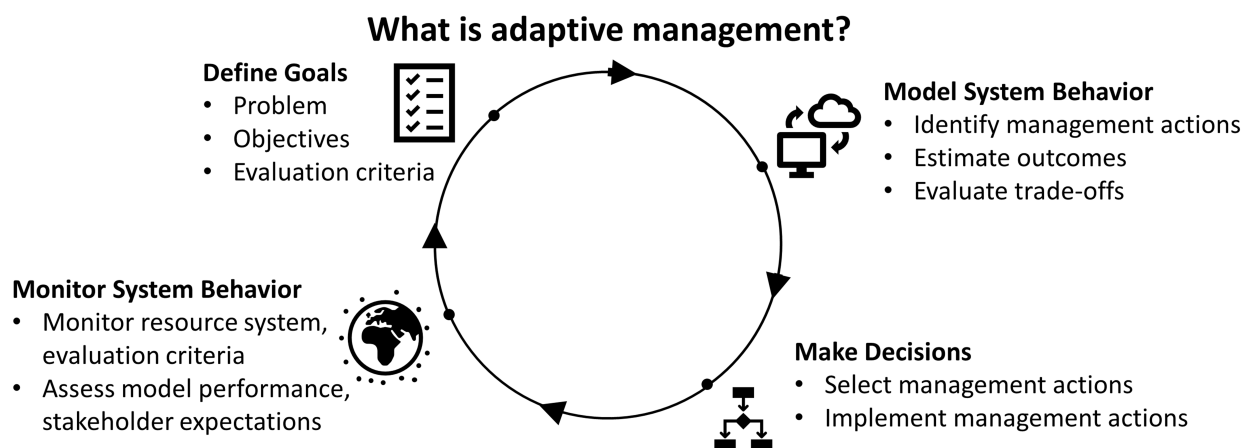


Figure 5.1: A Potential Adaptive Management Cycle.

One critical benefit of adaptive management is the potential for contingent agreement, whereby stakeholders that disagree on the likelihood of different outcomes can jointly agree

to management rules to guide responses to environmental trends that ultimately manifest without having to agree on a specific shared future environmental forecast *a priori*[117, p. 147]. In the space context, for instance, a stakeholder who believes LLC failure rates are likely to be 10% of spacecraft might reach consensus with an operator who believes their failure rate will be sub-1% with initially more lenient post-mission disposal timelines that become more strenuous should failure rates exceed a particular threshold.

A Department of the Interior technical guide [136] on adaptive management lists nine criteria that must be met for adaptive management to be appropriate:

1. Management decisions must be made;
2. Stakeholders can be engaged;
3. Management objectives must be explicitly describable;
4. Decision-making must be subject to uncertainty about the impacts of potential management actions;
5. It must be possible to model relationships between resources and management actions;
6. Monitoring can feasibly inform decision-making;
7. Progress toward achieving management objectives must be measurable;
8. Management actions must be adjustable in response to learning; and
9. The process must be feasible within legal constraints.

These criteria all reasonably hold true for space environment management. Decisions about mission authorization and debris mitigation/remediation need to be selected from among a variety of economically, legally, politically, and environmentally feasible options. Operators and other stakeholders are highly interested and want to be engaged. Sustainability-related objectives can be described at a high level and indeed have been in the internationally accepted definition of the long-term sustainability of the space environment. There is considerable uncertainty about both future conditions and relationships between management actions and the future debris population. Monitoring is possible, both directly for trackable space objects and indirectly using satellite failures and other proxies for lethal non-trackable (LNT) object strikes. Additionally, data collected by satellite operators for sub-lethal collisions can be used to infer other portions of the non-trackable population. Figures of merit can be measured against management objectives, as will be demonstrated in Section 5.2. Management actions can be adjusted over time in response to learning by stakeholders or through revisions to rules. Legal constraints on an adaptive management process for space are perhaps the hardest to characterize, absent a specific proposal for a governing body and structure. In principle, nothing would prohibit adaptive management on a voluntary opt-in basis by a group of concerned satellite operators. While adaptive approaches have been embraced by other portions of the U.S. government, adaptive management regimes are largely incompatible with the linearity and rigidity required for much of U.S. administrative law

[134]. We lack the expertise to determine whether such a structure could exist within existing FCC or Department of Commerce authorities and constraints, or if adaptive processes would require additional authorization from Congress. Resolving this issue is an important question that has strong implications for implementation.

Adaptive Governance

Adaptive governance expands adaptive management from seeking resiliency in the presence of uncertain ecological dynamics of a managed system to feature additional resiliency in the presence of economic, social, and political change [130]. It aims to facilitate coordination of resource use among users in a way that improves joint gains while reducing negotiation costs and ensuring sustainable outcomes [117, pg. 2]. A theoretic construct embraced by Ostrom and others conceptualizes adaptive governance as a set of nested management layers, with increasing burdens to change rules at each higher level [130], [137]. Within this structure, adaptive management forms the innermost loop, where the adaptive management system makes routine operational decisions about system monitoring, enforcement, resource appropriation, and information sharing. A collective rules layer provides mechanisms to revise resource management policies applied at the operational level. A highest constitutional level governs participation in the adaptive governance process and the governance structures used to make decisions regarding collective rules, as visualized in Figure 5.2. Adaptive regulation [138] is another similar framing but typically is focused on the involvement and actions of a regulator, whereas adaptive governance can include but does not necessarily presuppose such involvement.

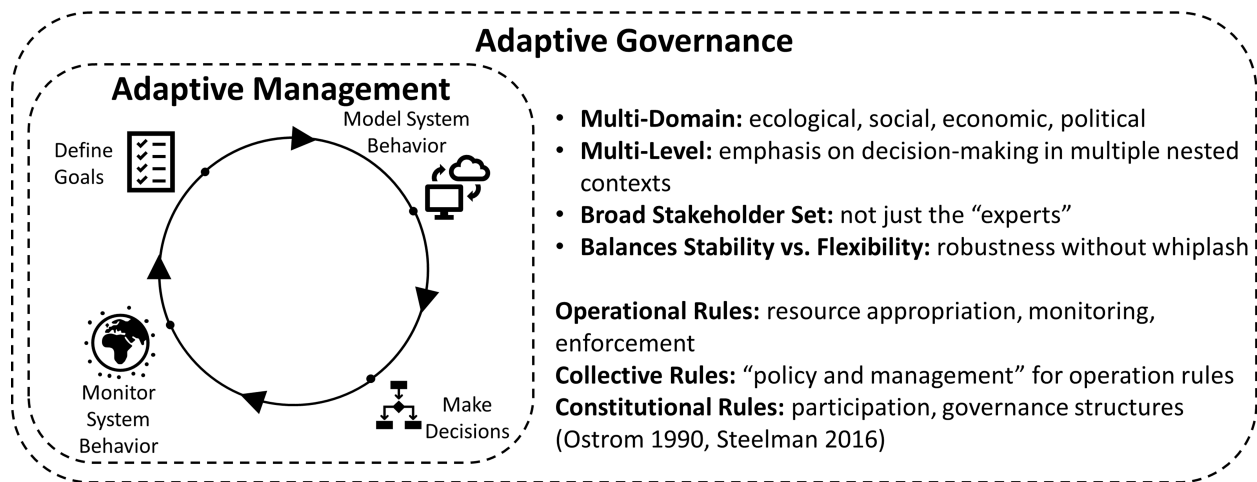


Figure 5.2: Adaptive Governance Overview.

Previous Work on Adaptive Governance and Space

Adaptive governance for space has been mentioned in several contexts but usually at a high level of abstraction. Oltrogge and Christensen [139] note the potential relevance of adaptive governance philosophies for the space domain to help achieve underlying stakeholder objectives in the presence of evolving economic, societal, and environmental contexts. Ezell [140]

conducts a high-level survey of existing space governance, generally favoring the adoption of more adaptive space governance mechanisms. Keles recommends implementation of adaptive governance by the United Nations Office of Outer Space Affairs and the ITU [141]. Keles also highlights Dynamic Adaptive Policy Pathways, an approach introduced by Haasnoot et al. [142] that identifies tipping points to key indicators and uses the performance of those indicators to inform shifts between various management strategies. While not explicitly framed in terms of adaptive governance, a recent European Space Policy Institute report on orbital capacity describes the use of the ESA Space Environment Capacity Concept to support coordination for sustainable orbital use in similar terms [20]. While these works all recognize the potential for adaptive management and governance in the space context, Miguard et al. notes that the space policy literature has “stopped short of extending those arguments into current governance frameworks that can be operationalized” [143].

5.1.3 Traditional Ecological Knowledge

Traditional ecological knowledge (TEK), the set of cultural knowledge, beliefs, and practices adapted and passed down through generations of Indigenous peoples, provides another frame and source of potential insight to inform adaptive space environment management and governance [144]. In discussing the potential role of TEK, this subsection takes an etic (the perspective of an outsider looking in) approach, seeking to understand and generalize from TEK from outside of the culture of Indigenous communities that hold TEK. While TEK is sometimes framed as a fundamentally different and incompatible knowledge process to be contrasted against Western science, these boundaries and distinctions are far from absolute and are sometimes unhelpful [144, pp. 13–14].

In many other contexts, such as agroforestry, medicine, and fisheries management, traditional knowledge provides concrete practices for management of particular natural resource systems. Because TEK is community-specific rather than homogeneous, and because space-flight is a relatively recent technological development, engaging with TEK is perhaps a bit different from areas where the question and domain directly relate to a lived environment or the activity of an Indigenous community. While there are some connections to traditional practices, including Indigenous astronomy, there is less of a history directly associated with issues of space sustainability. Nonetheless, it is still possible to learn from and apply learning and knowledge more broadly associated with TEK worldviews, social institutions, and management systems. Such engagement can help highlight inherent assumptions rooted in Western praxis, such as a tendency to quantify and value natural resource systems solely in economic terms based on extractive use rather than viewing them as intrinsically valuable and inherently deserving of preservation. Troster and Parotta [145] identify certain beliefs as commonly (but not universally) present in TEK natural resource management contexts. Many of these ideas are co-present in the framing taken in this chapter, rooted in socio-ecological systems and adaptive management. These include the connectedness of all things, the inherent need to view human actors as part of the system of analysis, the presence of path dependency in management, the importance of humility and adaptation in the presence of limited knowledge about natural systems, and the usefulness of training to identify and respond to relevant indicators of a natural system. In addition to general alignment with aspects of the analytical framing of the management problem, TEK provides several

normative ideas that may be helpful for discussions in the space environment management context. These include an emphasis on stewardship, promotion of equitable sharing, generosity and reciprocity, recognition of the inherent value of natural resources as ends and not just means, and a requirement for humans to engage in reciprocal thanks and giving as part of their interactions with the natural world. To the extent stakeholders choose to engage with such normative preferences, it may help promote enduring, effective, and stable management regimes. Berkes [144, p. 26] notes that multiple sources have investigated TEK approaches for common-pool resource management [146]–[148] (although many TEK holders would reject a management framing for one rooted in care or stewardship [144, p. 44]).

In addition to interpretation and generalization from an etic perspective, it is also possible to learn from emic approaches (those of insiders in the context of their own culture) and holders of TEK. For instance, Dan Hawk, the principal scientist for United First Nations Planetary Defense, has been a pioneering voice for the application of TEK to a variety of space issues, including space sustainability, planetary defense, and lunar surface operators.

While this thesis does not attempt to directly apply TEK or incorporate it into the proposed framework, TEK is an underutilized source of knowledge that holds significant promise for space sustainability. Combinations of TEK and Western science can provide synergistic benefits in resource stewardship contexts [144, p. 45]. However, TEK can be misapplied if removed from its cultural context and co-opted into non-Indigenous frameworks [144, p. 17]. Attempts to incorporate TEK into space governance should follow best practice for learning from TEK [144, p. 42], including participation of knowledge holders as equal stakeholders in the process, consent of the communities who hold TEK and respect for their intellectual property, and a willingness to continuously question one’s assumptions.

5.2 Methodology

In this chapter, the MOCAT-SSEM is used as a quantitative evolutionary space environment modeling tool to demonstrate several forms of support such a model could play to an adaptive governance process.

5.2.1 A Sketch of an Adaptive Space Environment Management Regime

There is not a single checklist to successfully implement adaptive management and governance. Rather, the process itself is context dependent and should be responsive to both technical and process learning. In this section, we will lay out a notional process and structure for adaptive space environment management and governance. The purpose of this description is to help concretize the description of the concepts described in Section 5.1 while recognizing that preconceived notions should give way during an actual implementation to outcomes of participatory collaborative stakeholder involvement processes.

The discussion in this section is informed by multiple sources, including Ferriter et al. [136], Allen et al. [134], Brunner et al. [116], and Steelamn [130], but does not explicitly follow a single structure from any of these works. While the discussion focuses primarily on

adaptive management rather than adaptive governance, elements of the latter involve similar thinking but also permit changes to stakeholder sets and governance systems to ensure continued effectiveness and responsiveness.

Leadership

A management regime needs an actor to implement and coordinate the process, building buy-in among stakeholders and facilitating participation in the governance structure. In the space debris context, two main kinds of stakeholders are perhaps the best fit.

The first would be a well-respected non-government organization with domain expertise that is widely respected by operators and other stakeholders and perceived as impartial. They could potentially partner with another group with deeper expertise in adaptive management and governance for natural resource systems, but likely without the same familiarity with space debris or the space community. Because such an organization or partnership is unlikely to have funding sufficient to support a long-term process, they would likely also have to attract a source of funding sufficient to sustain the process for at least several years. Such funding could come from corporate, government, or foundation sources. Funding would be necessary to support the activities of personnel from the supporting organizations, fund technical experts and supporting modeling work, and pay costs associated with travel and meetings to convene stakeholders. Funding might also be needed to support participation of stakeholders who are important to the process but lack financial resources to participate at their own cost.

Another option would see a government entity acting in the leadership and convening role. This could be a regulatory entity subject to compliance with relevant administrative law requirements or an entity with domain knowledge but that does not serve as a regulator. Personnel familiar with adaptive management could be detailed from the Department of the Interior or elsewhere to help support the process. The entity would need to ensure any necessary authorization to pursue the effort, as well as to maintain funding necessary to support the program over a multi-year initial period.

Stakeholder Engagement and Recruitment

One of the earliest tasks for the executive leadership team will be to develop awareness and interest in participation among relevant stakeholders. This group should include those who make use of the managed resource system, namely satellite operators, as well as those impacted by management decisions concerning resource allocation. Relevant cleavages among stakeholders may include orbit regime, Earth observation versus communications payloads, academic versus commercial operators, and operators of large constellations versus small numbers of bespoke satellites, as well as disagreements between large constellations of dozens of satellites (who may still rely on more manual processes to some extent) and large constellation operators (where scale means they must leverage even greater levels of autonomy). A key task for the recruited stakeholder group is to agree on scope, objectives, and feasible management actions. The management scheme would likely involve primarily commercial users and may be constrained to nations with particular geopolitical alignments. A failure to obtain global participation or global scope is not necessarily a problem. For instance, a

set of LEO-only operators may feel they will be better able to make progress discussing rules for their own regime if GEO operators, who compete with LEO operators in the communications market and (in the view of some LEO operators) have sometimes tried to leverage sustainability concerns for competitive reasons, are excluded. A process that involves only Western operators may still establish norms and best practices and improve the environment, even without full participation from geopolitical rivals. A more limited stakeholder set constrains the network effects associated with coordination but may still be preferable if it permits progress where a larger group can be intractable. Even under a polycentric coordination regime, individual coordination centers can still adaptively respond to changes to the environment, even if there are less-than-desirable levels of coordination among different power centers. Naturally, those excluded from such coordination efforts, whether certain operators or certain countries, are unlikely (especially initially) to view the outcomes of such efforts as legitimate.

Problem and Goal Identification

Once a stakeholder group is assembled, a key early step is to identify a problem and any associated high-level goal or goals. A reasonable starting point is concern that various factors will limit the ability of humans to conduct space activities. A potential high-level goal can be found in the United Nations Committee on the Peaceful Uses of Outer Space’s Guidelines on the Long-Term Sustainability of Outer Space Activities and their definition of the “Long-Term Sustainability of Outer Space Activities” as “the ability to maintain the conduct of space activities indefinitely into the future in a manner that realizes the objectives of equitable access to the benefits of the exploration and use of outer space for peaceful purposes, in order to meet the needs of the present generations while preserving the outer space environment for future generations” [149].

Nevertheless, this definition alone is not sufficient. Multiple factors potentially constrain human ability to make use of the space environment over time. In the realm of kinetic space safety, there are concerns related to the long-term sustainability of the space environment, operational threats to spaceflight safety and associated mitigation burden, and orbit coordination and cross-constellation orbital compatibility. Other potential limitations include access to communications spectrum to send and receive information between satellites and the ground, the risk to air and ground users from space debris that survives re-entering the Earth’s atmosphere, changes to climate from increasingly large amounts of aluminum and other materials being vaporized in the Earth’s upper atmosphere during post-mission disposal, and the carbon cost of spaceflight and associated terrestrial activities.

Kinetic space safety—avoiding physical collisions in space—is likely where any such effort will start, but the stakeholders must decide what, if any, additional areas to include and what additional technical expertise or additional stakeholders will need to be included to satisfactorily consider such goals.

Objective Definition

It is necessary to translate potentially qualitative problems and goals into objectives that can be expressed unambiguously in a feasible and measurable manner. This definition in

turn drives necessary modeling capabilities to support the adaptive management process. As distinct from scientific management, there are likely multiple objectives with differing importance to different stakeholders.

Defining Potential Management Actions

There are many ways to influence the space environment, including through new launches; promoting, disincentivizing, or coercing certain behaviors; monitoring and interacting with objects in space; and removing objects. While kinetic space safety actions are often divided between space debris mitigation and remediation, a plethora of more specific options are available. Some such topics include requirements for satellite maneuverability above a certain altitude threshold, system-wide limits on aggregate ground causality risk, requirements to remediate failed spacecraft that exceed a particular orbital lifetime or lifetime probability of collision, and conditional mission authorization based on model-derived compliance with management objectives. Stakeholders may decide that one or more of these actions are appealing and should be encouraged or required.

The set of identified potential management actions again creates requirements for supporting technical modeling. What distinguishes the selection of such management actions from business as usual in an adaptive management process includes: 1) the decision is being made through a participatory governance structure with strong buy-in from stakeholders; 2) technical expertise is provided to assist stakeholders in independently understanding and assessing the likely quantitative effect of proposed changes; and 3) decisions are regularly revisited as part of a structured decision-making process.

Model Identification and Adoption

Once objectives and potential management actions are identified, one or more modeling approaches need to be selected to support efforts to simulate management actions, estimate outcomes, and identify trade-offs.

Technical assistance will often need to be provided by experts to develop models, explain their limitations and sources of uncertainty, and ensure that suitable modeling approaches are identified that can measure the objectives of interest and other consequences of management actions. In many cases, more than one modeling approach may be used. In the space context, lower-fidelity SSEMs and heuristic methods used for discussion and preliminary evaluation could be augmented by higher-fidelity, full-scale three-dimensional MC techniques for final decision-making.

As part of this process, there will be a need to develop consensus on multiple modeling parameters, including initial starting populations, future solar weather predictions (which influence drag, the only natural sink on the space environment), launch models, and spacecraft physical and behavioral properties. Where possible, representative consensus values should be defined, with ranges of several values used for parameters where there is significant uncertainty and the environment is sufficiently sensitive to merit additional modeling runs. Launch models will likely begin as exogenous deterministic or stochastic models but evolve over time to be economically informed to better reflect reality.

Estimating Outcomes and Trade-Offs

Stakeholder intuition and models can be used to estimate the results of various management actions, either alone or in combination. The models can then be used to understand results for objectives relevant to stakeholders. In some cases, multiple objectives can be simultaneously accommodated through properly selected management actions; in others, stakeholders will need to explicitly trade between different, at least partially incompatible objectives.

Selecting Management Actions

From a set of enumerated management actions and their modeled outcomes and trade-offs, it will be necessary for stakeholders to select a set of management actions. These actions will be periodically revisited but generally used to guide routine administration by system managers. As part of the selection of management actions, stakeholders will need to balance the desirability of stability and therefore predictability versus flexibility to accommodate unexpected behavior and outcomes [150].

Implementing Management Actions

Once decisions are made, these management actions will need to be implemented. Depending on the management action, this implementation may be anything from almost self-executing to extremely complex and time consuming.

Monitoring

As part of the adaptive regime, stakeholders will need to agree to a monitoring plan. Monitoring can be used to understand the status of the selected objectives or the state of the resource system, compare stakeholder predictions versus actual environmental evolution, and calibrate and improve models.

Assessment

This step studies the results of management actions and uses learning from the adaptive management process to inform changes during the next iteration of the management loop.

5.2.2 Model Specifications

The previous subsection briefly described elements that might exist for adaptive management and governance of the space debris environment. In this section, several of these elements will be demonstrated explicitly using MOCAT-SSEM.

As explained previously, an adaptive management process relies on translating a problem and qualitative objectives into specific technical evaluation criteria that can be evaluated in a model run. As described above, such goals must be defined through broadly inclusive processes that understand and address differing needs among different sets of stakeholders. For the demonstration in this section, several nominal goals are demonstrated and implemented as indicator variables in MOCAT-SSEM.

Table 5.1: Reference Scenario Properties for Adaptive Demonstrations.

Field	Value
Start date	1 December 2022 0:00:00 UTC
Simulation duration [years]	200
Output steps	200
Density model	JB2008 Interpolated Density (generic high solar cycle prediction)
Number of shells	40
Minimum altitude [km]	200
Maximum altitude [km]	1400
Velocity of collisions [km/s]	10
Characteristic length [m]	0.01
Integrator	ode15s
Launch traffic model	Empirical fit to large constellation scenario

In the MOCAT-SSEM framework, global properties are set for certain scenario-wide attributes, as seen in Table 5.1. Other properties are set on a species-wide basis, as seen in Table 5.2. Equations are generated according to the general processes described in the introduction.

Initial Population and Launch Traffic

An initial traffic and future launch model is compiled and used in all simulation runs. The initial population is extracted from all two-line elements available with epochs between 2023-01-01 and 2023-01-03 with mean motion greater than three revolutions per day (to capture LEO objects), excluding analyst objects and the International Space Station (since its modules skew property statistics for satellite species). This approach ignores the population of initial non-trackable debris, although it is possible to incorporate this population using counts from the ESA’s MASTER [151] or NASA’s ORDEM [152]. If an object has multiple available states in this interval, the latest state is selected. Physical properties are estimated through fusion with the ESA’s DISCOS database [153], with interpolation laws used for missing objects as described in [33]. Object areas are derived from radius information subject to a circular area assumption, which is also used for the drag term B^* for each object with a drag coefficient C_D of 2.2, as commonly used for satellites [154].

A synthetic launch profile is created by fusing several sub-profiles. A baseline recurring launch rate is generated by repeating injection of launched objects each year from 2018 to 2022, with the date of launch randomized to occur sometime during the corresponding year

Table 5.2: Reference Species and Properties for Adaptive Demonstrations.

Symbol	S	S _u	S _{ns}	N	B
Description	Active station-keeping satellites, orbit-coordinated	Active station-keeping satellites	Non-station-keeping satellites	Debris (plus derelicts for S, S _u , S _{ns})	Rocket body
Cd	2.2	2.2	2.2	2.2	2.2
Mass [kg]	148, 750, 1250	260, 473	6	.00141, 0.5670	1783.94
Radius [m]	0.5, 2.0, 4.0	0.73, 2.08	0.11	0.01, 0.1321	2.69
Area [m ²]	0.79, 12.57, 50.26	1.67, 13.56	0.035	3.1416 x 10 ⁻⁴ , 0.0548	22.70
Active	true	true	true	false	false
Slotted	true	false	false	false	false
Drag	false	false	true	true	true
Maneuverable	true	true	false	false	false
Trackable	true	true	true	false, true	true
Mission lifetime	8	8	3	N/A	N/A
Post-mission disposal	.99	.65	N/A	N/A	N/A
Disposal altitude	0	0	N/A	N/A	N/A
Efficacy of collision avoidance vs. inactive	10 ⁻⁵	10 ⁻⁵	10 ⁻⁵	N/A	N/A
Efficacy of collision avoidance vs. active	10 ⁻⁵	10 ⁻⁵	10 ⁻⁵	N/A	N/A
Rocket body	false	false	false	false	true
Launch rate	Table 5.3 empirical fit	2018-2022 space-track empirical fit	2018-2022 space-track empirical fit	N/A	2018-2022 space-track empirical fit

of the recurring launch model. To this background population, a set of selected LLCs is added based on the values in Table 5.3. LLCs are assumed to replenish satellites at the end of mission lifetime for the duration of the simulation. A piece-wise interpolated launch rate is created by binning the future launch traffic model by altitude and mass-binned species, discretized with time resolution equivalent to the model output reporting criteria.

Modeled Species

More species improve fidelity but increase the number of modeled collision pairs, increasing computational cost and analysis burden. The species for the simulation were chosen through a combination of analysis and judgment. As a preliminary step, k-medians and k-means residuals were calculated for a combined set of initial and future launch model data for one to six clusters per class. Based on diminishing returns in these results, as well as the relative population size of various satellite types as seen in Table 5.4, a certain number of species were selected. The values for mass, area, radius, and lifetime were then set based on these results. Results for mass and area only are visualized for a class in Figure 5.3. Because the debris population is not known *a priori* and constitutes a relatively small portion of the data set, values were selected to model sub-trackable debris as well as trackable debris and derelicts for active species. The chosen species and properties are displayed in Table 5.2.

5.2.3 Indicator Variables

In addition to the features previously described, a new feature called “indicator variables” was added to MOCAT-SSEM. These are non-species quantities that can be customized to model, extract, and visualize behavior of interest that does not necessarily correspond to

Table 5.3: LLCs Included in Future Launch Model. Data courtesy of Dan Jang, based on FCC, ITU, and other sources/assumptions.

Constellation	Altitude	Inclination	Sats on stn	Sats off stn	Sats down	Total Sats Planned	FirstLaunch	FinishLaunch	mass	radius
Starlink	550	53	1419	35	251	1584	2018	2027	260	2
Starlink	570	70	170	234	3	720	2018	2027	260	2
Starlink	560	97.6	233	0	0	348	2018	2027	260	2
Starlink	540	53.2	1544	23	68	1584	2018	2027	260	2
Starlink	560	97.6	0	0	0	172	2018	2027	260	2
Starlink2A	530	43	0	288	2	2500	2023	2031	750	2
Starlink2A	525	53	0	0	0	2500	2023	2031	750	2
Starlink2A	535	33	0	0	0	2500	2023	2031	750	2
Starlink2	340	53	0	0	0	5280	2025	2031	1250	4
Starlink2	345	46	0	0	0	5280	2025	2031	1250	4
Starlink2	350	38	0	0	0	5280	2025	2031	1250	4
Starlink2	360	96.9	0	0	0	3600	2025	2031	1250	4
Starlink2	530	43	0	0	0	860	2025	2031	1250	4
Starlink2	525	53	0	0	0	860	2025	2031	1250	4
Starlink2	535	33	0	0	0	860	2025	2031	1250	4
Starlink2	604	148	0	0	0	144	2025	2031	1250	4
Starlink2	614	115.7	0	0	0	324	2025	2031	1250	4
OneWeb	1200	87.9	499	133	2	588	2019	2023	148	0.5
OneWeb	1200	55	0	0	0	128	2019	2023	148	0.5
OneWeb	1200	87.9	0	0	0	1764	2025	2028	148	0.5
OneWeb	1200	40	0	0	0	2304	2025	2028	148	0.5
OneWeb	1200	55	0	0	0	2304	2025	2028	148	0.5
Kuiper	590	33	0	0	0	782	2024	2029	700	1.5
Kuiper	590	30	0	0	0	2	2024	2029	700	1.5
Kuiper	610	42	0	0	0	1292	2024	2029	700	1.5
Kuiper	630	51.9	0	0	0	1156	2024	2029	700	1.5

Table 5.4: Objects in Initial Population and Future Launch Model. Numbers do not add up to 100% due to rounding.

Species	Count	Percentage
Non-station-keeping satellites	36,974	3.06
Station-keeping satellites	7,182	0.59
Coordinated satellites	1,120,127	92.77
Rocket bodies	7,182	0.59
Debris (initial + exogenous)	35,954	2.98

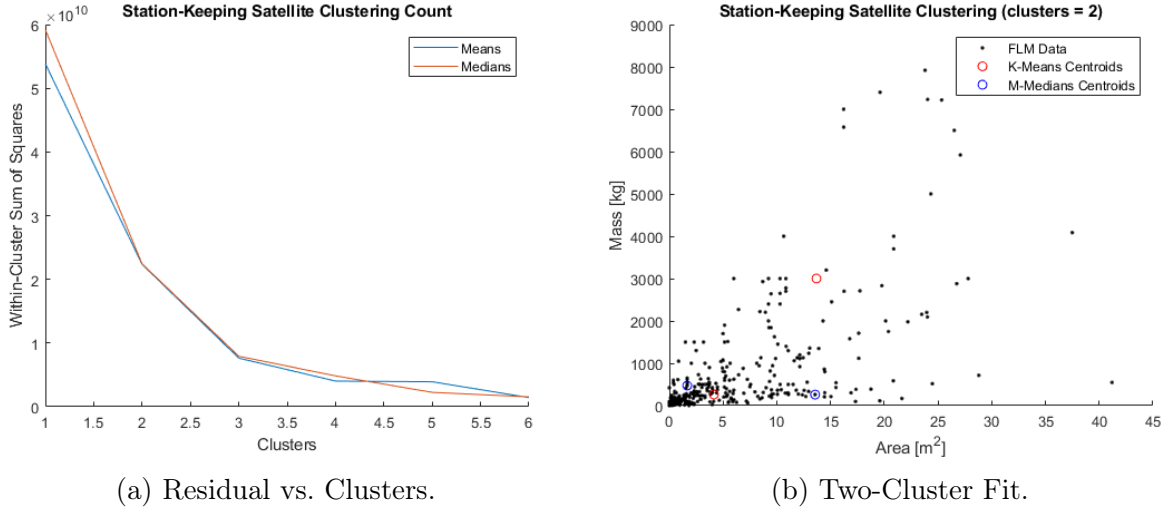


Figure 5.3: Area vs. Mass Analysis for Station-Keeping Satellites. While the knee in the residuals in (a) is at three clusters, a two-species representation is selected since station-keeping satellites represent a small portion of overall launch traffic.

the population of one or more species. Examples include collision rates, an aggregate count of failed post-mission disposal for a particular species in a particular shell, and economic formulas. For instance, the debris-induced cost model from [155] could be used to quantify the cost associated with debris as predicted by MOCAT-SSEM. In this work, indicator variables are constructed to measure quantities associated with potential indicators for various space environment goals that constrain orbital capacity. When compared against consensus targets for permissible values for these indicators, they provide feedback on the acceptability of environmental evolution in a given simulation. The modeled indicators in this work include long-term debris trends, active satellite losses to collisions, satellite maneuvers, and the amount of orbital space physically saturated by large constellation deployment.

As implemented in MOCAT-SSEM, indicator variables can be computed using additional ODEs (that are integrated by the chosen numerical integrator), as arbitrary functions of system state information at a particular moment in time, or as a numerical derivative of system state outputs. Helper functions were implemented that automatically compile each of these indicator variables depending on model scenario variables and species. The generic implementation is intended to support future research and stakeholder use with differing goals.

Long-Term Sustainability

A long-term sustainability constraint is intended to ensure that the amount of debris does not experience problematic long-term growth over the simulation period. In this demonstration, an indicator is implemented to ensure that the increase in the numerical derivative of the number of debris objects in any given altitude bin for any given species does not increase at the end of the simulation. Because the use of a density-informed drag model results in local periodic oscillations, this is evaluated using a linear fit to the total number of debris objects

of each species in each altitude bin, evaluated over the last quarter of the simulation period (150–200 years). Numerous other decisions could be reasonable here: looking at aggregate debris count or debris counts in broader regions of LEO rather than the specific altitude bin structure used in this simulation, quantifying debris in terms of kilograms or kilogram-years, or accepting a slight amount of growth or requiring decreases. For greater security, it would also be possible to impose a stability constraint, requiring the orbital solution to be able to accept an impulse of a certain quantity of debris at a particular altitude or altitudes without violating the constraint.

Operational Risk

This constraint seeks to ensure that short-term “pain” to satellite operators caused by debris does not exceed some impermissible threshold. This is evaluated in terms of both the estimated number of collision maneuvers that a given satellite must perform, as well as the percentage of active satellites in a particular altitude bin that are lost to collisions in a given year.

Collisions are evaluated following the approach described in Lifson et al. [100] and summarized in Subsection 5.1.1. Collisions between two active maneuverable spacecraft species are reduced by a factor α_{active}^2 , while collisions between an active satellite and a trackable non-maneuverable or inactive object are reduced by a factor of α . For conjunctions between two species with slotted orbit coordination effectiveness, ζ , a reduction of $1 - \zeta$ is applied to reflect the physical separation achieved by this coordination. There is no reduction in collisions that occur between inactive objects or between an active object and a lethal non-trackable object.

Recall that for a pair of species, Q_i and Q_j , the populations in each altitude bin are decreased by:

$$\dot{C}_i = \Gamma_{ij}\phi_{ij}Q_iQ_j \quad (5.12)$$

$$\dot{C}_j = \Gamma_{ji}\phi_{ji}Q_jQ_i \quad (5.13)$$

to model collisions. By summing the number of collisions generated for each species pair involving a species Q_i , it is possible to calculate aggregate collisions per year for a particular species in each altitude bin as a function of time. This quantity can also be computed for Q_i as a percentage by multiplying by the factor of $100/Q_i$.

$$\dot{C}_{i_{tot}} = \sum_{j=1}^k \Gamma_{ij}\phi_{ij}Q_iQ_j \quad (5.14)$$

where $j = 1..k$ reflects the index values of all other species against which Q_i could experience a collision. While not explicitly indicated, note that $\dot{C}_{i_{tot}}$ is a time-varying quantity that is altitude-bin dependent.

For a collision to occur between a pair of trackable objects where at least one object is active, collision avoidance must have failed. Maneuvers per year are considered to occur for active maneuverable species at a rate corresponding to the portion of intrinsic collision probability that is not mitigated by Γ . The number of maneuvers for a collision pair in an altitude bin can thus be estimated according to:

$$\dot{M}_{ij} = (1 + \Gamma_{ij})\phi_{ij}Q_iQ_j \quad (5.15)$$

For conjunctions between maneuverable slotted species with slotted orbit coordination effectiveness ζ , a correction factor of $\frac{1}{1-\zeta}$ is applied since the reduction in collision frequency due to this orbit coordination is assumed to occur without maneuvers due to physical orbit separation. For pairs of active objects, we divide the \dot{M}_{ij} contribution evenly between the two species, but this modeling assumption could be modified based on empirical information, for instance, if a particular species corresponds to an operator who prefers to maneuver during conjunction events.

The number of maneuvers per species per time period can then be summed across all relevant species pairs to estimate the number of maneuvers for a species per altitude bin at a particular time in Equation 5.16.

$$\dot{M}_i = \sum^n \dot{M}_{ij} \quad (5.16)$$

This can also be calculated as a per-spacecraft quantity by dividing by the total population Q_i at that time. This per-spacecraft quantity is naturally more useful for collision avoidance burden assessment purposes.

It is important to note that while this modeling approach will produce a maneuver estimate corresponding to the model dynamics, it is subject to non-trivial countervailing sources of error. It will often tend to overpredict maneuvers and collision events due to a reliance on the kinetic theory of gases to model cross-species interaction, and underpredict collision events since it assumes perfect knowledge of when a maneuver is required, with no wasted additional maneuvers. It further assumes that every maneuver is successful at preventing a collision.

In future validation work, the reliability of this indicator should be assessed against the number of potential collision volume incursions calculated within a full-scale 3D MC modeling using the cube method [156] for collision detection. The cube method similarly relies on the kinetic theory of gases but assumes that objects can only potentially collide during periods where they overlap within small cubes of space rather than the expansive bins assumed by MOCAT-SSEM. Outputs from cube method data will naturally need to be scaled to correct for the artificial dependency between derived maneuver counts and cube size. Outputs from both models should be compared against higher-fidelity data that either simulates time-varying object covariances and conjunction analysis pathways or against real historical data on maneuver frequency.

Intrinsic Capacity

Large constellations are typically designed to ensure that satellites within the constellation do not pose a threat of physical collision—referred to as fratricide—to other satellites within the same orbital shell of that constellation. Large constellations overlapping in orbital volume in an uncoordinated manner have the potential to generate significant numbers of close approaches that would necessitate analysis, coordination, and potential mitigation. To avoid this risk, it is reasonable to offset large constellations for mutual exclusion. Separation between large constellations was included as a recommended best practice within a recent

set of recommendations compiled by OneWeb, Iridium, and SpaceX through the American Institute of Aeronautics and Astronautics [2]. If such separation is done using compatible frozen orbits for each constellation, such separation can be accomplished within a relatively modest orbital volume, as described in Chapter 3 and Lifson et al. [93]. Assumptions for minimum acceptable spacing between satellites can be used to extrapolate the maximum number of allowable satellites in a particular orbital shell and the number of acceptable shells using power law fits to empirical two-body results following the methods in [22], [93] and described in Chapter 4. In Lifson et al. [100], these methods were applied to place a constraint on satellites within an SSEM for the purpose of system-wide optimization.

Here, intrinsic capacity, or the number of geometrically allowable and mutually compatible satellites in an orbital volume, is computed on a shell-wise basis using the equation:

$$N_{sat}(i, \alpha_i) = \left(\frac{\alpha(i)}{c(i)} \right)^{\frac{1}{b(i)}} \quad (5.17)$$

where N_{sat} is the number of satellites that can fit within a single shell, α_i is the minimum allowable separation distance between satellites, expressed in terms of either an angle or arc-length converted to an equivalent angle, and c and b are coefficients used to fit the power law to the satellite distribution, following the approach in [93], based on the interval from 500 to 10000 satellites using the 10 highest-capacity solutions for each N_{sat} . Intrinsic capacity is then computed for each bin based on an assumed exclusive height for each shell. The unconsumed intrinsic capacity in a given altitude bin is found as:

$$I_{free} = \frac{d}{h} * N_{sat}(i, \alpha_i) - \sum_i^{N_s} S_i(t) \quad (5.18)$$

where d is the altitude range of each altitude bin, h is the exclusive height assumed to be occupied by a given orbital shell, N_s is the number of species of satellites subject to orbit coordination, and $S_i(t)$ is the population of species S_i at time t . This model ignores inclination dependency, assumes a single allowable in-shell and between-shell separation distance, and does not consider the specifics of the physical geometry of each orbital shell subject to coordination. Nonetheless, it is helpful to limit capacity per altitude bin within the SSEM, recognizing that orbit coordination may impose constraints on orbital placement different than long-term sustainability, particularly if operators are assumed to conduct maneuvers to avoid collisions against trackable objects. This indicator is best used for first-pass analysis on plausibility of placement of large constellations in a compatible manner, to be replaced by actual constellation shell designs and physical geometry for specific overlap analysis for actual orbit coordination.

In this chapter, intrinsic capacity is computed assuming an inclination of 40° , a minimum in-shell separation distance of 60 km, and an exclusive orbital volume of 5 km per shell. These numbers are chosen as a fairly conservative bound for intrinsic capacity. For large constellations with electric propulsion, technically achievable separation distances may be much smaller than these values [95].

5.2.4 Non-Zero Altitude Disposal Orbits

Most previous MOCAT modeling approaches have supposed the instantaneous disposal of de-orbited satellites by removing them from the system. Gusmini et al. explicitly modeled transitions between shells for satellites with low-thrust propulsion [125].

In this work, an intermediate approach is implemented by adding a property “disposal-altitude” as an optional parameter for active satellite species. For a species where a non-zero disposal altitude is selected, satellites that successfully experience post-mission disposal at an altitude greater than the disposal altitude are incremented to k -th altitude bin of the debris species, N_i , that corresponds to the chosen satellite species. This approach is useful to simulate disposal orbits corresponding to various allowable maximum post-mission orbital lifetimes (e.g., a 25 year versus a 5 year rule, assuming circular disposal orbits). It is less suitable for studying elliptical disposal orbits, given the simplifications included in the current model.

Given a set of altitude bins, h , we can construct:

$$\begin{aligned} \text{altitude vector } h &= \begin{pmatrix} h_1 \\ \vdots \\ h_i \\ h_{i+1} \\ \vdots \\ h_n \end{pmatrix}, \\ \text{disposal vector } l &= \begin{pmatrix} l_1 = 1 \\ \vdots \\ l_i = 1 \\ l_{i+1} = 0 \\ \vdots \\ l_n = 0 \end{pmatrix}, \end{aligned} \tag{5.19}$$

and disposal altitude indicator

$$\iota = \begin{pmatrix} 0 \\ \vdots \\ \iota_i = 1 \\ \vdots \\ 0 \end{pmatrix}$$

We can add two additional terms to $\dot{\mathbf{C}}_{PMD}$ for species N_i to represent passivated disposal at altitudes below the cutoff and satellites from higher altitudes that maneuver to the disposal altitude before passivation:

$$\dot{\mathbf{C}}_{PMD} = \dot{\mathbf{C}}_{PMD} + lP_M \frac{Q_i}{\Delta t} + \iota P_M \frac{Q_i}{\Delta t} \sum_{j=i+1}^n C_j \tag{5.20}$$

If satellites were moved to a disposal altitude but retained collision avoidance capabilities, that would be modeled differently, with a transition between altitude bins for the same active species rather than to a debris species.

5.3 Results

This section demonstrates several potential roles that modeling could play within an adaptive governance regime using MOCAT-SSEM, including assessing marginal traffic for compatibility with environmental objectives, modeling effects of environmental changes, and estimating effects of various actions, either individually or in concert. While not demonstrated here, MOCAT-SSEM could also be used to assess the impact of different factors that change endogenous launch rates (i.e., launch rates determined dynamically in the simulation based on agent-based logic, environmental states, and future expectations), examine impacts of changes on system-wide optimization solutions, and evaluate the relative impact of a particular mission on the environment.

The purpose of these demonstrations is to show in concrete terms how evolutionary space debris modeling could be used to support an adaptive governance process. These examples are not intended to indicate that any particular management concept should be unilaterally implemented by a regulator, but rather to demonstrate how quantitative models could be used to support analysis and potential implementation of such management actions if they were endorsed by stakeholders in a relevant adaptive process.

The results in this section use an uncalibrated model built using the MOCAT-SSEM framework, which features multiple substantial simplifying assumptions. Verification and validation work is ongoing, with only limited calibration work published to date for simpler MOCAT SSEM models [120]. Calibration is still being implemented into the full MOCAT-SSEM framework to support multiple mass-binned species and other features. In particular, because the uncalibrated MOCAT-SSEM model used in this work employs a collision model that assumes that all fragments from a collision are deposited in the altitude bin where the collision occurs and that collision probability is dependent on the kinetic theory of gases, it tends to overstate the number of collisions that result. Accordingly, the results from this work are at best indicative of potential trends and should not be used to inform decision-making without further verification.

5.3.1 Adaptive Authorization Pathway

In the first modeling approach under this section, MOCAT-SSEM is configured to measure indicators for long-term sustainability, operational collision avoidance, and intrinsic capacity. Figure 5.4 shows how assumptions feed into the model, which produces outputs for metrics relating to various capacity constraints, indicating whether the constraints are satisfied on a shell-wise basis. For the purpose of this example, the following constraints are assumed. In an actual adaptive process, these would be determined through a consensus approach based on discussions between stakeholders.

1. **Long-Term Sustainability:** The numerical derivative of the number of debris objects in any altitude bin for each species shall be non-positive, as measured by the slope coefficient of a linear fit to the last 50 years of the simulation period. This fit period is used to avoid having periodic effects due to solar cycle expansion and contraction influence this indicator.

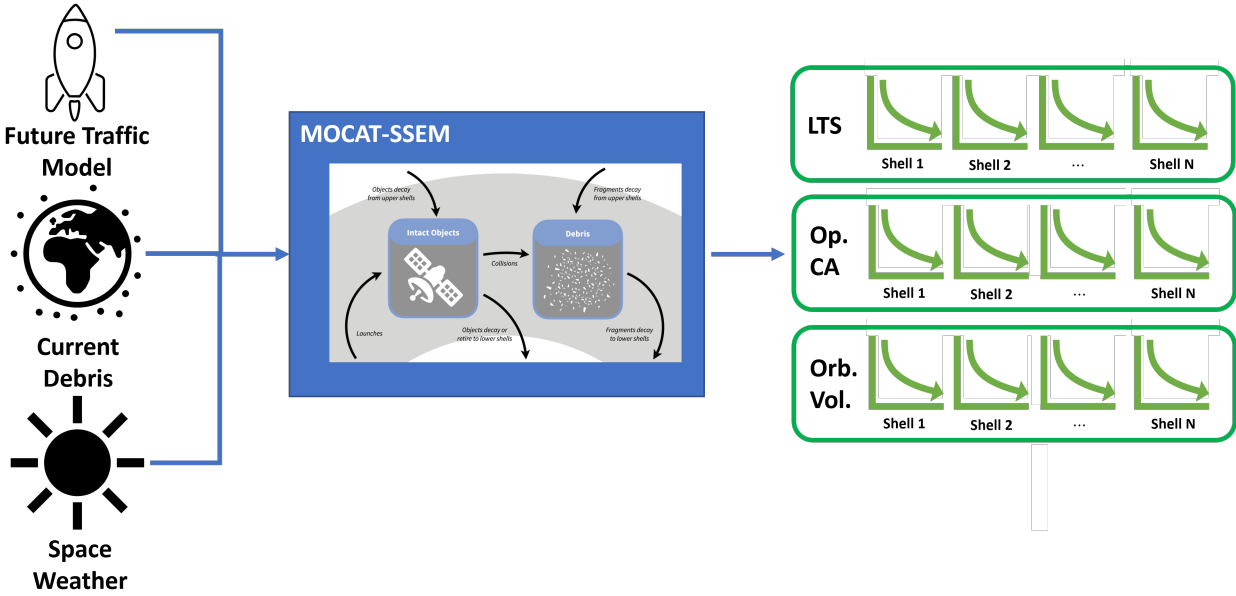


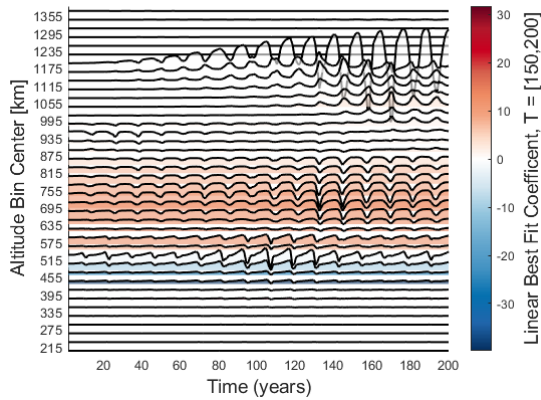
Figure 5.4: Baseline Modeling Process Diagram.

2. **Operational Collision Avoidance:** No more than 1% of satellites within any given species in any given altitude bin shall be lost in a given year to collision events. A given satellite shall not have to perform more than 12 collision avoidance maneuvers per year.
3. **Intrinsic Capacity:** The number of satellites within large constellations shall not exceed the quantity associated with preserving 60 km between satellites within shells and 5 km between shells.

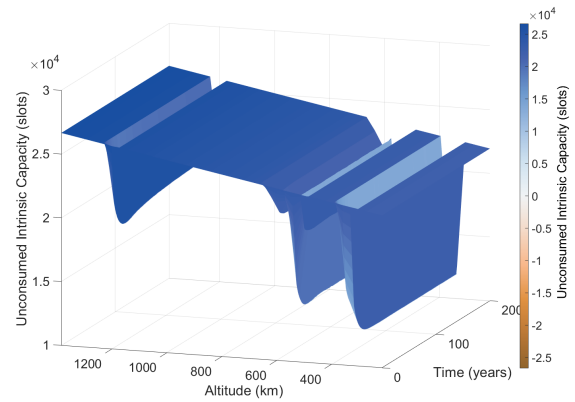
The model is then run and these constraints are evaluated to assess whether or not they are met.

Baseline Model

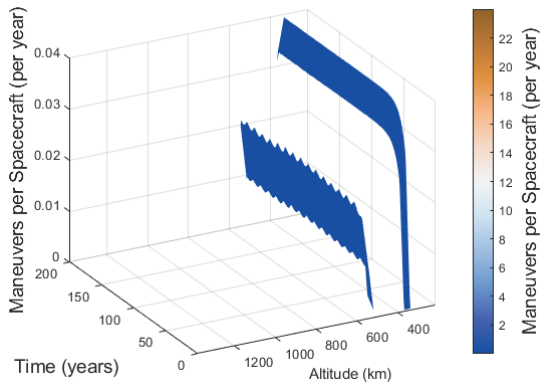
In Figure 5.5, we see various outputs for the model run, with good values in blue and bad values in red. In Figure 5.5a, we see data for the LNT species indicating that while there are strong oscillatory effects at high altitudes, they do not necessarily violate the constraint. However, there is an altitude range in the middle of the graph from approximately 575 to 875 km where the constraint is not met. While only one species is displayed in this chapter due to space limitations, in practice all populations would be reviewed, either individually or in aggregate. In Figure 5.5b, we see dips in intrinsic capacity associated with the various modeled LLCs, but note that there is still remaining excess intrinsic capacity. In Figure 5.5c, a per-species quantity is shown, and we see that about 1 in 25 S_{1250} spacecraft will have to maneuver each year to avoid a collision with a tracked object, well below the threshold. In Figure 5.5d, we see a violation of the operational collision avoidance constraint at high altitudes far into the future. Because high-altitude debris is not mitigated earlier in the



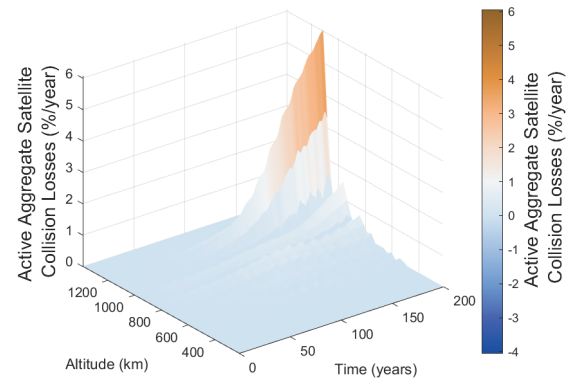
(a) Population Trends for LNT Debris Population.



(b) Intrinsic Capacity.



(c) Collision Avoidance Maneuvers per Spacecraft for S_{1250kg} Species.



(d) Aggregate Collision Losses for Active Spacecraft.

Figure 5.5: Baseline Constraint Satisfaction. The intrinsic capacity and shown maneuver constraints are satisfied globally, while the aggregate collision loss and population trends show altitudes that violate the chosen constraints. This is described further in Subsection 5.3.1

simulation, it gradually fragments over time into a large amount of LNT debris, making the orbit unacceptably dangerous. In this baseline model run, we see that not all constraints are met. This indicates that action will be needed as part of the governance process. Stakeholders could choose to revise constraints on indicators, adopt additional mitigation or remediation actions, or limit traffic.

Safe-Harbor Review

In this example, we assume that the adaptive governance institution decides to implement a process whereby constellations are evaluated using the modeling tool to ensure the environment remains compliant with the goals for various indicators in the presence of the new traffic. We further assume that there is a regulator involved in the process with authority to

approve or reject proposed traffic. This assumption simplifies the description of the workflow but is not an inherent requirement. A similar process could be conducted on the basis of a processing round rather than per application. Likewise, similar review could be used to inform a safe-harbor provision to avoid more detailed scrutiny of a constellation’s orbital use rather than an approval or denial decision. For simplicity in this example, a single constellation will be considered, and the information from the SSEM model run alone is used to qualify for a safe-harbor condition rather than to provide an approval or denial decision. As described here, the regulator only considers whether the added traffic remains within the capacity as defined by the chosen indicators. It does not make any evaluation on efficiency of orbital use or other trade-offs (although an adaptive governance system could impose such a consideration).

The fictitious applicant, AstroCorp., proposes a consistently replenished satellite constellation of 200 24 kg 12U CubeSats without propulsion or maneuverability at 500 km. Satellites operate for one year. This is modeled with two new species, shown in Table 5.5. In the model, the paired derelict class is excluded from being spawned by collision events and the initial/future launch model to preserve traceability. AstroCorp. adds their mission to the baseline model run and finds that the net contribution from their mission to any of the constraints is negligible. They demonstrate, as seen in Figure 5.6 and 5.7, that the constellation produces few collisions and requires few maneuvers by other maneuverable actors to avoid either the satellites or debris. They do not use intrinsic capacity and have negligible effect on long-term sustainability due to their altitude. The regulator thus permits AstroCorp. to use a streamlined capacity review process that waives certain analysis requirements.

While AstroCorp. received accelerated review, the opposite is also possible. A constellation that showed problematic changes to indicators could be subject to higher scrutiny or potentially be required to revise their constellation to comply with the modeling outcomes determined by the adaptive process.

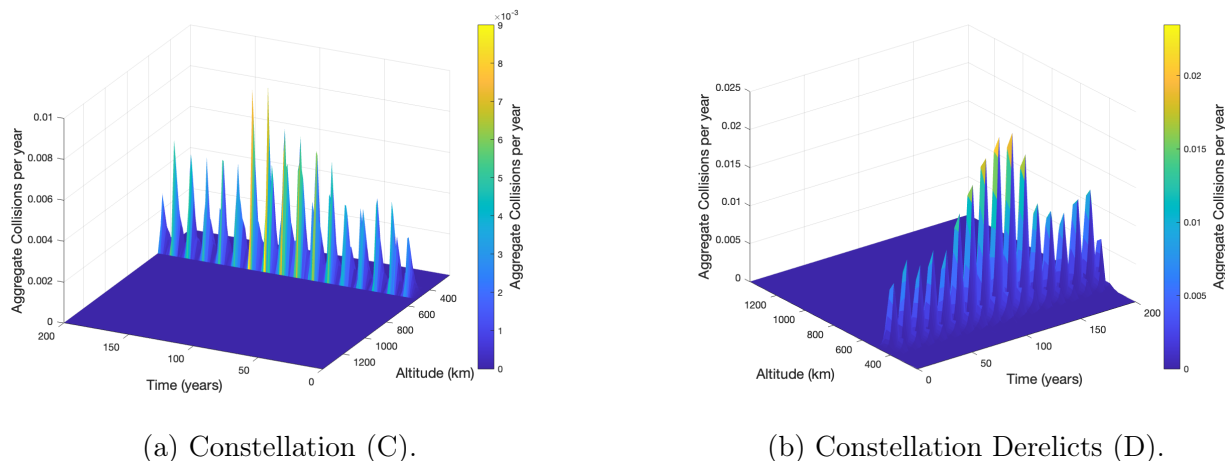
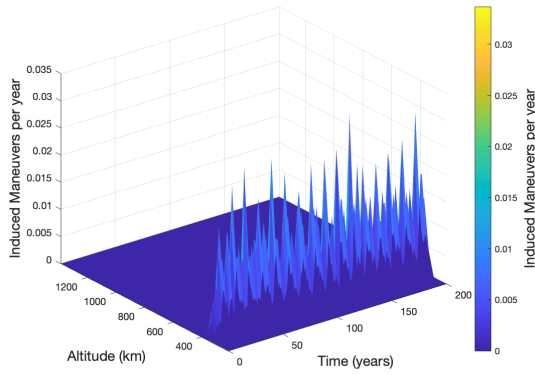


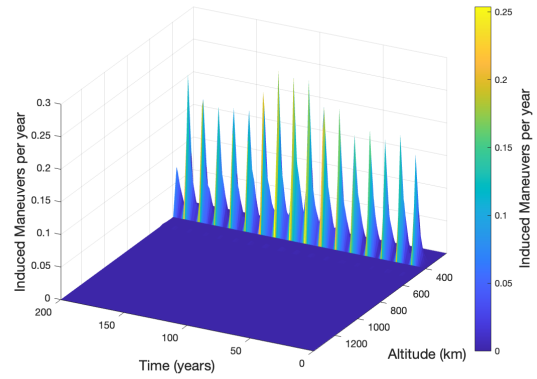
Figure 5.6: Additional Aggregate Collisions from the New Constellation (C) and Constellation Derelicts (D). There is additional collision risk near AstroCorp.’s operational altitude from operational satellites and satellites that fail on-orbit, but the risk is minimal.

Table 5.5: Species and Properties for Additional Species Added for Demonstration Case

Symbol	C	N_c
Description	Candidate Constellation Streamlined Review (Section 5.3.1)	Paired Debris Class Streamlined Review (Section 5.3.1)
Cd	2.2	2.2
Mass [kg]	24	24
Radius [m]	0.261	0.261
Area [m²]	0.681	0.681
Active	true	false
Slotted	false	false
Drag	true	true
Maneuverable	false	false
Trackable	true	true
Mission lifetime	1	N/A
Post-mission disposal	N/A	N/A
Disposal altitude	N/A	N/A
Efficacy of collision avoidance vs. inactive	N/A	N/A
Efficacy of collision avoidance vs. active	N/A	N/A
Rocket body	false	false
Launch rate	empirical fit (200 sat @ 500 km, replenished every 1 years)	N/A



(a) Constellation (C).



(b) Constellation Derelicts (D).

Figure 5.7: Additional Induced Maneuvers from the New Constellation (C) and Constellation Derelicts (D). The additional maneuvers induced by the constellation and its derelicts are minimal.

Table 5.6: Fragment Counts for the Simulated ASAT Missile Test

	$N_{0.0014137\text{kg}}$	$N_{0.567\text{kg}}$	$N_{6\text{kg}}$
Fragments	56,037	608	45

5.3.2 Adaptation to Changes to Environmental Conditions

In this example, an ASAT missile test is modeled as occurring 8.0402 years into the simulation (chosen arbitrarily) at 800 km involving a 500 kg object with a 2 m radius and an 8000 kg object with a 32 meter radius. The event generates the fragment counts in Table 5.6. Those fragments are modeled as being deposited into the altitude bin containing 800 km, although this assumption is not particularly realistic. Recall also that the initial population excludes the substantial amounts of sub-trackable debris already at these altitudes. In comparing Figures 5.8a and 5.8b, the sharp spike in debris creation due to the ASAT event is clearly visible, with the region already violating the long-term sustainability constraint and continuing to do so after the test. However, the long-term slope of the line remains similar. Based on predicted LNT collision rates and the background environment, adaptive management participants could discuss if they need to adapt any decision rules in response to the event, such as discouraging traffic to impacted altitudes, encouraging additional spacecraft shielding, or pursuing enhanced on-site monitoring to better estimate LNT flux.

5.3.3 Decision Support to Changes to Behavior

Another major category where integrated modeling can be helpful is in assessing the approximate outcomes of various interventions. Comparing a model run with and without an intervention is valuable for assessing a wide range of potential interventions to understand trade-offs. Such interventions might include use of cross-operator orbit coordination between LLCs, greater or less compliance with PMD requirements, or changes to maximum post-orbit

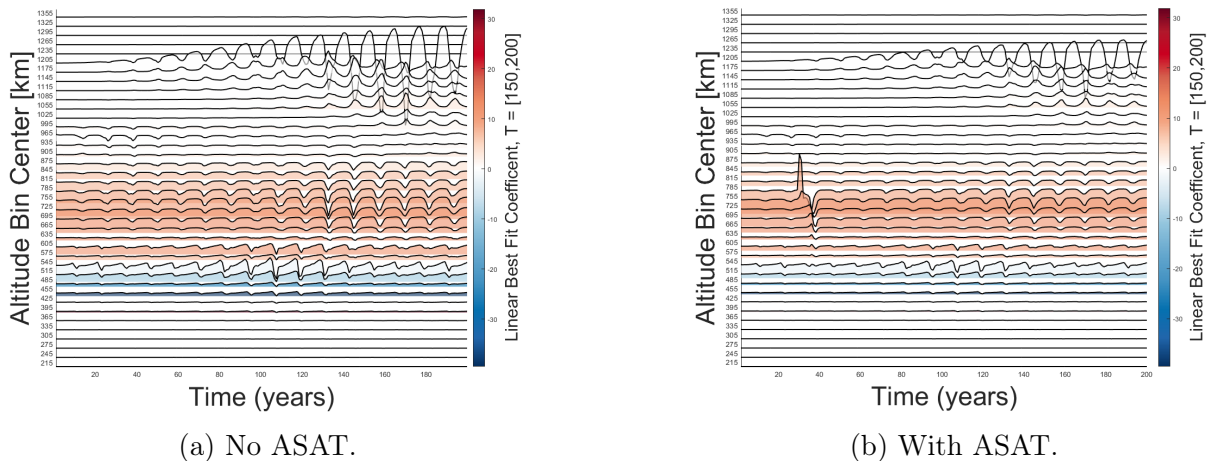


Figure 5.8: Long-term Sustainability Constraint, Evaluated with and without ASAT Test.

lifetime. Because the behavior of individual spacecraft does not need to be explicitly simulated to represent such actions in an SSEM, it is often easy to represent such changes by altering parameters or with minimal additions to the model. This section provides an example using the non-zero altitude disposal introduced in Section 5.2.4.

Post-Mission Disposal Altitude

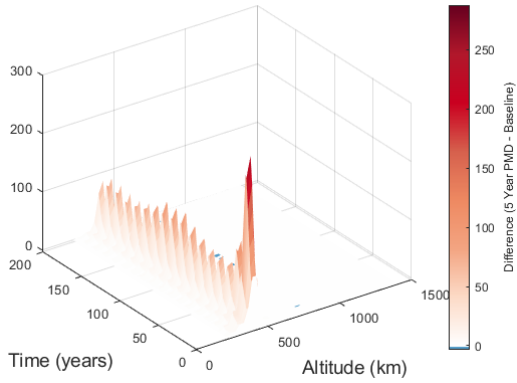
In this example, stakeholders are considering implementing a five-year rule for maximum post-mission orbital lifetime. They assume that, despite requesting that operators de-orbit as soon as possible, many operators will only passivate spacecraft at altitudes sufficient to comply with this rule. To model this effect, the PMD equations are changed so that maneuverable non-LLC spacecraft, S_u , that successfully complete PMD above the disposal altitude are no longer immediately removed from the scenario but deposited into a disposal orbit sufficient to de-orbit in five years or less.

For each species of S_u , this altitude was estimated by propagating a representative satellite until it reached 200 km using the Orekit astrodynamics library’s implementation of the DSST with a modified Harris Priester atmosphere model (429 km for S_{260kg} and 573 km for S_{473km}).

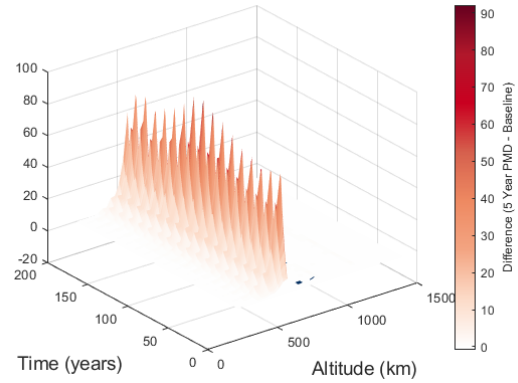
A comparison was conducted between instantaneous disposal and this new behavior. As seen in Figure 5.9, we see the expected increases in derelict populations from the new policy. Figure 5.10a shows that the policy results in between 0.1–0.25 additional low-altitude collision events per year, while Figure 5.10b shows up to about a half an additional maneuver per spacecraft per year for the S_{u473kg} species.

5.4 Summary and Future Work for Chapter 5

This chapter considered space environment management in the context of prior learning on governance of natural resource systems and demonstrates how evolutionary space environ-

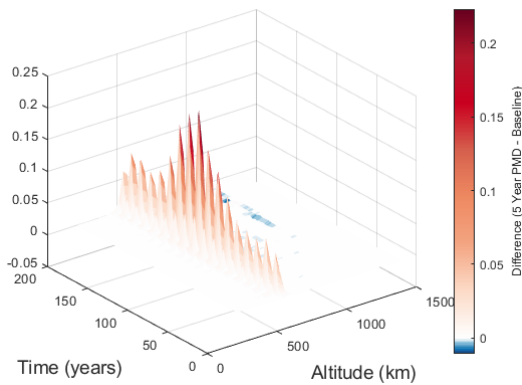


(a) N_{260kg} Population Difference.

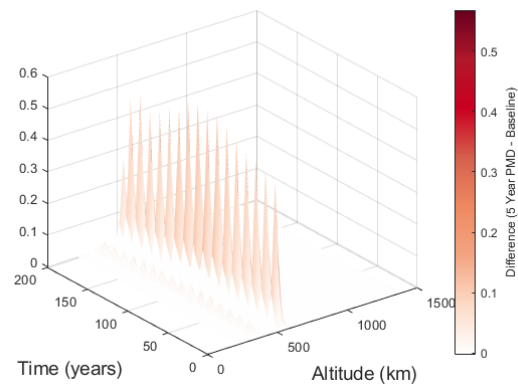


(b) N_{473kg} Population Increase.

Figure 5.9: Derelict Population Increases from Five-Year Rule versus Instantaneous Disposal.



(a) N_{473kg} Additional Collisions.



(b) $S_{u_{473kg}}$ Additional Collision Avoidance Maneuvers per Spacecraft.

Figure 5.10: Derelict Population Burden from Five-Year Rule versus Instantaneous Disposal.

ment models could be used to support adaptive management and governance processes. This role was demonstrated using MOCAT-SSEM and a set of notional constraints to orbital capacity that capture different potential stakeholder interests. More technical work is needed to calibrate, verify, and validate MOCAT-SSEM and build community familiarity with the entire MOCAT.

This chapter has made the case that incorporating evolutionary environmental modeling more directly into deliberations around orbital use is a necessary change if we want to improve the quality of decision-making on space debris mitigation and remediation. Several steps are necessary to achieve this shift. First, across a variety of fora, we need to develop consensus around measurable technical definitions for what we mean by space sustainability, the factors we believe constrain our use of the space environment, relevant modeling assumptions, and indicators that capture the aspects that matter to different classes of stakeholders. Second, we need to build community confidence in and ability to use modeling tools, as well as devote resources to make them available and usable to stakeholders. Trusted, accessible, sufficiently-capable models are a critical prerequisite for successful adaptive management. Third, we need to start to incorporate notions of orbital capacity into our decision-making—whether because capacity constrains our actions or because the data show that it does not. Shared resources that are finite need to be understood and used efficiently and equitably. At the same time, it is important to avoid the siren’s call of scientific management. Incorporating evolutionary space environment models more directly into management decision-making is important but will likely not lead to success if used as part of a highly centralized process mediated by adversarial legal interactions between stakeholders. Fourth and lastly, work is needed to socialize these ideas within the space community, determine potential convening organizations, and build stakeholder support and participation. Whether efforts coalesce around a convening government entity, a voluntary private effort, or another structure, it will take significant will and a groundswell of support to build and maintain relevant structures and institutions to support improved decision-making processes.

Chapter 6

Quantifying the Benefit of Orbit Coordination between LLCs

This chapter seeks to quantify benefits from an orbit coordination scheme such as that proposed in Chapter 3. These benefits come from two main effects. First, orbit coordination produces a reduction in conjunction events between on-station spacecraft that need to be analyzed, coordinated, and potentially mitigated by maneuvers. Second, if collision avoidance efficacy is less than perfect, such coordination also reduces the frequency of collision events arising from unsuccessfully mitigated or missed high-risk conjunctions (and associated fragmentation products).

The analysis in this chapter uses MC techniques and primarily focuses on avoidable conjunctions rather than collisions, following advice that arose from the interviews in Chapter 4. Colvin et al. [155] conducted extensive stakeholder engagement to estimate the monetary cost of conjunction risk assessment and collision avoidance and found burden associated with risk analysis and maneuvers to be relatively small for most classes of payloads. Nonetheless, the sheer frequency of conjunctions associated with non-coordinated orbits could challenge the feasibility of even highly automated workflows, increase the risk of accidents associated with coordination failures, and turn even modest marginal costs into significant aggregate sums.

MOCAT-MC, while higher fidelity than SSEM models, still involves significant simplifying assumptions that diverge from the actual space environment, including simplified satellite station-keeping, the use of the cube model to estimate long-term collision rates for active constellations, and a single future launch traffic scenario. Nonetheless, the simulation is intended to provide at least indicative evidence about the magnitude of benefits to orbit coordination between large constellations. Quantifying such benefits may be helpful when engaging with and seeking to persuade additional stakeholders, even though benefit quantification was generally not necessary to persuade the stakeholders interviewed in Chapter 4.

Analysis examining changes to orbital capacity and collision rates as a function of the active-on-active collision avoidance failure rate was conducted with the MOCAT-4S SSEM, an SSEM that distinguishes between unslotted spacecraft and constellations with coordinated mutually exclusive orbits, in D’Ambrosio et al. [99] and Lifson et al. [100]. In this work, an optimization was conducted for a constant launch rate, Λ , subject to constraints on

intrinsic capacity, long-term sustainability, and the ratio of slotted to unslotted launch rates. That work found only limited gains to the overall number of admissible satellites and reductions to collision rates from orbital coordination at plausible collision avoidance maneuver failure rates. While preliminary work to estimate maneuver rates using MOCAT-SSEM was presented in Subsection 5.2.3, significantly more work is necessary to verify and qualify the approach before it would be suitable for this form of analysis.

6.1 Relevant Prior Analyses

Multiple prior analyses have looked at the conjunction and collision burden associated with large constellations. Alfano, Oltrogge, and Shepperd [62], [86], [157] developed and used NEAT to assess rates of conjunctions and predicted collisions for various classes of objects. In their most recent work, the authors found significant active-on-active collision risk in the approximately 400–600 km altitude range, but also that this risk was dominated by risk associated with the active-on-debris population across most of this altitude range. Viasat used the NEAT tool to estimate warnings, maneuvers, and collisions versus the trackable catalog over 15 years and found what they considered concerning numbers of potential conjunctions, maneuvers, and collisions for Astra, China SatNet, Lynk, OneWeb, and SpaceX (both Gen1 and Gen2), absent mitigations [158].

6.2 MOCAT-MC

MOCAT-MC is an MC evolutionary space environment model [33], [61], [121]. The model features an analytic propagator including atmospheric drag using the JB2008 model and the J_2 perturbation [33]. ASOs are divided into active and inactive objects. The mean semi-major axis of an active object is restored to the mean semi-major axis of its reference orbit every five days. At the end of their operational lifetime, active satellites undergo post-mission disposal with a certain configurable probability. Satellites from large constellations complete post-mission disposal with an efficacy of 90%, other satellites at 80%, and rocket bodies at 55%. Disposed objects are removed instantly from the simulation. Fragmentation events generate fragments following the NASA SBM with the distinctions implemented between catastrophic and non-catastrophic collisions [128]. While MOCAT-MC can model spontaneous explosions, none are included in the simulations in this chapter.

6.2.1 Collision Modeling

Collisions are estimated using the cube method [66]. The environment of interest is divided into cubes. At a regular sampling rate, each cube is examined. If two objects are present in the same cube, they are assumed to have a possibility of collision defined according to the kinetic theory of gases, similar to the assumption employed in MOCAT-SSEM on a shell-by-shell basis:

$$P_{i,j} = s_i s_j v_r \sigma V \tag{6.1}$$

where the probability of collision between objects i and j is calculated as the product of their spatial densities, s_i and s_j , the relative velocity of the collision, v_r , the sum of their cross-sectional area, σ , and the volume of the cube considered by the model, V . In this work, cubes with a side length of 10 km are used. Trackability is demonstrated using an altitude-based empirical formula from Jang et al. [33]. If a collision occurs, fragments are generated following the NASA SBM and propagated forward. No reduction to collision probability is applied for conjunctions vs. non-trackable objects. For trackable objects and active spacecraft, various reduction factors are applied. α is a reduction factor for conjunctions between an active and a trackable inactive object. α_a is a reduction factor for conjunctions between two active non-constellation objects. $\alpha_{c_{intra}}$ is the fraction of collision avoidance failure for conjunctions within a particular constellation and is assumed to be 0 due to the widespread use of safe-by-design orbits. $\alpha_{c_{inter}}$ is the fraction of collision avoidance failure between constellation spacecraft from different constellations. A generic high solar cycle prediction is used as the input to the JB2008 model.

6.2.2 Baseline Traffic Model

The scenario simulated employs a composite future launch model, combining repeating historical traffic and proposed large constellations. The future constellation launch model uses the data from Jang et al. [61] and reproduced in Table 3 of Appendix E. The list of constellations is derived from the ITU, FCC, and other data sources as a guess for constellations that will be launched. It assumes that satellites are directly injected to their operational altitude (i.e., orbit-raises are neglected) and that each shell is continuously replenished after reaching full deployment for the remainder of the simulation. A non-constellation future traffic model is also used, assuming that traffic from 2018 to 2022 is repeated indefinitely into the future with the launch date randomized within one time-tick of the MC simulation (set to five days in this work) within the year of the cycle where it originally occurred. The injection mean anomaly of traffic is also randomized.

6.2.3 Method

For the analysis in this section, two MOCAT-MC scenarios were assessed with differing collision avoidance behavior. The difference in collision avoidance behavior is summarized in Table 6.1. The first models the baseline traffic for the constellations included in the baseline traffic model in Section 6.2.2. In this model run, all active spacecraft are assumed to be maneuverable and capable of avoiding collisions with other active spacecraft with perfect efficacy. A rate of failure of 1% is assumed for active versus inactive traffic, modeling that collision avoidance efficacy may not be universally well performed across all traffic but assuming that all active-on-active conjunctions result in perfect collision avoidance. In the second run, we assume that a low but non-zero rate of failure occurs across all active-on-object conjunctions, assuming that constellation shells are safe by design. The rate of 10^{-5} was chosen to represent a plausible but high failure bound on collision avoidance efficacy.

In each run, every conjunction is logged to compare the evolution, quantity, and percentage of cube interactions for active-on-active and other object pair types. This quantity is

Table 6.1: Collision Avoidance Failure Rate

	Scenario 1	Scenario 2
α	0.01	10^{-5}
α_a	0	10^{-5}
$\alpha_{c_{intra}}$	0	0
$\alpha_{c_{inter}}$	0	10^{-5}

used as a proxy for conjunction volume. We also compare collision rates and the long-term evolution of the debris environment between the two simulations.

It is important to know that there are several significant limitations with this approach. First, the station-keeping and propagation approach is relatively crude and does not necessarily accurately preserve constellation structure and object reference trajectories. Second, the cube method does not accurately predict when objects could collide. For instance, objects in circular orbits 10 km apart directly above and below one another will be detected as a conjunction but may actually be passively safe by design. Third, we do not know how the constellations included in this simulation will orient and maintain their operational orbits. These limitations mean that conjunctions and collisions from the simulation are potentially indicative of burdens that could be avoided through coordinated orbit design, but that there is potentially significant unquantified modeling error associated with the specific numbers produced in these results.

6.2.4 Results

In each scenario, 10 runs were performed. Post-mission disposal failures and collision events are stochastically generated in each run, and launch traffic is randomized as described previously. The displayed results are averaged results across the runs.

Scenario 1: Perfect Active-on-Active Collision Avoidance

As can be seen in Figures 6.1 and 6.2, the populations in the simulation are unsustainable, with increasing numbers of conjunctions between debris and derelicts over time. Almost immediately as large constellations are deployed, constellation-on-constellation conjunctions (which exclude intra-shell events) dominate other types of conjunctions, before eventually being overtaken by debris-involving events. As seen in Figure 6.3, which contains only conjunctions involving active spacecraft, we see that constellation-on-constellation events constitute a significant fraction of conjunctions. Per-pair statistics are listed in Table 5 in Appendix E. This result should provide powerful motivation to mitigate avoidable constellation-on-constellation events through orbit coordination.

Next, we examine the contribution of individual constellations to the conjunction volume. Figure 6.4 tracks the number of conjunctions across different operators for constellation-on-constellation conjunctions. Starlink, China SatNet, and Astra show particularly high rates of conjunctions, which is expected given the size and altitudes of those constellations. Per-pair statistics are listed in Table 4 in Appendix E.

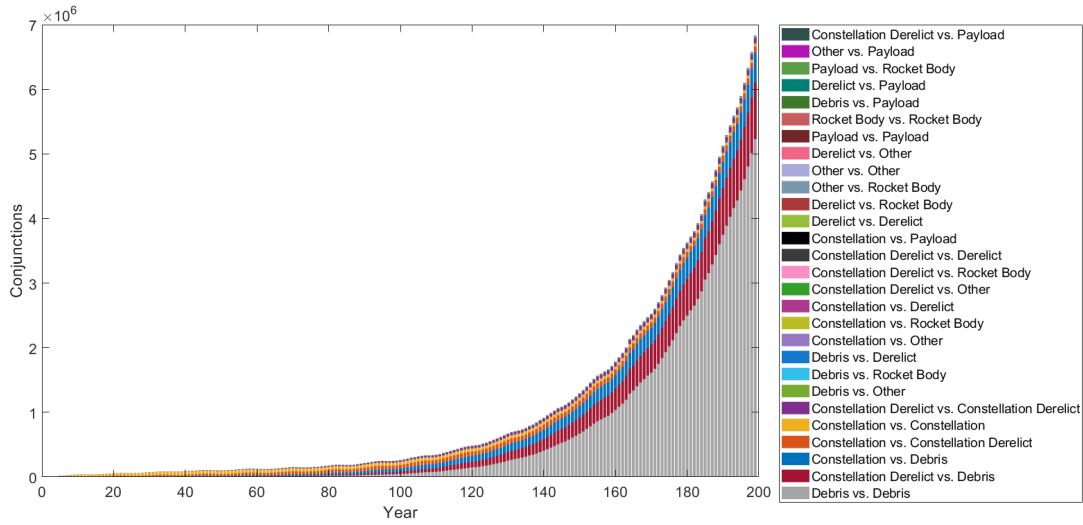


Figure 6.1: Scenario 1: Object Type Pairs for Conjunctions. The scenario experiences runaway debris growth.

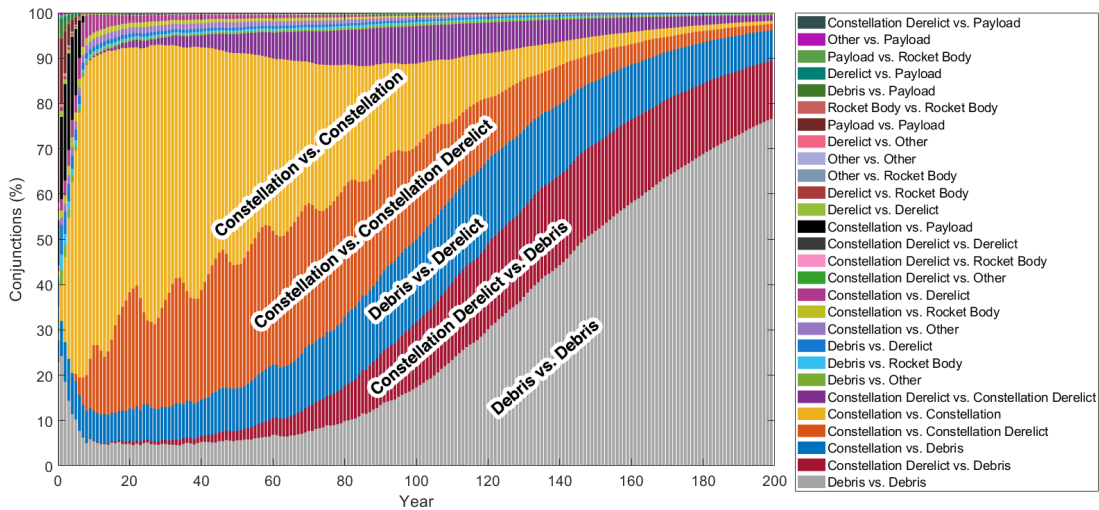


Figure 6.2: Scenario 1: Object Type Pairs for Conjunctions (Percentage). Cross-constellation events form a substantial portion of conjunctions until debris growth dominates.

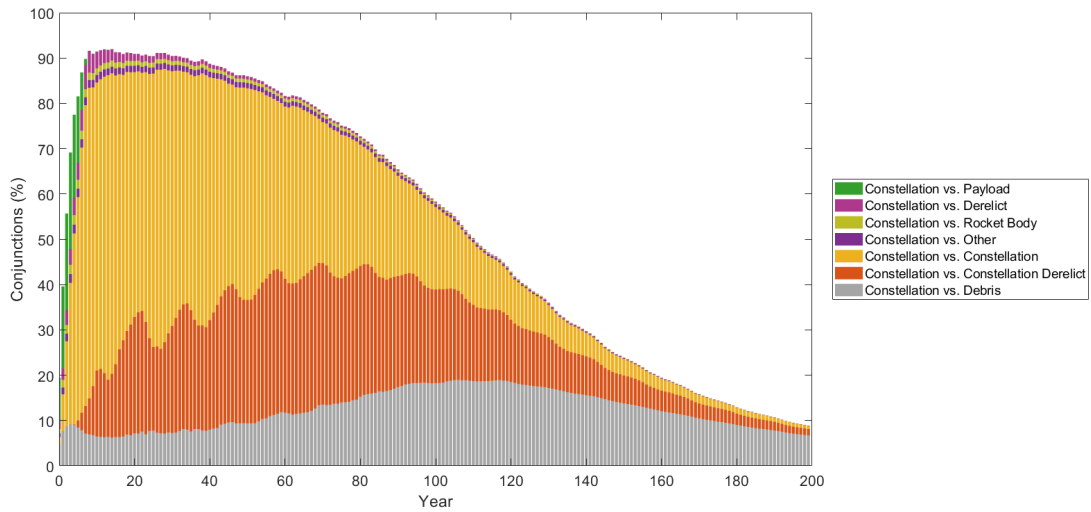


Figure 6.3: Scenario 1: Object Type Pairs for Conjunctions, Pairs involving Constellations Only (Percentage).

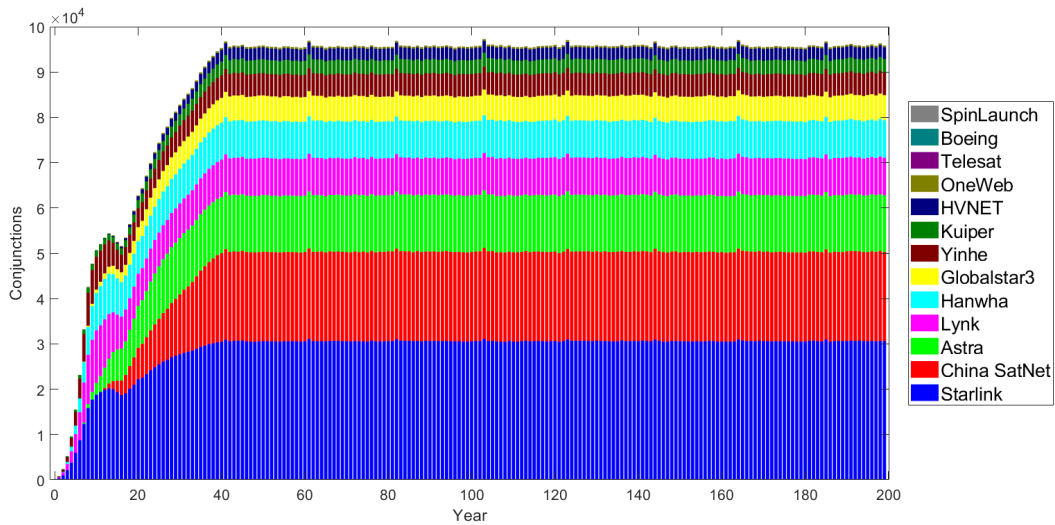


Figure 6.4: Scenario 1: Constellation-on-Constellation Conjunctions by Constellation.

Scenario 2: Imperfect Active-on-Active Collision Avoidance

This scenario was intended to explore the consequences for the LEO environment from a low but non-zero collision avoidance failure rate. The simplified modeling used assumes that all conjunctions require a collision avoidance maneuver. If a maneuver fails, we simulate a fragmentation event. Surprisingly, with a maneuver failure rate of 10^{-5} , none of the 10 simulation runs generated a constellation-on-constellation collision. We thus conclude that, to the extent the MOCAT-MC run accurately models this operational choice, there are limited benefits to mitigated collisions from orbit coordination, as high-efficacy collision avoidance systems seem adequate to mitigate trackable active-on-active collision risk.

6.3 Conclusion

This brief chapter quantifies the benefits from large constellation orbit coordination. Using MOCAT-MC, it found that constellation-on-constellation conjunctions constitute a significant portion of overall conjunction burden (sometimes over 60%), particularly in the early years following large constellation deployment before derelicts and debris events eventually dominate quasi-constant constellation-on-constellation burden. Unexpectedly, large constellation collision risk was totally mitigated by the combination of low in-cube intrinsic collision probability and high-efficacy (10^{-5} failure rate) collision avoidance. We conclude that the benefits from orbit coordination in terms of collisions, orbital capacity, and the overall evolution of the space environment are limited.

Even if overlapping large constellations would not result in additional collisions due to highly reliable and effective collision avoidance capability, results demonstrating the significant burden associated with the sheer number of constellation-on-constellation conjunctions provide strong quantitative support to the assertion that large constellations should be deployed with coordinated, mutually exclusive orbits.

Chapter 7

Summary and Future Work

7.1 Summary

This thesis makes the case that orbit coordination for inherent orbital separation is a useful tool to help enable additional safe density of orbital use. It also provides a necessary, if not sufficient, framework to understand orbital use, particularly for large constellations. Chapter 3 demonstrates techniques to design and efficiently tessellate orbital shells that are self-safe and mutually safe. It also presents techniques to estimate or assess the shapes of these shells and the improvements to intrinsic orbital capacity associated with coordination. Chapter 4 synthesizes work on intrinsic capacity to describe further how intrinsic capacity can be used to quantify and support rational, efficient, and equitable use of orbital volume. It then describes potential pathways to implementation and assesses these pathways with a limited set of current and future large constellation operators. Chapter 5 pivots slightly, describing adaptive governance frameworks and their applicability to orbital capacity and space sustainability, demonstrating the integration of MOCAT-SSEM into various governance-support roles. Chapter 6 quantifies the benefits of slotting using MOCAT-MC, demonstrating that orbit coordination schemes have the potential to avoid a significant portion of orbital conjunctions that would occur without mutually exclusive constellation orbits.

7.2 Contributions

Each body chapter makes intellectual contributions. In Chapter 3, extremely large osculating 2D-LFCs are demonstrated for the first time and applied to provide a potential solution to real-world orbital compatibility problems, as well as to derive recommendations on efficient orbital use that improve orbital density by a factor of 2–20 times compared to non-coordinated alternatives. Simplified practical tools for estimating geometry in the latitude-altitude plane are also presented which enable approximate stacking analysis at considerably less complexity and computational burden than fully defining and propagating large constellations. In Chapter 4, the corpus of our prior work on slotting is placed in an applied context to illustrate practical uses and make the work accessible to regulatory engineers and subject-matter experts supporting policymakers. This is accompanied by the first extensive policy analysis on pathways to implement slot-based orbit coordination and the

consequences for achieving various potential policy objectives. Chapter 5 provides a detailed and quantitative integration of a LEO evolutionary environmental model into an adaptive governance framework for space sustainability. Chapter 6 provides suggestive quantitative evidence that underscores the significant numbers of conjunctions that can be avoided by an orbit coordination scheme, a quantification that, to our knowledge, has not yet been explicitly calculated in the published literature.

7.3 Future Work

There are multiple areas where the work described in this thesis could be expanded. In Chapter 3, work could be done to develop screening tools to tractably assess in-shell minimum separation distances for osculating constellation designs and to determine achievable shell widths in the presence of sudden changes to solar weather and atmospheric density estimation error. In Chapter 4, accessible public tools could be developed to implement the kinds of capacity analysis considered in Section 4.2. Additional analysis could be conducted to quantify the general cost of failing to plan ahead when designing constellations to be reconfigurable for expansion. Significantly more stakeholders could be interviewed to develop a better sense of stakeholder opinions on orbit coordination, particularly among non-Western operators. In Chapter 5, work could be done to begin implementing an adaptive management and governance regime and to explore productive national resource management concepts from other non-space domains as well as TEK. Work is needed to complete verification and validation for MOCAT-SSEM, develop supporting documentation, and add additional features such as elliptical orbit support. In Chapter 6, analysis fidelity could be significantly improved by use of a model that maintains satellite orbits according to actual control laws and realistic (speculative) reference trajectories, tracking estimated covariances, conjunctions, maneuvers, and collisions based on actual probabilities of collision. Incorporation of the NEAT method into MOCAT-MC might help to reduce some of the potential false positives associated with use of the cube method for conjunction estimation across geometrically structured sets of constellations.

7.4 Final Remarks

This work is united by a fundamentally translational objective: to provide an engineering and governance framework with which to inform and support decisions about intrinsic capacity as part of broader discussions on orbital use. The work in this thesis, and associated collaborations, has sought to demonstrate analytical tools to discuss potential orbital use with precision in both an engineering and policy context. These methods can be used to assess the efficiency with which operators make use of space, quantify remaining occupiable orbital volume, improve resource use, and provide technical rigor to support conversations about equity in orbital use.

It is our fervent belief that such conversations can, and should, be held now in an inclusive manner across a variety of fora. Early conversations and coordination can lock in low-cost, win-win coordination and orbital separation. In contrast, the longer we delay, the

more we risk locking in suboptimal architectures, to the detriment of future missions and the environment. Coordination will be especially critical in an international context given the likely juxtaposition of large Western and Chinese constellation shells at multiple LEO altitudes. Fortunately, the technical recommendations proposed in this work already align with engineering design choices (e.g., near-circular shells, frozen orbits, and uniform constellations) that most large constellations already select for self-motivated engineering reasons. Communication and coordination mechanisms and governance can and should grow from this happy accident. If we make the effort, our design choices can ensure that there remains ample room in LEO for new entrants and emerging space operators. It can also ensure that we are well poised for potential shell-sharing coordination mechanisms when required by the eventual density of orbital operations.

Appendices

A Initial Equinoctial Elements for Constellation Seed Orbits

This appendix contains computed equinoctial elements for the seed orbit for each of the major constellations displayed and analyzed in this paper.

Table 1: Seed Trajectories for Constellations

Constellation	a [m]	e_x	e_y	h_x	h_y	l_m [rad]
SpaceX 604 km	6989892.306	-0.0011007277	0.0005397019	3.4834154926	0.0062728318	3.1383439840
Amazon 610 km	6994747.474	-0.0009463572	0.0005784624	0.3842483520	-0.0006048589	3.1357222512
SpaceX 614 km	7001489.016	-0.0006185179	0.0012116838	1.5901223905	0.0014565147	3.1377484004
SpaceX 614 km Uncoordinated	7001405.495	-0.0006223543	-0.0018674285	1.5901242611	0.0014527746	3.1439014133
Amazon 630 km	7013732.330	-0.0007865047	0.0009351080	0.4870550411	-0.0006328345	3.1357521642
China SatNet 30	7507996.598	-0.0009763066	0.0004924818	0.2680843684	-0.0004260772	3.1348149832
China SatNet 40	7515642.664	-0.0008465491	0.0005592872	0.3641333208	-0.0005120975	3.1357970080
China SatNet 50	7520732.068	-0.0007094399	0.0007767660	0.4664840525	-0.0005519432	3.1361103191
China SatNet 60	7529540.884	-0.0005786868	0.0015461783	0.5775216509	-0.0005329314	3.1351482035
Hughes	7541153.023	-0.0006396936	0.0010086038	0.5207427699	-0.0005482596	3.1359544848
600 km $N_o = 19$, $N_{s_o} = 26$, $N_c = 6$	6985254.219	-0.0006719853	0.0018982970	0.5775442909	-0.0006136269	3.1413693443
550km, $i = 30$	6932603.639	-0.0011455768	0.0005415725	0.2681075439	-0.0005535049	3.1371553429
550km, $i = 35$	6935353.386	-0.0010720349	0.0005423213	0.3154746793	-0.0006333956	3.1384523595
550km, $i = 40$	6938050.383	-0.0009938381	0.0005491323	0.3641596411	-0.0007248931	3.1403373716
550km, $i = 45$	6941217.582	-0.0009129501	0.0006264725	0.4144118096	-0.0008545479	-3.1397805723
550km, $i = 87$	6932957.670	0.0007308090	0.0012092678	0.9279451772	-0.1967928843	-0.2240373901

B Radial Distance Derivatives

The following are the derivative terms used for the mean elements-based shell width estimation model, which include the J_2 short-periodic variations. Similar to the corresponding section of the paper, the orbital elements in these formula (but not osculating radius) refer to J_2 mean rather than osculating elements.

$$\frac{dr}{da} = \frac{J_2 R_{\oplus}^2 \left(\cos(2\theta + 2\omega) \sin(i)^2 - (3 \cos(i)^2 - 1) \left(\frac{2\sqrt{1-e^2}}{(e \cos(\theta)+1)^2} + \frac{e \cos(\theta)}{\sqrt{1-e^2+1}} + 1 \right) \right)}{4 a^2 (e^2 - 1)} - \frac{e^2 - 1}{e \cos(\theta) + 1} \quad (1)$$

$$\begin{aligned} \frac{dr}{de} &= \frac{a \cos(\theta) (e^2 - 1)}{(e \cos(\theta) + 1)^2} - \frac{2 a e}{e \cos(\theta) + 1} \\ &+ \frac{J_2 e R_{\oplus}^2 \left(\cos(2\theta + 2\omega) \sin(i)^2 - (3 \cos(i)^2 - 1) \left(\frac{2\sqrt{1-e^2}}{(e \cos(\theta)+1)^2} + \frac{e \cos(\theta)}{\sqrt{1-e^2+1}} + 1 \right) \right)}{2 a (e^2 - 1)^2} \\ &+ \frac{J_2 R_{\oplus}^2 (3 \cos(i)^2 - 1) \left(\frac{\cos(\theta)}{\sqrt{1-e^2+1}} - \frac{2e}{\sqrt{1-e^2} (e \cos(\theta)+1)^2} - \frac{4 \cos(\theta) \sqrt{1-e^2}}{(e \cos(\theta)+1)^3} + \frac{e^2 \cos(\theta)}{\sqrt{1-e^2} (\sqrt{1-e^2+1})^2} \right)}{4 a (e^2 - 1)} \end{aligned} \quad (2)$$

$$\frac{dr}{d\omega} = \frac{a e \sin(\theta) (e^2 - 1)}{(e \cos(\theta) + 1)^2} - \frac{J_2 R_{\oplus}^2 \left(2 \sin(2\theta + 2\omega) \sin(i)^2 - \left(\frac{e \sin(\theta)}{\sqrt{1-e^2+1}} - \frac{4 e \sin(\theta) \sqrt{1-e^2}}{(e \cos(\theta)+1)^3} \right) (3 \cos(i)^2 - 1) \right)}{4 a (e^2 - 1)} \quad (3)$$

$$\frac{dr}{di} = - \frac{\cos(i) \sin(\phi) \left(\frac{J_2 R_{\oplus}^2 \left(2 \sin(2\theta + 2\omega) \sin(i)^2 - \left(\frac{e \sin(\theta)}{\sqrt{1-e^2+1}} - \frac{4 e \sin(\theta) \sqrt{1-e^2}}{(e \cos(\theta)+1)^3} \right) (3 \cos(i)^2 - 1) \right)}{4 a (e^2 - 1)} - \frac{a e \sin(\theta) (e^2 - 1)}{(e \cos(\theta) + 1)^2} \right)}{\sin(i)^2 \sqrt{1 - \frac{\sin(\phi)^2}{\sin(i)^2}}} \quad (4)$$

Finally, the circular version of these equations can be derived by using the following substitution:

$$e = \sqrt{e_x^2 + e_y^2} \quad (5)$$

$$\cos(\theta) = \frac{e_x}{\sqrt{e_x^2 + e_y^2}} \sqrt{1 - \frac{\sin(\phi)^2}{\sin(i)^2}} + \frac{e_y}{\sqrt{e_x^2 + e_y^2}} \frac{\sin(\phi)'}{\sin(i)} \quad (6)$$

$$\cos(2\omega) = 1 - 2 \left(\frac{\sin(\phi)'}{\sin(i)} \right)^2 \quad (7)$$

where $e_x = e \cos(\omega)$, $e_y = e \sin(\omega)$

C LEO Operator Interview Questions

This appendix contains the interview questions provided in advance to interviewees and used to guide semi-structured interviews.

Interview Questions

Definitions:

- A **slot** is a three-dimensional, time-varying region of space used to constrain the location for a particular satellite or satellites. Note that, as used here, slot does not necessarily presuppose assignment by a regulatory body.
- A **shell** is an orbital region associated with the volume swept out over time by one or more slot locations spread across one or more orbital planes. Shells may be designed to preserve a minimum separation distance between slots within the shell.
- **Allocation** refers to the process for determining the structure of a set of slots and/or shells including factors like phasing, orbital planes, satellites per orbital plane, and inclination.
- **Assignment** refers to the process of granting permission to an operator to use a particular set of slots for some period of time.

Questions:

1. About the Interviewee
 - a. Please describe your educational and professional background and your current role within your organization.
2. Framing Questions
 - a. What do you believe are the most important steps for operators to take to ensure space sustainability? Regulators?
 - b. What practices do you believe are most important to mitigate the risk associated with cross-operator conjunctions?
3. Operator Practices

If your organization does not operate or plan to operate satellites, please answer based on what you believe are practices among operators with which you are familiar.

 - a. How do you/will you coordinate between satellites in your own constellation(s) to prevent endogenous collisions?
 - b. How do you coordinate with adjacent or overlapping constellations controlled by other operators to prevent collisions?
 - c. How do you coordinate to avoid and/or mitigate conjunctions during shell-crossing events?
 - d. How do you determine when to start coordinating with another operator, and at what stage in development do you usually start?
4. Orbit Coordination

Miles will explain ARCLab's work on slotting, in-shell & between shell separation distances, and the potential for shell-sharing, using Figures 1 and 2.

 - a. What benefits do you believe cross-operator orbit coordination could achieve?
 - b. What, if any, concerns would you have about a system for orbit coordination and/or slotting?
 - c. What kinds of analysis would be useful to quantify the benefits associated with LEO on-station orbit coordination?
5. Implementation Process

Form Rev. April 15, 2023

There are several ways that LEO orbital coordination could emerge. Miles will explain various options using Table 1.

- a. What kind of system implementation process, allocation mechanisms, and licensing schemes would be desirable and/or acceptable? Do you have any thoughts about which forms or forms would be most desirable? Most likely?
 - b. Do you believe that this above chart omits any major options?
 - c. What do you believe would be necessary at a technical level to facilitate cross-operator shell coordination? Shell sharing?
6. Orbital Capacity Modeling
- a. How do you define orbital capacity?
 - b. What do you believe constrains orbital capacity? Now? In the future?
 - c. How should the concept of orbital capacity be used?
 - d. What kinds of questions would you want to answer with an orbital capacity tool? What would make a tool useful to you?
 - e. What kinds of assumptions do you believe should be used to model:
 - i. Future launch traffic
 - ii. Collision avoidance between active spacecraft
 - iii. Spontaneous explosions/satellite failures
 - iv. Solar cycle/atmospheric density
 - v. Post-mission disposal rates
 - vi. Active debris removal
 - vii. Other important considerations for capacity
7. Questions
- a. Is there anything else you would like to tell me?

Approach to Solving the Satellite Placement Problem

- Break problem into concentric quasi-spherical **shells**, spacing shells to ensure non-overlap, even with perturbations.
- Define **satellite locations (slots)** in each shell to ensure a minimum in-shell separation distance, α .
- Adjust slots slightly to account for **non-spherical Earth effects**.
- (Optionally) Leave an empty **“street” layer** for maneuvers between “parking” layers.

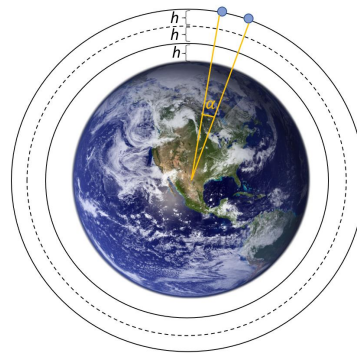


Figure 1: Approaches to Solving the Satellite Placement Problem

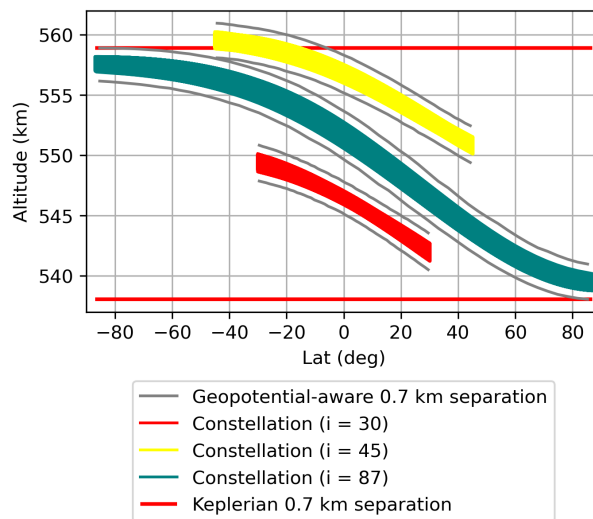


Figure 2: Example of Three Orbital Shells Viewed in Latitude/Altitude Space

Table 1: Pathways to Implementation of Slot-Based LEO Orbit Coordination

Approach	Enforcement	Shell/Slot Allocation	Shell/Slot Assignment
Norms-Based	None	First mover	First come
Inter-operator negotiated legal coordination mechanism	Contracts	Contract parties	Negotiated agreement (not binding on others)
	State regulator	Involved operators (approved by state regulator)	Only binding on those under state regulator jurisdiction
Launching state authorization conditions	State regulator	State regulator	State regulator
Internationally coordinated shell design and/or allocation & assignment framework	States	Agreement between states through international entity	States through process at international entity (first come vs. planning issues like GEO?)

D LEO Operator Interviewees

The following individuals were interviewed for this work. All individuals listed by name gave permission to be identified with the given name, title, and company affiliation.

Table 2: LEO Operator Interviewees

Name	Title	Company	Interview Time
Anonymous		Anonymous LEO Operator	Jun 2023
Ryan Shepperd	Lead SSA Engineer	Iridium Communications	May 2023
Jason Parker	Flight Dynamics Specialist	Telesat	Jul 2023
Nicholas Bijmens	Senior Engineer, LEO Regulatory Integration	Telesat	May 2023

E Chapter 6 Supplementary Tables

Table 3 is referenced in Section 6.2.2 and draws on data from the ITU, FCC, and Jonathan’s Space Pages¹.

Table 3: Future Constellation Launch Model

Constellation	Altitude [km]	Inclination [deg]	Satellites On Station	Satellites Off Station	Satellites Deorbited	Total Satellites Planned	First Launch	Finish Launch	Mass [kg]	Radius [m]	Mission Life [year]
Starlink	550	53.0	1,419	35	251	1,584	2018	2027	260	2.00	8
Starlink	570	70.0	170	234	3	720	2018	2027	260	2.00	8
Starlink	560	97.6	233	0	0	348	2018	2027	260	2.00	8
Starlink	540	53.2	1,544	23	68	1,584	2018	2027	260	2.00	8
Starlink	560	97.6	0	0	0	172	2018	2027	260	2.00	8
Starlink2A	530	43.0	0	288	2	2,500	2023	2031	750	2.00	8
Starlink2A	525	53.0	0	0	0	2,500	2023	2031	750	2.00	8
Starlink2A	535	33.0	0	0	0	2,500	2023	2031	750	2.00	8
Starlink2	340	53.0	0	0	0	5,280	2025	2031	1250	4.00	8
Starlink2	345	46.0	0	0	0	5,280	2025	2031	1250	4.00	8
Starlink2	350	38.0	0	0	0	5,280	2025	2031	1250	4.00	8
Starlink2	360	96.9	0	0	0	3,600	2025	2031	1250	4.00	8
Starlink2	530	43.0	0	0	0	860	2025	2031	1250	4.00	8
Starlink2	525	53.0	0	0	0	860	2025	2031	1250	4.00	8
Starlink2	535	33.0	0	0	0	860	2025	2031	1250	4.00	8
Starlink2	604	148.0	0	0	0	144	2025	2031	1250	4.00	8
Starlink2	614	115.7	0	0	0	324	2025	2031	1250	4.00	8
OneWeb	1200	87.9	499	133	2	588	2019	2023	148	0.50	8
OneWeb	1200	55.0	0	0	0	128	2019	2023	148	0.50	8
OneWeb	1200	87.9	0	0	0	1,764	2025	2028	148	0.50	8
OneWeb	1200	40.0	0	0	0	2,304	2025	2028	148	0.50	8
OneWeb	1200	55.0	0	0	0	2,304	2025	2028	148	0.50	8
Kuiper	590	33.0	0	0	0	782	2024	2029	700	1.50	8
Kuiper	590	30.0	0	0	0	2	2024	2029	700	1.50	8
Kuiper	610	42.0	0	0	0	1,292	2024	2029	700	1.50	8
Kuiper	630	51.9	0	0	0	1,156	2024	2029	700	1.50	8
China SatNet	590	85.0	0	0	0	480	2035	2055	260	2.00	8
China SatNet	600	50.0	0	0	0	2,000	2035	2055	260	2.00	8
China SatNet	508	60.0	0	0	0	3,600	2035	2055	260	2.00	8
China SatNet	1145	30.0	0	0	0	1,728	2035	2055	260	2.00	8
China SatNet	1145	40.0	0	0	0	1,728	2035	2055	260	2.00	8
China SatNet	1145	50.0	0	0	0	1,728	2035	2055	260	2.00	8
China SatNet	1145	60.0	0	0	0	1,728	2035	2055	260	2.00	8
Yinhe	511	63.5	6	0	0	1,000	2020	2030	230	0.70	8
Hanwha	500	97.5	0	0	0	2,000	2025	2035	260	2.00	8
Lynk	500	97.5	4	0	3	2,000	2020	2030	125	0.50	8
Astra	700	0.0	0	0	0	40	2030	2045	500	2.49	8
Astra	690	98.0	0	0	0	504	2030	2045	500	2.49	8
Astra	700	55.0	0	0	0	1,792	2030	2045	500	2.49	8
Astra	380	97.0	0	0	0	2,240	2030	2045	500	2.49	8
Astra	390	30.0	0	0	0	4,896	2030	2045	500	2.49	8
Astra	400	55.0	0	0	0	4,148	2030	2045	500	2.49	8
Boeing	1056	54.0	0	0	0	132	2025	2030	260	2.00	8
Telesat	1015	99.0	0	0	0	78	2023	2033	260	2.00	8
Telesat	1325	50.9	0	0	0	220	2023	2033	260	2.00	8
Telesat	1015	99.0	0	0	0	351	2023	2033	260	2.00	8
Telesat	1325	50.9	0	0	0	1,320	2023	2033	260	2.00	8
HVNET	1150	55.0	0	0	0	1,440	2030	2045	260	2.00	8
SpinLaunch	830	55.0	0	0	0	1,190	2030	2045	150	1.66	8
Globalstar3	485	55.0	0	0	0	1,260	2030	2045	260	2.00	8
Globalstar3	515	70.0	0	0	0	100	2030	2045	260	2.00	8
Globalstar3	600	55.0	0	0	0	900	2030	2045	260	2.00	8
Globalstar3	620	98.0	0	0	0	100	2030	2045	260	2.00	8
Globalstar3	700	55.0	0	0	0	720	2030	2045	260	2.00	8

Table 4 is referenced in Section 6.2.4.

Table 5 is referenced in Section 6.2.4.

¹<https://www.planet4589.org/space/>

Table 4: Operator vs. Operator Conjunctions

Constellation Pair	Conjunctions	Conjunctions (%)
Astra vs. Starlink	2215252.8	24.13
Guanwang vs. Starlink	1530311.1	16.67
Lynk vs. Starlink	671229.2	7.31
Hanwha vs. Starlink	626208.4	6.82
Starlink vs. Yinhe	559981.8	6.10
Hanwha vs. Lynk	553094.3	6.02
Guanwang vs. HVNET	410856.2	4.48
Guanwang vs. Hanwha	309778.1	3.37
Guanwang vs. Lynk	309357.6	3.37
Globalstar3 vs. Guanwang	293614.2	3.20
Guanwang vs. Kuiper	286655.8	3.12
Guanwang vs. Yinhe	222918.2	2.43
Globalstar3 vs. Starlink	213633.1	2.33
Kuiper vs. Starlink	169418.6	1.85
Astra vs. Globalstar3	168678.9	1.84
Globalstar3 vs. Kuiper	123440.3	1.34
Lynk vs. Yinhe	119852.5	1.31
Hanwha vs. Yinhe	108678.4	1.18
Globalstar3 vs. Lynk	88696.3	0.97
Globalstar3 vs. Hanwha	88125.0	0.96
Globalstar3 vs. Yinhe	39591.0	0.43
Guanwang vs. OneWeb	35507.6	0.39
HVNET vs. OneWeb	35397.0	0.39
Boeing vs. Telesat	590.6	0.01
Kuiper vs. OneWeb	109.6	0.00
Astra vs. Kuiper	67.2	0.00
OneWeb vs. Starlink	50.4	0.00
OneWeb vs. Telesat	15.6	0.00
Kuiper vs. Yinhe	5.9	0.00
Boeing vs. OneWeb	3.3	0.00
Globalstar3 vs. OneWeb	2.0	0.00

Table 5: Object Type vs. Object Type Conjunctions

Object Type Pair	Conjunctions	Conjunctions (%)
Debris vs. Debris	125774694.9	58.28
Constellation Derelict vs. Debris	32348296.7	14.99
Constellation vs. Debris	22683311.0	10.51
Constellation vs. Constellation Derelict	13383085.9	6.2
Constellation vs. Constellation	12530224.7	5.81
Constellation Derelict vs. Constellation Derelict	6324920.2	2.93
Debris vs. Other	746555.2	0.35
Debris vs. Derelict	428157.8	0.2
Debris vs. Rocket Body	415469.9	0.19
Constellation vs. Other	409631.6	0.19
Constellation vs. Rocket Body	250672.5	0.12
Constellation vs. Derelict	197539.2	0.092
Constellation Derelict vs. Other	116270.1	0.054
Constellation Derelict vs. Rocket Body	58340.8	0.027
Constellation Derelict vs. Derelict	46271.7	0.021
Constellation vs. Payload	23897.6	0.011
Derelict vs. Derelict	13834.0	0.0064
Derelict vs. Rocket Body	11427.8	0.0053
Derelict vs. Other	9437.8	0.0044
Payload vs. Payload	9308.6	0.0043
Other vs. Rocket Body	8762.6	0.0041
Other vs. Other	8330.6	0.0039
Rocket Body vs. Rocket Body	4711.3	0.0022
Debris vs. Payload	1834.2	0.00085
Derelict vs. Payload	613.5	0.00028
Payload vs. Rocket Body	375.0	0.00017
Other vs. Payload	297.7	0.00014
Constellation Derelict vs. Payload	197.1	9.10×10^{-5}

References

- [1] T. Maclay, W. Everetts, and D. Engelhardt, *Responsible satellite operations in the era of large constellations*, Jan. 2019. [Online]. Available: <https://spacenews.com/op-ed-responsible-satellite-operations-in-the-era-of-large-constellations/>.
- [2] Iridium, OneWeb, and SpaceX, “Satellite Orbital Safety Best Practices,” AIAA, Reston, VA, Tech. Rep., 2022, pp. 1–14. [Online]. Available: <https://assets.oneweb.net/s3fs-public/2022-09/Satellite%20Orbital%20Safety%20Best%20Practices.pdf>.
- [3] J. Zoller, C. A. Keisner, and W. Lewis, *Petition for Reconsideration of Kuiper Systems LLC*, Washington, DC, 2020. [Online]. Available: <https://www.fcc.gov/ecfs/search/search-filings/filing/1092552081258>.
- [4] R. Pritchard-Kelly, B. Weimer, D. Svor, and T. Hastings, *Opposition and Response of Oneweb*, Washington, DC, 2020. [Online]. Available: <https://www.fcc.gov/ecfs/search/search-filings/filing/1125914700201>.
- [5] J. P. Janka, A. R. Mehlman, and J. S. Taubman, *Consolidated Opposition to Petitions for Reconsideration*, Washington, DC, 2020. [Online]. Available: <https://www.fcc.gov/ecfs/search/search-filings/filing/11242734224280>.
- [6] A. L. Allison and B. A. Olcott, *Reply of The Boeing Company*, Washington, DC, 2020. [Online]. Available: <https://www.fcc.gov/ecfs/search/search-filings/filing/121004544084>.
- [7] N. G. Spina, *Comments of Kepler Communications Inc.* Washington, DC, 2020. [Online]. Available: <https://www.fcc.gov/ecfs/search/search-filings/filing/1125185066832>.
- [8] J. S. Taubman and C. D. Bair, *Reply of Viasat, Inc.* Washington, DC, 2022. [Online]. Available: https://licensing.fcc.gov/myibfs/download.do?attachment_key=14961092.
- [9] Space Exploration Technologies Corp., *SpaceX Ex Parte (7-15-19)*, Washington, DC, 2019. [Online]. Available: https://licensing.fcc.gov/myibfs/download.do?attachment_key=1795124.
- [10] J. N. Zoller and C. A. Keisner, *Reply Comments of Kuiper Systems LLC*, Washington, DC, 2022. [Online]. Available: https://licensing.fcc.gov/myibfs/download.do?attachment_key=14889612.

- [11] Federal Communications Commission, *Order and Authorization*, Washington, DC, 2022. [Online]. Available: <https://docs.fcc.gov/public/attachments/FCC-22-91A1.pdf>.
- [12] Scientific and Technical Subcommittee of the Committee on the Peaceful Uses of Outer Space, “Report of the Scientific and Technical Subcommittee on its sixtieth session, held in Vienna from 6 to 17 February 2023,” United Nations, Vienna, Austria, Tech. Rep., 2023. [Online]. Available: <https://documents-dds-ny.un.org/doc/UNDOC/GEN/V23/011/65/PDF/V2301165.pdf?OpenElement>.
- [13] A. L. Allison, *The ITU and Managing Satellite Orbital and Spectrum Resources in the 21st Century*. Cham, Switzerland: Springer Cham, 2014, p. 94. DOI: [10.1007/978-3-319-05314-1](https://doi.org/10.1007/978-3-319-05314-1).
- [14] R. Kopeć, “Geostationary Belt – State’s Territory or Province of Mankind?” *Rev. of Nationalities*, vol. 8, no. 1, pp. 167–178, Feb. 2019. DOI: [10.2478/pn-2018-0011](https://doi.org/10.2478/pn-2018-0011).
- [15] C. Guzman Gomez and Y. Cordoba A, “The Equitable Access to the Geo for Developing Countries: A Pending Challenge,” in *Proc. of the Int. Astronautical Cong.*, Beijing, China, 2013, pp. 1–5. [Online]. Available: https://papers.ssrn.com/sol3/papers.cfm?abstract_id=2960223.
- [16] Working Party 4A, “Annex 20 to Working Party 4A Chairman’s Report SUPPORTING MATERIAL THAT WAS DEVELOPED TO ADDRESS WRC-23 AGENDA ITEM 7 – TOPIC A,” Geneva, Switzerland, Tech. Rep., 2023, pp. 1–67. [Online]. Available: https://www.itu.int/dms_ties/itu-r/md/19/wp4a/c/R19-WP4A-C-0978!N20!MSW-E.docx.
- [17] People’s Republic of China, *Proposed new Question [NGSO ORBIT/SPECTRUM] CONDUCT STUDIES ON THE ORBIT AND SPECTRUM RESOURCES CAPACITY FOR NON-GSO SATELLITE SYSTEMS*, Dubai, United Arab Emirates, 2023.
- [18] F. Letizia, B. Bastida Virgili, and S. Lemmens, “Assessment of orbital capacity thresholds through long-term simulations of the debris environment,” *Advances in Space Res.*, vol. 72, no. 7, 2022. DOI: [10.1016/j.asr.2022.06.010](https://doi.org/10.1016/j.asr.2022.06.010).
- [19] G. A. Henning, D. L. Mains, J. C. Maldonado, M. E. Sorge, G. E. Peterson, A. B. Jenkin, and J. Zundel, “Finding the Upper Threshold of LEO Activity That Makes Long-Term Space Operations Unsustainable,” in *73rd Int. Astronautical Cong.*, Paris, France: International Astronautical Federation, 2022, pp. 1–16.
- [20] M. Renčelj, S. Dalledonne, C. Poirier, and L. Pohl, “Space Environment Capacity: Policy, regulatory and diplomatic perspectives on threshold-based models for space safety & sustainability,” European Space Policy Institute, Vienna, Austria, Tech. Rep., 2022. [Online]. Available: <https://www.espi.or.at/events/limited-orbital-environments-capacity-approaches-to-outer-space/>.
- [21] D. Arnas, M. Lifson, R. Linares, and M. E. Avendaño, “Definition of Low Earth Orbit slotting architectures using 2D lattice flower constellations,” *Advances in Space Res.*, vol. 67, no. 11, pp. 3696–3711, Jun. 2021. DOI: [10.1016/j.asr.2020.04.021](https://doi.org/10.1016/j.asr.2020.04.021).

- [22] M. Avendaño, D. Arnas, R. Linares, and M. Lifson, “Efficient search of optimal Flower Constellations,” *Acta Astronautica*, vol. 179, pp. 290–295, Feb. 2021. DOI: [10.1016/j.actaastro.2020.10.026](https://doi.org/10.1016/j.actaastro.2020.10.026).
- [23] D. Arnas and R. Linares, “Non-Self-Intersecting Trajectories and Their Applications to Satellite Constellation Design and Orbital Capacity,” *J. of Guidance, Control, and Dynamics*, vol. 46, no. 3, 2023. DOI: [10.2514/1.G007208](https://doi.org/10.2514/1.G007208). arXiv: [/arxiv.org/abs/2110.07823](https://arxiv.org/abs/2110.07823) [[https:](https://)].
- [24] D. Arnas and R. Linares, “Uniform Satellite Constellation Reconfiguration,” *J. of Guidance, Control, and Dynamics*, vol. 45, no. 7, Feb. 2022. DOI: [10.2514/1.G006514](https://doi.org/10.2514/1.G006514).
- [25] M. Lifson, “A Study of Emerging Space Nation and Commercial Satellite Operator Stakeholder Preferences for Space Traffic Management,” M.S. thesis, Massachusetts Institute of Technology, Cambridge, MA, 2020.
- [26] D. J. Kessler and B. G. Cour-Palais, “Collision Frequency of Artificial Satellites: The Creation of a Debris Belt,” *J. of Geophysical Res.*, vol. 83, no. A6, p. 2637, 1978. DOI: [10.1029/JA083iA06p02637](https://doi.org/10.1029/JA083iA06p02637).
- [27] J.-C. Liou, D. Hall, P. Krisko, and J. Opiela, “LEGEND – a three-dimensional LEO-to-GEO debris evolutionary model,” *Advances in Space Res.*, vol. 34, no. 5, pp. 981–986, Jan. 2004. DOI: [10.1016/j.asr.2003.02.027](https://doi.org/10.1016/j.asr.2003.02.027).
- [28] B. Bastida Virgili, “DELTA (Debris Environment Long Term Analysis),” *6th Int. Conf. on Astrodynamics Tools and Techniques*, 2016.
- [29] A. Jenkin, M. Sorge, G. Peterson, J. McVey, and B. Yoo, “100-Year Low Earth Orbit Debris Population Model,” in *Astrodynamics Specialists Conf.*, Girdwood, AK: AAS/AIAA, 2011.
- [30] J.-C. Liou, N. Johnson, and N. Hill, “Controlling the Growth of Future LEO Debris Populations with Active Debris Removal,” *Acta Astronautica*, vol. 66, no. 5–6, pp. 648–653, Mar. 2010. DOI: [10.1016/j.actaastro.2009.08.005](https://doi.org/10.1016/j.actaastro.2009.08.005).
- [31] J. C. Liou, “An Active Debris Removal Parametric Study for LEO Environment Remediation,” *Advances in Space Res.*, vol. 47, no. 11, 2011. DOI: [10.1016/j.asr.2011.02.003](https://doi.org/10.1016/j.asr.2011.02.003).
- [32] J.-C. Liou, M. Matney, A. Vavrin, A. Manis, and D. Gates, “Project Review: NASA ODPO’s Large Constellation Study,” *Orbital Debris Quart. News*, vol. 22, no. 3, Sep. 2018. [Online]. Available: <https://www.orbitaldebris.jsc.nasa.gov/quarterly-news/pdfs/odqnv22i3.pdf>.
- [33] D. Jang, D. Gusmini, P. M. Siew, A. D’Ambrosio, S. Servadio, P. Machuca, and R. Linares, “Monte Carlo Methods To Model The Evolution Of The Low Earth Orbit Population,” in *33rd AAS/AIAA Space Flight Mechanics Meeting*, Austin, TX: AAS/AIAA, 2023.
- [34] C. Bombardelli, E. M. Alessi, A. Rossi, and G. B. Valsecchi, “Environmental effect of space debris repositioning,” *Advances in Space Res.*, vol. 60, no. 1, pp. 28–37, 2017. DOI: [10.1016/j.asr.2017.03.044](https://doi.org/10.1016/j.asr.2017.03.044).

- [35] D. Mcknight, R. Witner, F. Letizia, *et al.*, “Identifying the 50 statistically-most-concerning derelict objects in LEO,” *Acta Astronautica*, vol. 181, pp. 282–291, 2021. DOI: [10.1016/j.actaastro.2021.01.021](https://doi.org/10.1016/j.actaastro.2021.01.021).
- [36] C. Pardini and L. Anselmo, “Evaluating the environmental criticality of massive objects in LEO for debris mitigation and remediation,” *Acta Astronautica*, vol. 145, pp. 51–75, 2018. DOI: [10.1016/j.actaastro.2018.01.028](https://doi.org/10.1016/j.actaastro.2018.01.028).
- [37] C. Pardini and L. Anselmo, “Characterization of abandoned rocket body families for active removal,” *Acta Astronautica*, vol. 126, pp. 243–257, 2016. DOI: [10.1016/j.actaastro.2016.04.035](https://doi.org/10.1016/j.actaastro.2016.04.035).
- [38] C. Kebschull, J. Radtke, and H. Krag, “Deriving a priority list based on the environmental criticality,” in *Proc. of the 65th Int. Astronautical Cong.*, Toronto, Canada: International Astronautical Federation, 2014.
- [39] J. Utzmann, M. Oswald, S. Stabroth, P. Voigt, A. Wagner, and L. Retat, “Ranking and characterization of heavy debris for active removal,” in *Proc. of the 63rd Int. Astronautical Cong.*, Naples, Italy: International Astronautical Federation, 2012.
- [40] T. Yasaka, “Can we have an end to the debris issue?” In *62nd Int. Astronautical Cong.*, International Astronautical Federation, 2011.
- [41] J.-C. Liou and N. L. Johnson, “A Sensitivity Study of the Effectiveness of Active Debris Removal in LEO,” *Acta Astronautica*, vol. 64, no. 2-3, pp. 236–243, Jan. 2009. DOI: [10.1016/J.ACTAASTRO.2008.07.009](https://doi.org/10.1016/J.ACTAASTRO.2008.07.009).
- [42] H. Krag, S. Lemmens, and F. Letizia, “Space Traffic Management Through the Control of the Space Environment’s Capacity,” in *1st IAA Conf. on Space Sit. Awareness*, Orlando, FL: International Academy of Astronautics, 2017.
- [43] F. Letizia, S. Lemmens, B. Bastida Virgili, and H. Krag, “Application of a debris index for global evaluation of mitigation strategies,” *Acta Astronautica*, vol. 161, pp. 348–362, Aug. 2019. DOI: [10.1016/j.actaastro.2019.05.003](https://doi.org/10.1016/j.actaastro.2019.05.003).
- [44] F. Letizia, S. Lemmens, and H. Krag, “Environment capacity as an early mission design driver,” *Acta Astronautica*, vol. 173, pp. 320–332, 2020. DOI: [10.1016/j.actaastro.2020.04.041](https://doi.org/10.1016/j.actaastro.2020.04.041).
- [45] C. Colombo, M. Trisolini, J. L. Gonzalo, L. Giudici, S. Frey, E. Kerr, N. Sánchez-Ortiz, F. Letizia, and S. Lemmens, “Design of a software to assess the impact of a space mission the space environment,” in *8th Euro. Conf. on Space Debris*, T. Flohrer, S. Lemmens, and F. Schmitz, Eds., Darmstadt, Germany: ESA Space Debris Office, 2021. [Online]. Available: <https://conference.sdo.esoc.esa.int/proceedings/sdc8/paper/289>.
- [46] A. Rossi, G. B. Valsecchi, and E. M. Alessi, “The criticality of spacecraft index,” *Advances in Space Res.*, vol. 56, no. 3, pp. 449–460, 2015. DOI: [10.1016/j.asr.2015.02.027](https://doi.org/10.1016/j.asr.2015.02.027).

- [47] A. Rossi, H. Lewis, A. White, L. Anselmo, C. Pardini, H. Krag, and B. Bastida Virgili, “Analysis of the consequences of fragmentations in low and geostationary orbits,” *Advances in Space Res.*, vol. 57, no. 8, pp. 1652–1663, 2016. DOI: [10.1016/j.asr.2015.05.035](https://doi.org/10.1016/j.asr.2015.05.035).
- [48] A. Rossi, E. M. Alessi, G. B. Valsecchi, H. Lewis, J. Radtke, C. Bombardelli, and B. B. Virgili, “A Quantitative Evaluation of the Environmental Impact of the Mega Constellations,” in *7th Euro. Conf. on Space Debris*, Darmstadt, Germany, 2017.
- [49] L. Anselmo and C. Pardini, “Dimensional and scale analysis applied to the preliminary assessment of the environment criticality of large constellations in LEO,” *Acta Astronautica*, vol. 158, pp. 121–128, 2019. DOI: [10.1016/j.actaastro.2017.09.028](https://doi.org/10.1016/j.actaastro.2017.09.028).
- [50] C. Pardini and L. Anselmo, “Environmental sustainability of large satellite constellations in low earth orbit,” *Acta Astronautica*, vol. 170, pp. 27–36, May 2020. DOI: [10.1016/j.actaastro.2020.01.016](https://doi.org/10.1016/j.actaastro.2020.01.016).
- [51] V. Trozzi, M. Trisolini, and C. Colombo, “Analysis of possible definitions of the space environment capacity to pursue long-term sustainability of space activities,” in *72nd Int. Astronautical Cong.*, Dubai, United Arab Emirates: International Astronautical Federation, 2021.
- [52] D. J. Kessler and P. D. Anz-Meador, “Critical number of spacecraft in low Earth orbit: Using satellite fragmentation data to evaluate the stability of the orbital debris environment,” *European Space Agency (Special Publication)*, vol. 1, no. 473, pp. 265–272, 2001. [Online]. Available: <https://conference.sdo.esoc.esa.int/proceedings/sdc3/paper/97/SDC3-paper97.pdf>.
- [53] A. Rao and F. Letizia, “An integrated debris environment assessment model,” in *8th Euro. Conf. on Space Debris*, T. Flohrer, S. Lemmens, and F. Schmitz, Eds., Darmstadt, Germany: ESA Space Debris Office, 2021. [Online]. Available: <https://conference.sdo.esoc.esa.int/proceedings/sdc8/paper/206/SDC8-paper206.pdf>.
- [54] JASON, “The Impacts of Large Constellations of Satellites,” MITRE Corporation, McLean, VA, Tech. Rep., 2020. [Online]. Available: https://www.nsf.gov/news/special_reports/jasonreportconstellations/.
- [55] J. Drmola and T. Hubik, “Kessler Syndrome: System Dynamics Model,” *Space Policy*, vol. 44-45, pp. 29–39, 2018. DOI: [10.1016/j.spacepol.2018.03.003](https://doi.org/10.1016/j.spacepol.2018.03.003).
- [56] G. L. Somma, C. Colombo, and H. G. Lewis, “A Statistical LEO Model to Investigate Adaptable Debris Control Strategies,” in *7th European Conference on Space Debris*, ESA Space Debris Office, Ed., Darmstadt, Germany, 2017.
- [57] C. Kebschull, P. Scheidemann, S. Hesselbach, J. Radtke, V. Braun, H. Krag, and E. Stoll, “Simulation of the space debris environment in LEO using a simplified approach,” *Advances in Space Res.*, vol. 59, no. 1, pp. 166–180, 2017. DOI: [10.1016/j.asr.2016.08.005](https://doi.org/10.1016/j.asr.2016.08.005).
- [58] A. V. Gheorghie and D. E. Yuchnovicz, “The Space Infrastructure Vulnerability Cadastre: Orbital Debris Critical Loads,” *International Journal of Disaster Risk Science*, vol. 6, no. 4, pp. 359–371, 2015. DOI: [10.1007/s13753-015-0073-2](https://doi.org/10.1007/s13753-015-0073-2).

- [59] H. G. Lewis, G. G. Swinerd, R. J. Newland, and A. Saunders, “The fast debris evolution model,” *Advances in Space Res.*, vol. 44, no. 5, pp. 568–578, 2009, ISSN: 02731177. DOI: [10.1016/j.asr.2009.05.018](https://doi.org/10.1016/j.asr.2009.05.018).
- [60] A. M. Bradley and L. M. Wein, “Space debris: Assessing risk and responsibility,” *Advances in Space Res.*, vol. 43, no. 9, pp. 1372–1390, May 2009. DOI: [10.1016/j.asr.2009.02.006](https://doi.org/10.1016/j.asr.2009.02.006).
- [61] D. Jang, P. M. Siew, P. Machuca, and R. Linares, “Monte Carlo Methods For Lethal Non-Trackable Objects and the Future Leo Population Evolution,” in *Advanced Maui Optical and Space Surveillance Technologies Conf.*, Maui, HI: Maui Economic Development Board, 2023.
- [62] S. Alfano and D. Oltrogge, “Volumetric assessment of satellite encounter rates,” *Acta Astronautica*, vol. 152, pp. 891–907, 2018. DOI: [10.1016/j.actaastro.2018.09.030](https://doi.org/10.1016/j.actaastro.2018.09.030).
- [63] D. S. McKnight and F. R. Di Pentino, “New insights on the orbital debris collision hazard at GEO,” *Acta Astronautica*, vol. 85, pp. 73–82, 2013, ISSN: 0094-5765. DOI: [10.1016/j.actaastro.2012.12.006](https://doi.org/10.1016/j.actaastro.2012.12.006). [Online]. Available: <https://www.sciencedirect.com/science/article/pii/S0094576512004869>.
- [64] E. J. Öpik, “Collision Probabilities with the Planets and the Distribution of Interplanetary Matter,” *Proc. of the Royal Irish Acad. Sec. A: Mathematical and Physical Sci.*, vol. 54, pp. 165–199, Jan. 1951. [Online]. Available: <http://www.jstor.org/stable/20488532>.
- [65] G. W. Wetherill, “Collisions in the asteroid belt,” *J. of Geophysical Research*, vol. 72, no. 9, pp. 2429–2444, May 1967. DOI: [10.1029/JZ072i009p02429](https://doi.org/10.1029/JZ072i009p02429).
- [66] J.-C. Liou, D. Kessler, M. Matney, and G. Stansbery, “A New Approach to Evaluate Collision Probabilities Among Asteroids, Comets, and Kuiper Belt Objects,” in *34th Annu. Lunar and Planetary Sci. Conf.*, League City, Texas, 2003.
- [67] H. G. Lewis, S. Diserens, T. Maclay, and J. P. Sheehan, “Limitations of the cube method for assessing large constellations,” in *1st Int. Orbital Debris Conf.*, Sugar Land, Texas, 2019.
- [68] N. Reiland, A. J. Rosengren, R. Malhotra, and C. Bombardelli, “Assessing and minimizing collisions in satellite mega-constellations,” *Advances in Space Res.*, vol. 67, no. 11, pp. 3755–3774, Jun. 2021. DOI: [10.1016/j.asr.2021.01.010](https://doi.org/10.1016/j.asr.2021.01.010).
- [69] F. R. Hoots, L. L. Crawford, and R. L. Roehrich, “Analytic Method To Determine Future Close Approaches Between Satellites,” *Celestial Mechanics*, vol. 33, pp. 143–158, 1984. DOI: [10.1007/BF01234152](https://doi.org/10.1007/BF01234152).
- [70] Y. JeongAhn and R. Malhotra, “Simplified Derivation of the Collision Probability of Two Objects in Independent Keplerian Orbits,” *Astronomical J.*, vol. 153, no. 5, p. 235, 2017. DOI: [10.3847/1538-3881/aa6aa7](https://doi.org/10.3847/1538-3881/aa6aa7).
- [71] Y. JeongAhn and R. Malhotra, “The current impact flux on Mars and its seasonal variation,” *Icarus*, vol. 262, pp. 140–153, 2015. DOI: [10.1016/j.icarus.2015.08.032](https://doi.org/10.1016/j.icarus.2015.08.032).
- [72] D. Mortari, M. Wilkins, and C. Bruccoleri, “The Flower Constellations,” *J. of the Astronautical Sci.*, vol. 52, pp. 107–127, 2004. DOI: [10.1007/BF03546424](https://doi.org/10.1007/BF03546424).

- [73] D. Mortari and M. P. Wilkins, “Flower Constellation Set Theory Part I: Compatibility and Phasing,” *IEEE Trans. on Aerospace & Electronic Systems*, vol. 44, no. 3, pp. 953–963, Jul. 2008. DOI: [10.1109/TAES.2008.4655355](https://doi.org/10.1109/TAES.2008.4655355).
- [74] M. P. Wilkins and D. Mortari, “Flower Constellation Set Theory Part II: Secondary Paths and Equivalency,” *IEEE Trans. on Aerospace & Electronic Systems*, vol. 44, no. 3, pp. 964–976, Jul. 2008. DOI: [10.1109/TAES.2008.4655356](https://doi.org/10.1109/TAES.2008.4655356).
- [75] M. E. Avendano and D. Mortari, “New Insights on Flower Constellations Theory,” *IEEE Trans. on Aerospace & Electronic Systems*, vol. 48, no. 2, pp. 1018–1030, Apr. 2012. DOI: [10.1109/TAES.2012.6178046](https://doi.org/10.1109/TAES.2012.6178046).
- [76] M. E. Avendaño, J. J. Davis, and D. Mortari, “The 2-D lattice theory of Flower Constellations,” *Celestial Mechanics and Dynamical Astronomy*, vol. 116, no. 4, pp. 325–337, Aug. 2013. DOI: [10.1007/s10569-013-9493-8](https://doi.org/10.1007/s10569-013-9493-8).
- [77] D. Arnas, D. Casanova, and E. Tresaco, “n-Dimensional congruent lattices using necklaces,” *Advances in Space Res.*, vol. 67, no. 11, pp. 3725–3743, Jun. 2021. DOI: [10.1016/J.ASR.2020.04.045](https://doi.org/10.1016/J.ASR.2020.04.045).
- [78] D. Arnas, D. Casanova, and E. Tresaco, “4D Lattice Flower Constellations,” *Advances in Space Res.*, vol. 67, no. 11, pp. 3683–3695, Jun. 2021. DOI: [10.1016/J.ASR.2020.04.018](https://doi.org/10.1016/J.ASR.2020.04.018).
- [79] J. Davis, M. Avendano, and D. Mortari, “Elliptical Lattice Flower Constellations for Global Coverage,” *Advances in the Astronautical Sci.*, vol. 136, Jan. 2010.
- [80] D. Casanova, M. Avendaño, and E. Tresaco, “Lattice-preserving Flower Constellations under J2 perturbations,” *Celestial Mechanics and Dynamical Astronomy*, vol. 121, no. 1, pp. 83–100, 2015. DOI: [10.1007/s10569-014-9583-2](https://doi.org/10.1007/s10569-014-9583-2).
- [81] D. Arnas, “Necklace Flower Constellations,” Ph.D. dissertation, Univ. de Zaragoza, Zaragoza, Spain, 2018.
- [82] D. Arnas and D. Casanova, “Nominal definition of satellite constellations under the Earth gravitational potential,” *Celestial Mechanics and Dynamical Astronomy*, vol. 132, no. 3, p. 19, 2020, ISSN: 1572-9478. DOI: [10.1007/s10569-020-09958-4](https://doi.org/10.1007/s10569-020-09958-4).
- [83] D. Arnas, D. Casanova, and E. Tresaco, “Time distributions in satellite constellation design,” *Celestial Mechanics and Dynamical Astronomy*, vol. 128, pp. 197–219, Jun. 2017. DOI: [10.1007/s10569-016-9747-3](https://doi.org/10.1007/s10569-016-9747-3).
- [84] D. Arnas, D. Casanova, and E. Tresaco, “2D Necklace Flower Constellations,” *Acta Astronautica*, vol. 142, pp. 18–28, Jan. 2018. DOI: [10.1016/j.actaastro.2017.10.017](https://doi.org/10.1016/j.actaastro.2017.10.017).
- [85] D. Arnas, D. Casanova, E. Tresaco, and D. Mortari, “3-Dimensional Necklace Flower Constellations,” *Celestial Mechanics and Dynamical Astronomy*, vol. 129, no. 4, pp. 433–448, Dec. 2017. DOI: [10.1007/s10569-017-9789-1](https://doi.org/10.1007/s10569-017-9789-1).
- [86] S. Alfano, D. L. Oltrogge, and R. Shepperd, “LEO Constellation Encounter and Collision Rate Estimation: An Update,” *Proc. of the 2nd IAA Conf. on Space Sit. Awareness*, Jan. 2020.

- [87] A. Anilkumar, S. Aoyama, B. Baseley-Walker, *et al.*, “Space Traffic Management Final Report,” International Space University, Beijing, China, Tech. Rep., 2007. [Online]. Available: https://isulibrary.isunet.edu/doc_num.php?explnum_id=99.
- [88] B. Weeden and K. Shortt, “Development of an Architecture of Sun-Synchronous Orbital Slots to Minimize Conjunctions,” in *SpaceOps 2008*, 2008, pp. 1–15. DOI: [10.2514/6.2008-3547](https://doi.org/10.2514/6.2008-3547).
- [89] K. D. Bilimoria and R. A. Krieger, “Slot Architecture for Separating Satellites in Sun-Synchronous Orbits,” in *AIAA SPACE 2011 Conf. & Expo.*, Long Beach, CA: American Institute of Aeronautics and Astronautics, 2011. DOI: [10.2514/6.2011-7184](https://doi.org/10.2514/6.2011-7184).
- [90] E. Watson, “Sun-Synchronous Orbit Slot Architecture Analysis and Development,” M.S. thesis, California Polytechnic State University, San Luis Obispo, CA, May 2012, pp. 1–56. DOI: [10.15368/theses.2012.50](https://doi.org/10.15368/theses.2012.50).
- [91] C. D. Noyes, “Characterization of the Effects of a Sun-Synchronous Orbit Slot Architecture on the Earth’s Orbital Debris Environment,” M.S. thesis, California Polytechnic State University, San Luis Obispo, CA, Jun. 2013. DOI: [10.15368/theses.2013.66](https://doi.org/10.15368/theses.2013.66).
- [92] C. Bombardelli, G. Falco, D. Amato, and A. J. Rosengren, “Space Occupancy in Low-Earth Orbit,” *J. of Guidance, Control, and Dynamics*, vol. 44, no. 4, pp. 684–700, Mar. 2021. DOI: [10.2514/1.G005371](https://doi.org/10.2514/1.G005371).
- [93] M. Lifson, D. Arnas, M. E. Avendaño, and R. Linares, “A Method for Generating Closely Packed Orbital Shells and the Implication on Orbital Capacity,” in *AIAA SciTech Forum & Expo. 2023*, National Harbor, MD: AIAA, 2023.
- [94] M. Lara and R. P. Russell, “Fast design of repeat ground track orbits in high-fidelity geopotentials,” *J. of the Astronautical Sci.*, vol. 56, no. 3, pp. 311–324, Aug. 2008. DOI: [10.1007/BF03256555](https://doi.org/10.1007/BF03256555).
- [95] G. Lavezzi, M. Lifson, S. Servadio, and R. Linares, “An Analysis of Orbital Separation Distances to Support Space Traffic Management,” in *AAS/AIAA Astrodynamics Specialist Conf.*, Big Sky, MT: AAS/AIAA, 2023.
- [96] D. Arnas, D. Casanova, and E. Tresaco, “2D Necklace Flower Constellations applied to Earth observation missions,” *Acta Astronautica*, vol. 178, pp. 203–215, Jan. 2021. DOI: [10.1016/j.actaastro.2020.09.010](https://doi.org/10.1016/j.actaastro.2020.09.010).
- [97] M. Lifson, D. Arnas, M. Avendaño, and R. Linares, “Low Earth Orbit Slotting: Implications for Orbit Design and Policy,” in *8th Annu. Space Traffic Manage. Conf.*, Austin, TX: IAA, 2022, pp. 1–23.
- [98] C. Colombo, M. Trisolini, A. Muciaccia, L. Giudici, J. L. Gonzalo, S. Frey, B. Campo, F. Letizia, and S. Lemmens, “Evaluation of the Space capacity share used by a mission,” in *73rd Int. Astronautical Cong.*, Paris, France: International Astronautical Federation, Sep. 2022.

- [99] A. D’Ambrosio, M. Lifson, D. Jang, C. Pasiecznik, and R. Linares, “Projected Orbital Demand and LEO Environmental Capacity,” in *23rd Advanced Maui Optical and Space Surveillance Technologies*, Maui, HI: Maui Economic Development Board, 2022.
- [100] M. Lifson, A. D’Ambrosio, D. Arnas, and R. Linares, “How many satellites can we fit in Low Earth Orbit?: Capacity Integrating Risk-Based and Intrinsic Methods,” in *2022 AAS/AIAA Astrodynamics Specialist Conference*, Charlotte, North Carolina: AAS/AIAA, 2022.
- [101] M. Lifson, D. Jang, and R. Linares, “Space Environmental Governance and Decision Support using Source-Sink Evolutionary Environmental Models,” in *Advanced Maui Optical and Space Surveillance Technologies Conf.*, Maui, HI: Maui Economic Development Board, 2023.
- [102] D. A. Vallado, *Fundamentals of Astrodynamics and Applications*, 3rd ed. New York: Springer, 2007, pp. 1–1055.
- [103] S. A. Holmes and W. E. Featherstone, “A unified approach to the Clenshaw summation and the recursive computation of very high degree and order normalised associated Legendre functions,” *J. of Geodesy*, vol. 76, no. 5, pp. 279–299, 2002. DOI: [10.1007/s00190-002-0216-2](https://doi.org/10.1007/s00190-002-0216-2).
- [104] R. A. Broucke and P. J. Cefola, “On the equinoctial orbit elements,” *Celestial Mechanics*, vol. 5, no. 3, pp. 303–310, 1972. DOI: [10.1007/BF01228432](https://doi.org/10.1007/BF01228432).
- [105] S. Bruinsma, G. Thuillier, and F. Barlier, “The DTM-2000 empirical thermosphere model with new data assimilation and constraints at lower boundary: accuracy and properties,” *J. of Atmospheric and Solar-Terrestrial Physics*, vol. 65, no. 9, pp. 1053–1070, Jun. 2003. DOI: [10.1016/S1364-6826\(03\)00137-8](https://doi.org/10.1016/S1364-6826(03)00137-8).
- [106] R. S. Park, W. M. Folkner, J. G. Williams, and D. H. Boggs, “The JPL Planetary and Lunar Ephemerides DE440 and DE441,” *Astronomical J.*, vol. 161, no. 3, p. 105, Feb. 2021. DOI: [10.3847/1538-3881/abd414](https://doi.org/10.3847/1538-3881/abd414).
- [107] R. Storn and K. Price, “Differential Evolution – A Simple and Efficient Heuristic for global Optimization over Continuous Spaces,” *J. of Global Optimization*, vol. 11, no. 4, pp. 341–359, 1997. DOI: [10.1023/A:1008202821328](https://doi.org/10.1023/A:1008202821328).
- [108] G. W. Rosborough and C. A. Ocampo, “Influence of Higher Degree Zonals on the Frozen Orbit Geometry,” in *Proc. of the AAS/AIAA Astrodynamics Conf.*, vol. 2, Durango, CO: Univelt Inc, 1991, pp. 1291–1304.
- [109] J. H. Kwok, *The artificial satellite analysis program (ASAP). Version 2.0*, English. Pasadena, CA: Jet Propulsion Laboratory, 1987.
- [110] D. Goldman, *SpaceX Gen2 System Amendment (SAT-AMD-20210818-00105)*, Washington, DC, 2022. [Online]. Available: https://licensing.fcc.gov/cgi-bin/ws.exe/prod/ib/forms/reports/swr031b.hts?q_set=V_SITE_ANTENNA_FREQ.file_numberC/File+Number/%3D/SATAMD2021081800105&prepare=&column=V_SITE_ANTENNA_FREQ.file_numberC/File+Number.

- [111] D. Kaufman, *Technical Appendix: Application of Kuiper Systems LLC for Authority to Launch and Operate a Non-Geostationary Satellite Orbit System in V-band and Ku-band Frequencies (SAT-LOA-20211104-00145)*, Washington, DC, 2021. [Online]. Available: https://licensing.fcc.gov/cgi-bin/ws.exe/prod/ib/forms/reports/swr031b.hts?q_set=V_SITE_ANTENNA_FREQ.file_numberC/File+Number/%3D/SATLOA2021110400145&prepare=&column=V_SITE_ANTENNA_FREQ.file_numberC/File+Number.
- [112] P. Rosenberger, *Technical Appendix: Application for Modification (SAT-MOD-20230228-00043)*, Washington, DC, 2023. [Online]. Available: https://licensing.fcc.gov/cgi-bin/ws.exe/prod/ib/forms/reports/swr031b.hts?q_set=V_SITE_ANTENNA_FREQ.file_numberC/File+Number/%3D/SATMOD2023022800043&prepare=&column=V_SITE_ANTENNA_FREQ.file_numberC/File+Number.
- [113] C. Ravishankar, *Technical Appendix: Technical Overview of the HVNET System (SAT-PPL-20211104-00142)*, Washington, DC, 2021. [Online]. Available: https://licensing.fcc.gov/cgi-bin/ws.exe/prod/ib/forms/reports/swr031b.hts?q_set=V_SITE_ANTENNA_FREQ.file_numberC/File+Number/%3D/SATPPL2021110400142&prepare=&column=V_SITE_ANTENNA_FREQ.file_numberC/File+Number.
- [114] N. Bernard, L. Maisonobe, L. Barbulescu, P. Bazavan, S. Scortan, P. J. Cefola, M. Casasco, and K. Merz, “Validating short periodics contributions in a draper semi-analytical satellite theory implementation: the orekit example,” in *25th Int. Symp. on Space Flight Dyn.*, Munich, Germany, 2015.
- [115] D. Casanova, M. E. Avendano, and D. Mortari, “Design of flower constellations using necklaces,” *IEEE Trans. on Aerospace and Electronic Systems*, vol. 50, no. 2, pp. 1347–1358, Apr. 2014. DOI: [10.1109/TAES.2014.120269](https://doi.org/10.1109/TAES.2014.120269).
- [116] R. D. Brunner, T. A. Steelman, L. Coe-Juell, C. M. Cromley, C. M. Edwards, and D. W. Tucker, *Adaptive governance : integrating science, policy, and decision making*. New York, NY: Columbia University Press, 2005.
- [117] J. T. Scholz and B. Stiftel, *Adaptive governance and water conflict : new institutions for collaborative planning*. Washington, DC: Resources for the Future, 2005.
- [118] D. L. Talent, “Analytic model for orbital debris environmental management,” *Journal of Spacecraft and Rockets*, vol. 29, no. 4, pp. 508–513, 1992. DOI: [10.2514/3.25493](https://doi.org/10.2514/3.25493).
- [119] G. L. Somma, H. G. Lewis, and C. Colombo, “Sensitivity analysis of launch activities in Low Earth Orbit,” *Acta Astronautica*, vol. 158, no. May 2018, pp. 129–139, 2019. DOI: [10.1016/j.actaastro.2018.05.043](https://doi.org/10.1016/j.actaastro.2018.05.043).
- [120] P. Machuca, P. A. Johnson, D. Jang, P. M. Siew, and R. Linares, “Efficiently Forecasting Resident Space Object Populations: a Calibrated Source-sink Evolutionary Model and a Machine-learning Algorithm,” in *Space Capacity Workshop*, Milan, Italy, 2023.

- [121] D. Jang, A. D’Ambrosio, M. Lifson, C. Pasiecznik, and R. Linares, “Stability of the LEO Environment as a Dynamical System,” in *23rd Advanced Maui Optical and Space Surveillance Technologies*, Maui, HI: Maui Economic Development Board, 2022.
- [122] A. D’Ambrosio, M. Lifson, and R. Linares, *The Capacity of Low Earth Orbit Computed using Source-sink Modeling*, 2022. DOI: [10.48550/ARXIV.2206.05345](https://doi.org/10.48550/ARXIV.2206.05345).
- [123] A. D’Ambrosio, S. Servadio, P. M. Siew, D. Jang, M. Lifson, and R. Linares, “Analysis of the LEO orbital capacity via probabilistic evolutionary model,” in *2022 AAS/AIAA Astrodynamics Spec. Conf.*, Charlotte, NC: AAS/AIAA, 2022.
- [124] C. Pasiecznik, A. D’Ambrosio, D. Jang, and R. Linares, “A Dynamical System Analysis of the Effects of the Launch Rate Distribution on the Stability of a Source-Sink Orbital Debris Model,” in *Int. Astronautical Cong.*, Paris, France: International Astronautical Federation, 2022.
- [125] D. Gusmini, A. D. Ambrosio, S. Servadio, P. D. Lizia, and R. Linares, “The Effects of Orbit Raising and Decay in Orbital Capacity Models,” in *33rd AAS/AIAA Space Flight Mechanics Meeting*, Austin, TX: AAS/AIAA, 2023.
- [126] M. Lifson, D. Jang, C. Pasiecznik, and R. Linares, “MOCAT-SSEM: A Source-Sink Evolutionary Model for Space Debris Environment Evolutionary Modeling,” in *9th Annu. Space Traffic Manage. Conf.*, Austin, TX: IAA, 2023.
- [127] B. R. Bowman, W. K. Tobiska, F. A. Marcos, C. Y. Huang, C. S. Lin, and W. J. Burke, “A new empirical thermospheric density model JB2008 using new solar and geomagnetic indices,” in *AIAA/AAS Astrodynamics Specialist Conference*, Honolulu, HI: AIAA/AAS, 2008. DOI: [10.2514/6.2008-6438](https://doi.org/10.2514/6.2008-6438).
- [128] N. Johnson, P. Krisko, J.-C. Liou, and P. Anz-Meador, “NASA’s new breakup model of evolve 4.0,” *Advances in Space Res.*, vol. 28, no. 9, pp. 1377–1384, Jan. 2001. DOI: [10.1016/S0273-1177\(01\)00423-9](https://doi.org/10.1016/S0273-1177(01)00423-9).
- [129] P. H. Krisko, “Proper implementation of the 1998 NASA breakup model,” *Orbital Debris Quarterly News*, vol. 15, no. 4, pp. 1–10, 2011.
- [130] T. Steelman, “Adaptive governance,” in *Handbook on Theories of Governance*, C. Ansell and J. Torfing, Eds., Cheltenham, U.K.: Edward Elgar Publishing, 2016, ch. 50.
- [131] B. C. Chaffin, H. Gosnell, and B. A. Cosens, “A decade of adaptive governance scholarship: synthesis and future directions,” *Ecology and Soc.*, vol. 19, no. 3, 2014. DOI: [10.5751/ES-06824-190356](https://doi.org/10.5751/ES-06824-190356).
- [132] R. D. Brunner and A. H. Lynch, *Adaptive governance and climate change*. Boston, MA: American Meteorological Society, 2010.
- [133] L. Gunderson and S. S. Light, “Adaptive management and adaptive governance in the everglades ecosystem,” *Policy Sci.*, vol. 39, no. 4, pp. 323–334, 2006. DOI: [10.1007/s11077-006-9027-2](https://doi.org/10.1007/s11077-006-9027-2).

- [134] C. R. Allen, J. J. Fontaine, K. L. Pope, and A. S. Garmestani, “Adaptive management for a turbulent future,” *J. of Env. Manage.*, vol. 92, no. 5, pp. 1339–1345, May 2011. DOI: [10.1016/J.JENVMAN.2010.11.019](https://doi.org/10.1016/J.JENVMAN.2010.11.019).
- [135] R. A. Kagan, *Adversarial Legalism: The American Way of Law, Second Edition*, 2nd ed. Cambridge, MA and London, U.K.: Harvard University Press, 2019. DOI: [doi:10.4159/9780674242678](https://doi.org/10.4159/9780674242678).
- [136] O. B. Ferriter, B. K. Williams, R. C. Szaro, *et al.*, “Adaptive Management,” U.S. Department of the Interior, Tech. Rep., 2009.
- [137] E. Ostrom, *Governing the Commons: The Evolution of Institutions for Collective Action*. Cambridge, U.K.: Cambridge University Press, 2015. DOI: [DOI:10.1017/CBO9781316423936](https://doi.org/10.1017/CBO9781316423936).
- [138] IRGC, “Planning Adaptive Risk Regulation, Conference Report,” EPFL International Risk Governance Center, Lausanne, Switzerland, Tech. Rep. Jan. 2016. [Online]. Available: <https://discovery.ucl.ac.uk/id/eprint/1508413/1/Planning%20Adaptive%20Regulation%20IRGC%20January%202016%20Conference%20Report.pdf>.
- [139] D. L. Oltrogge and I. A. Christensen, “Space governance in the new space era,” *J. of Space Safety Eng.*, vol. 7, no. 3, pp. 432–438, 2020. DOI: [10.1016/j.jsse.2020.06.003](https://doi.org/10.1016/j.jsse.2020.06.003).
- [140] C. Ezell, “Space Governance : Risks, Frameworks, and Futures,” Space Futures Initiative, Cambridge, MA, Tech. Rep., 2022, pp. 1–83. [Online]. Available: https://spacefuturesinitiative.org/images/Space_Governance_Risks_Frameworks_and_Futures.pdf.
- [141] O. F. Keles, “Telecommunications and Space Debris: Adaptive Regulation Beyond Earth,” *Telecommun. Policy*, vol. 47, no. 3, 2023. DOI: [10.1016/j.telpol.2023.102517](https://doi.org/10.1016/j.telpol.2023.102517).
- [142] M. Haasnoot, J. H. Kwakkel, and W. E. Walker, “Dynamic adaptive policy pathways : A method for crafting robust decisions for a deeply uncertain world,” *Glob. Env. Change*, vol. 23, no. 2, pp. 485–498, 2013. DOI: [10.1016/j.gloenvcha.2012.12.006](https://doi.org/10.1016/j.gloenvcha.2012.12.006).
- [143] M. R. Migaud, R. A. Greer, and J. B. Bullock, “Developing an Adaptive Space Governance Framework,” *Space Policy*, vol. 55, p. 101400, 2021. DOI: [10.1016/j.spacepol.2020.101400](https://doi.org/10.1016/j.spacepol.2020.101400).
- [144] F. Berkes, *Sacred Ecology*. Milton Park, U.K.: Taylor & Francis, 2017.
- [145] J. A. Parrotta and R. L. Trosper, Eds., *Traditional Forest-Related Knowledge: Sustaining Communities, Ecosystems and Biocultural Diversity*. London, U.K.: Springer Dordrecht, 2011, vol. 49, p. 622.
- [146] E. N. Anderson, *Ecologies of the Heart: Emotion, Belief, and the Environment*. Oxford, U.K.: Oxford University Press, 1996.
- [147] D. Deur and N. J. Turner, *Keeping it Living: Traditions of Plant Use and Cultivation on the Northwest Coast of North America*. Seattle, WA: University of Washington Press, 2005.

- [148] D. N. Pandey, *Ethnoforestry: Local Knowledge for Sustainable Forestry and Livelihood Security*. New Delhi, India: Himanshu Publications, 1998.
- [149] Chair of the Working Group on the Long-term Sustainability of Outer Space Activities, “Guidelines for the Long-Term Sustainability of Outer Space Activities,” United Nations Committee on the Peaceful Uses of Outer Space, Vienna, Austria, Tech. Rep., 2018. [Online]. Available: https://www.unoosa.org/res/oosadoc/data/documents/2018/aac_1052018crp/aac_1052018crp_20_0_html/AC105_2018_CRP20E.pdf.
- [150] R. K. Craig, A. S. Garmestani, C. R. Allen, C. A. T. Arnold, H. Birgé, D. A. DeCaro, A. K. Fremier, H. Gosnell, and E. Schlager, “Balancing stability and flexibility in adaptive governance: an analysis of tools available in U.S. environmental law.,” eng, *Ecology and Soc.*, vol. 22, no. 2, pp. 1–3, Jun. 2017. DOI: [10.5751/ES-08983-220203](https://doi.org/10.5751/ES-08983-220203).
- [151] V. Braun, A. Horstmann, S. Lemmens, and C. Wiedemann, “Recent Developments in Space Debris Environment Modelling , Verification and Validation With MASTER,” in *8th Euro. Conf. on Space Debris*, Darmstadt, Germany: ESA Space Debris Office, 2021, pp. 20–23.
- [152] M. Matney, P. Anz-meador, A. King, A. Manis, and J. H. Seago, “An Overview of NASA’s Newest Engineering Model, ORDEM 4.0,” in *2nd International Orbital Debris Conference*, Houston, TX: Universities Space Research Association, Lunar and Planetary Institute, 2023.
- [153] F. Mclean, S. Lemmens, Q. Funke, and V. Braun, “DISCOS 3: An improved data model for ESA’s database and information system characterising objects in space,” *7th Euro. Conf. on Space Debris, Darmstadt*, vol. 7, no. 151, pp. 1–4, 2017.
- [154] D. A. Vallado and D. Finkleman, “A critical assessment of satellite drag and atmospheric density modeling,” *Acta Astronautica*, vol. 95, pp. 141–165, 2014. DOI: [10.1016/j.actaastro.2013.10.005](https://doi.org/10.1016/j.actaastro.2013.10.005).
- [155] T. J. Colvin, J. Karcz, and G. Wusk, “Cost and Benefit Analysis of Orbital Debris Remediation,” NASA Office of Technology, Policy, and Strategy, Washington D.C., Tech. Rep., 2023. [Online]. Available: <https://www.nasa.gov/offices/otps/home/index.html>.
- [156] J. -. Liou, D. J. Kessler, M. Matney, and G. Stansbery, “A New Approach to Evaluate Collision Probabilities Among Asteroids, Comets, and Kuiper Belt Objects,” in *Lunar and Planetary Science Conference*, S. Mackwell and E. Stansbery, Eds., ser. Lunar and Planetary Science Conference, Mar. 2003, p. 1828.
- [157] D. Oltrogge and S. Alfano, “Efficient assessment of long-term encounter rates with CSSI’s volumetric encounter method,” 2022.
- [158] Viasat, “Managing Mega-Constellation Risks in LEO,” 2022. [Online]. Available: [https://www.viasat.com/content/dam/us-site/corporate/documents/Viasat%20White%20Paper-Managing%20Mega-Constellation%20Risks%20in%20LEO%20\(Updated%20Nov%202022\)%20\(A4\).pdf](https://www.viasat.com/content/dam/us-site/corporate/documents/Viasat%20White%20Paper-Managing%20Mega-Constellation%20Risks%20in%20LEO%20(Updated%20Nov%202022)%20(A4).pdf).